DIPLOMARBEIT

Ligandenaustauschreaktionen von Au Nanoclustern

ausgeführt am

Institut für Materialchemie
der Technischen Universität Wien

unter der Anleitung von

Univ.Prof. Dr. Günther Rupprechter
Dr. Noelia Barrabés Rabanal

durch

Vera Truttmann, BSc.
Lindenbauergasse 7/2
1110 Wien

Wien, im Dezember 2017

MASTER THESIS

Ligand Exchange Reactions of Au Nanoclusters

carried out at the

Institute of Materials Chemistry
of TU Wien

under the supervision of

Univ.Prof. Dr. Günther Rupprechter
Dr. Noelia Barrabés Rabanal

by

Vera Truttmann, BSc.
Lindenbauergasse 7/2
1110 Wien

Vienna, December 2017

Kurzfassung

Die Eigenschaften von ligandenstabilisierten Au Nanoclustern werden sowohl durch deren Größe, als auch durch die chemische Natur der Liganden beeinflusst. Modifikation derselben lässt sich mithilfe von Ligandenaustauschreaktionen bewerkstelligen, welche damit ausge-zeichnete Möglichkeiten zur gezielten Veränderung der Clustereigenschaften darstellen. Zudem können diese Reaktionen auch als Alternativstrategie zur Synthese von Clustern herangezogen werden, welche nicht aus den üblicherweise verwendeten Ausgangsstoffen zugänglich sind.

Für praktische Anwendungen, z.B. als Katalysator oder als Sensor, werden die Cluster für gewöhnlich auf oxidischen Supportmaterialien immobilisiert. Um ein besseres Verständnis derartiger Anwendungsprozesse und auch von Au Nanoclustern im Allgemeinen zu erlangen, sind Studien der Wechselwirkungen zwischen Cluster und Supportmaterial notwendig. Eine Möglichkeit dafür stellen Vergleiche der Ligandenaustauschreaktionen von gelösten und immobilisierten Clustern dar. Bislang wurden jedoch nur Untersuchungen der Ligandenaustauschreaktionen in flüssiger Phase publiziert.

Im Rahmen dieser Arbeit wurde zum ersten Mal ein Ligandenaustausch von immobilisierten $Au_{11}(PPh_3)_7Cl_3$ Nanoclustern mit Thiolliganden beobachtet. Zur Untersuchung der Austauschreaktionen wurden drei verschiedene Systeme verwendet: (1) freie Cluster in Lösung, (2) Cluster immobilisiert auf planaren Al_2O_3 oder ZnSe Oberflächen und (3) Cluster abgelagert auf SiO_2 oder Al_2O_3 Pulvern.
Für die Reaktionen in Lösung konnte ein Wachstum der Cluster von Au_{11} zu Au_{25} beobachtet werden, jedoch nicht für Cluster, die auf planaren Oberflächen oder Pulvern immobilisiert waren. Im Fall der Systeme (1) und (2) war der Ligandenaustausch zudem nicht vollständig und führte zu Produkten, die sowohl Triphenylphosphin und Chlor, als auch Thiole als Liganden aufwiesen. Für jene Cluster, die auf Metalloxidpulvern immobilisiert wurden, ist die Anzahl der ausgetauschten Liganden noch Gegenstand laufender Untersuchungen.

Zudem wurden auch Ligandenaustauschreaktionen von Au_{15} Nanoclustern in Lösung mit einem großen Überschuss an 2-Phenylethanthiol untersucht, wobei $Au_{20}(SC_2H_4Ph)_{16}$ entstand. Diese Reaktion stellt eine bisher unbekannte, unkompliziert durchzuführende Synthese von Au_{20} Clustern in hoher Ausbeute dar.

Abstract

The properties of monolayer protected Au nanoclusters are known to be size-dependent, and strongly related to the nature of the protecting ligand. Modification of the surface ligands can be accomplished by a ligand exchange reaction. This represents a valuable pathway for tuning the cluster properties, as well as alternative synthetic pathways of cluster species, which cannot be easily obtained from standard precursor materials.

For applications such as catalysis or sensing, the clusters are usually immobilized on metal oxides. For a better understanding of these processes and of Au nanoclusters in general, studying the interaction between cluster and support is crucial. One approach is provided by comparison of ligand exchange reactions of dissolved and deposited clusters. However, so far only ligand exchange reactions with Au nanoclusters in solution have been published.

Within this thesis, ligand exchange of immobilized $Au_{11}(PPh_3)_7Cl_3$ clusters and thiol ligands is reported for the first time. The reactions were studied using three different systems: (1) free clusters in solution, (2) cluster dropcast films on planar Al_2O_3 or ZnSe and (3) clusters supported on SiO_2 or Al_2O_3 powders.
For the reaction in solution, growth of the cluster core from Au_{11} to Au_{25} was observed, whereas no major change in size was found for reactions with cluster dropcast films or clusters supported on oxide powder material. Only incomplete exchange was observed for system (1) and (2), with all triphenylphosphine, thiol and chloride being present in the ligand shell of the product. For the powder-supported clusters, the number of exchanged ligands remains to be identified in future work.

In addition, ligand exchange in solution, starting from crude Au_{15} with a large excess of 2-phenylethanethiol was investigated, resulting in the formation of $Au_{20}(SC_2H_4Ph)_{16}$. This presents a new, facile approach for synthesizing Au_{20} clusters in high yield.

Acknowledgments

Contents

Nomenclature

Acronyms

Symbol	Description
(A)BF	(Annular) Bright Field
(HA)ADF	(High Angular) Annular Dark Field
(S)TEM	(Scanning) Transmission Electron Microscopy
aliph.	aliphatic system
arom.	aromatic ring/system
ATR	Attenuated Total Reflectance
bend.	bending; in IR code
br	broad; in NMR and IR code
CD	Circular Dichroism
EXAFS	Extended X-ray Absorption Fine Structure
FT-IR	Fourier Transform Infrared (Spectrometer)
HOMO	Highest Occupied Molecular Orbital
ip./op.	in-plane/out-of-plane; in IR code
IR	Infrared
IRRAS	Infrared Reflection-Absorption Spectroscopy

LE	Ligand Exchange
LIA	Lock-in Amplifier
LUMO	Lowest Unoccupied Molecular Orbital
MALDI	Matrix-Assisted Laser Desorption Ionization
MCT	Mercury Cadmium Telluride (Detector)
MS	Mass Spectroscopy
n.a.	not assigned; in IR code
PEM	Photoelastic Modulator
PM	Polarization Modulation
PM-IRRAS	Polarization-Modulation Infrared Reflection-Absorption Spectroscopy
RT	Room Temperature
RTOF	Reflectron Time-of-Flight
s, d, t, q, m	Singlet, Doublet, Triplet, Quartet, Multiplet; in NMR code
s, m, w	strong, middle, weak; in IR code
scis.	scissoring; in IR code
SEC	Size Exclusion Chromatography
SLS	Swiss Light Source
stretch.	stretching; in IR code
TOF	Time-of-Flight
UV-Vis	Ultraviolet-Visible

XAFS	X-ray Absorption Fine Structure
XAS	X-ray Absorption Spectroscopy
XPS	X-ray Photoelectron Spectroscopy

Chemicals

Symbol	Description
2-PET	2-Phenylethanethiol
BINAS	1,1'-Binaphtyl-2,2'-dithiol
DCM	Dichloromethane
DCTB	*trans*-2-[3-(4-*tert*-Butylphenyl)-2-methyl-2-propenylidene]malononitrile
EtOH	Ethanol
GSH	L-Glutathione reduced
MeOH	Methanol
Oct	Octyl
SG	Thiolate form of L-Glutathione
SR	Thiolate
TBAB	Borane *tert*-Butylamine
TBBT	*tert*-butylbenzothiol
THAP	2',4',6'-Trihydroxyacetophenone Monohydrate
THF	Tetrahydrofuran
TMS	Tetramethylsilane

TOAB	Tetraoctylammoniumbromide	
TPP	Triphenylphosphine	

Greek Symbols

Symbol	Description	Unit
δ	Chemical Shift	ppm
λ	Wavelength	nm
ν	Stretching vibration	
$\tilde{\nu}$	Wavenumber	cm^{-1}

Product Abbreviations

Symbol	Description
A	Compound A
F1-F4	Products from LE with Dropcast Films
P1-P4	Products from LE with Powder Samples
S1-S3	Products from LE in Solution with GSH

Roman Symbols

Symbol	Description	Unit
f	Frequency	Hz
A	Absorption	a.u.
E	(Photon) Energy	eV
eq.	equivalent	
M	Molar Mass	g/mol
m	Mass	kg
m/z	Mass over Charge	Da
n	Molar Amount	mol

1. Introduction

Au nanoclusters consist of a core of Au atoms in the nanometer regime, which is stabilized by a monolayer of protecting ligands [1]. The properties of these clusters depend on the size of the cluster core, as well as on their chemical composition. The ability to precisely tune this parameters has made clusters an interesting research subject within the last years, opening up a broad range of applications [2, 3], as is illustrated in Figure 1.1.
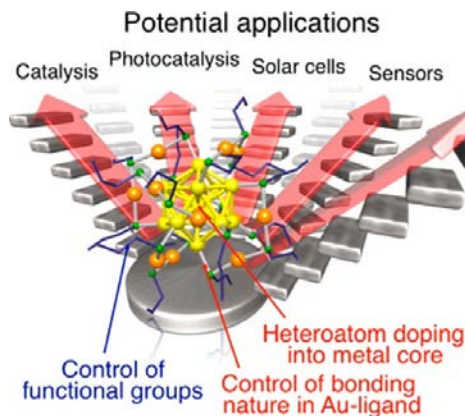
Figure 1.1.: Potential applications and possibilities for modifying the properties of thiolate protected Au nanoclusters. Reproduced from [2].

Au nanoparticles have been studied for years, due to their interesting catalytic activity [4–6] for sizes smaller than 2 nm, when the properties of bulk gold are lost and a molecular-like electronic structure is observed [7]. However, the investigation of these catalysts is demanding because of the polydisperse particle size [5]. This can be overcome by using Au nanoclusters instead, which can be synthesized with specific numbers of atoms [2].

It was found that clusters with certain numbers of Au atoms in the core were significantly more stable than others [8, 9], for example $[Au_{25}(SR)_{18}]^-$ [10–13] or $Au_{102}(SR)_{44}$ [8, 9, 12]. These cluster often exhibit closed electron shells, thereby following the series of electron magic numbers (n = 2, 8, 18, 20, 34, 40, 58 ...). In 2008, a formula for the calculation of the free-electron count n_e was derived:

$$n_e = N \cdot \nu_A - M - z \tag{1.1}$$

In this equation, n_e is equal to the number of free electrons, N to the number of Au atoms, ν_A to the effective valence of the Au atoms (ν_A is equal to 1 for Au nanoclusters), M to the number of ligands withdrawing a single electron from the Au core and z to the charge of the cluster. The concept is easily applied to systems with different types of metal atoms and ligands, by using modified variables ν_A and M [8, 12]. However, several exceptions of the magic numbers rule are known, for example $Au_{25}(SR)_{18}$, which is very stable although having only 7 free electrons [14]. This is due to the fact that the formula can be applied to spherical clusters only [8, 14].

For creating new, specifically functionalized clusters with precise magnetic, electronic, optical and catalytic properties, different strategies can be applied. One example is to change the size of the Au core, but also doping with other metals, producing bi- or trimetallic clusters, can be done. A third approach is the modification of the ligand shell, which will be discussed in more detail in the following [2].

1.1. Comparison of Phosphine and Thiolate Protected Au Nanoclusters

Au nanoclusters are known to bind different kinds of ligands, including thiolates [1], phosphines [15], alkynes [3, 16–18], selenides [3, 19–21] or tellurides [3, 22]. Among these, phosphines and thiolates are the most studied ones [3].
However, their chemical nature and therefore also the bonding motive to the cluster are quite different [23]. Phosphines belong to the neutral 'L-type' ligands, which coordinate to the Au core through their lone electron pair. Thiolates and halides, however, are 'X-type' ligands and negatively charged, balancing the positive charge of the Au core [23, 24]. As phosphines are not able to compensate for the positive Au cluster core, bonding of a second, 'X-type' ligand is required, creating mixed ligand shell clusters [23]. Halides, nitrates, $PF_6{}^+$ and $SbF_6{}^+$ are all able to function as secondary ligands [15, 23].

Another difference is the bonding motive to the metal core: Phosphines only bind end-on, meaning that one P atom is bound to one Au atom only [23]. Thiolate ligands, however, usually form so-called 'staple motives' around the cluster core, where one thiolate is bond to two Au atoms. These staples exist in different length and are of the general type [-S(R)-Au-S(R)-]$_n$ [23, 25], as is illustrated in Figure 1.2. Apart from that, thiolates can also be three- or four-coordinated to the metal core [23].

(a) $Au_{25}(SR)_{18}$ (b) staple motive
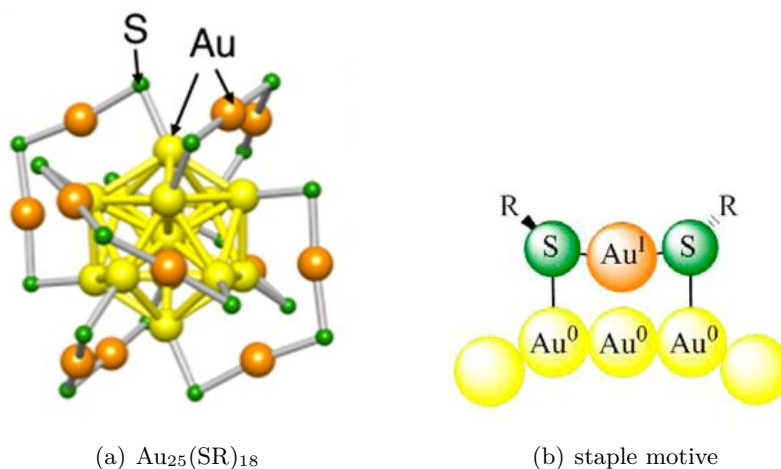
Figure 1.2.: Yellow: Au(0) core; orange: Au(1) in the staple motive; green: thiol ligands. The organic framework of the ligand is not shown. (a) Structure of $Au_{25}SR_{18}$. Adapted from [2]. (b) Staple motive of thiolate protected Au nanoclusters. Adapted from [26].

Although phosphine protected Au nanoclusters were the first ones investigated [1, 3], within the last years, clusters protected by thiolates received much more attention in research due to their higher stability [27]. However, due to their different geometrical structure and electronic properties, the magic atom number configurations of phosphine and thiolate protected Au nanoclusters are not the same. As a result, smaller clusters ($< Au_{13}$) are easily accessible using phosphines as ligands [1], while the corresponding thiolate protected clusters are difficult to obtain [27]. This can be explained by increased stabilization through the direct bonding between the phosphine ligands and the metal core (no staples) [1].

1.2. Phosphine Protected Au_{11} Nanoclusters

The discovery of triarylphosphine protected Au_{11} nanoclusters, often also called undecagold, dates back to the 1960s [28, 29]. According to the equation of Walter *et al.*, $Au_{11}(PPh_3)_7Cl_3$ has a closed electron shell, accounting for its high stability [12, 30].

Only in 2014, McKenzie *et al.* reported crystal structures and spectral data (NMR and UV-Vis) of two different undecagold clusters, $Au_{11}(PPh_3)_7Cl_3$ and $[Au_{11}(PPh_3)_8Cl_2]Cl$. The structures differ slightly, as is shown in Figure 1.3. Moreover, distinct differences in the optical properties, as well as in stability and reactivity were observed. $Au_{11}(PPh_3)_7Cl_3$ is not stable in halogenated solvents, decomposing within a few hours at room temperature. $[Au_{11}(PPh_3)_8Cl_2]Cl$, on the other hand, does not show significant signs of degradation even after several months [31]. The remarkable differences in the ligand exchange reaction activity

will be discussed in Chapter 1.4.2.

(a) $Au_{11}(PPh_3)_7Cl_3$ (b) $[Au_{11}(PPh_3)_8Cl_2]Cl$
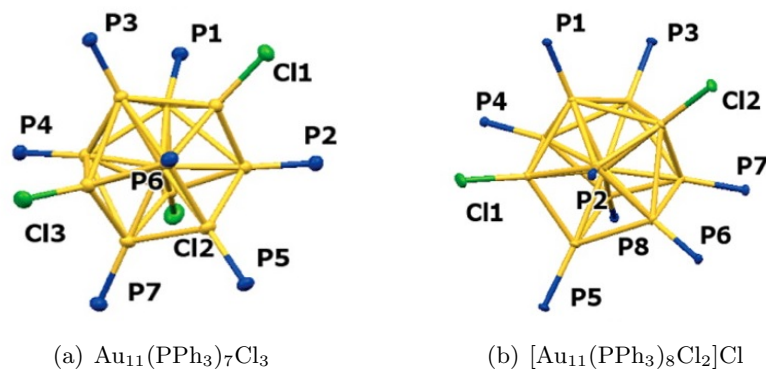
Figure 1.3.: Yellow: Au; blue: P; green: Cl. The organic framework of the ligand is not shown. Adapted from [31].

The 'X-type' ligand in Au_{11} necessary for charge compensation is usually the anion of the precursor $AuX(PPh_3)$ (see next Chapter). Chlorides [31, 32], bromides [33], iodides [34, 35] and thiocyanates [28] are all known to coordinate to Au_{11}. In addition, also thiolates were shown to bind to phosphine protected undecagold clusters [30, 36, 37]. In that case, the thiol ligands do not form staple bonds, but only coordinate to one single Au atom each [30, 37].

1.2.1. Supported Au_{11} Nanoclusters

Au nanoclusters have been found to be active for different types of liquid phase reactions, such as alcohol oxidation [38–40], cyclohexane oxidation [13, 41] or styrene oxidation [42–44]. For that purpose, the cluster is usually immobilized on a metal oxide support material, for example Al_2O_3 or CeO_2 [13]. However, only a few reports for triphenylphosphine protected Au_{11} supported on metal oxides have been published up to now.

Zheng *et al.* suggested interactions between the dipoles on the surface of a support material and the polarizeable cluster core to be the main bonding motive during the supporting process of monodisperse clusters [38]. However, Tsukuda and coworkers instead claimed interactions between the OH-groups of the silica and the polarized ligand shell to control the supporting process of Au_{11}. They further showed that the cluster adsorbs on mesoporous silica very readily, when CH_2Cl_2 is used as solvent. By adding increasing amounts of EtOH to the solution, the immobilization efficiency decreased, but a more homogenous distribution could be reached. This was attributed to the higher polarity of the solvent hindering the interactions between ligands and silica [39].

Removal of Au_{11} from the SiO_2 support by washing with EtOH was observed by Liu *et al.*, suggesting that the impregnation did not lead to irreversible structural changes [39]. Anderson *et al.* showed that treatment of triphenylphosphine protected Au_8, Au_9 and Au_{11} on titania with toluene at $100\,°C$ lead only to partial removal of both cluster and ligands from the support. However, a fraction of the residual immobilized clusters formed Au–O bonds [7].

Oxidation of Au_{11} on silica was also reported by Lim *et al.* [45, 46]. They found that in general, odd-numbered clusters (like Au_5, Au_7 and Au_{13}) supported on silica were highly inert against oxidation at ambient conditions, with Au_{11} being the only exception.

The stability of the other odd-numbered clusters was attributed to a charge transfer from the cluster to the support, making them even-numbered with a closed shell and therefore unreactive [45, 46]. It was further shown that very different behavior was observed for clusters immobilized on graphite [45, 47]. Thus, the interaction between cluster and support material seems to play a key role [45].

Partial removal of the ligands of Au_{11} on mesoporous silica at $200\,°C$ for $2\,h$ did not lead to an increase in core size, if the impregnation was done in a 1:5 EtOH/DCM mixture. The calcinated sample was then found to be a very active and recyclable catalyst for alcohol oxidation [39]. However, increasing core sizes were obtained if the calcination was pursued for $8\,h$ or longer due to aggregation, which resulted in less active catalysts [40]. Lim *et al.* observed no aggregation of small Au nanoclusters (2-13 core atoms) for calcination up to $250\,°C$ [45].

1.3. Synthesis of Ligand Protected Au Nanoclusters

1.3.1. Synthesis of Thiolate Protected Au Nanoclusters

The procedures for synthesis of thiolate-protected Au nanoclusters typically follow the method published by Brust *et al.* In short, $HAuCl_4 \cdot 3\,H_2O$ is dissolved in H_2O and transferred into the organic layer with the aid of a phase-transfer agent, followed by removal of the aqueous layer. Next, the thiol ligand is added in excess and the mixture is reduced by $NaBH_4$ [48]. This protocol has been modified for selective synthesis of several clusters, e.g. $Au_{25}(SR)_{18}$ [49–53], $Au_{38}(SR)_{24}$ [54, 55] or $Au_{144}(SR)_{60}$ [56]. The formation of a specific product can vary depending on different parameters, for example the chosen solvent [50, 56, 57], usage of a mono- or biphasic mixture [49, 50], pH range [51, 58, 59], reaction temperature [49, 50], nature [60] and amount of added ligand [61, 62], stirring speed [49, 50, 61, 63] and the aging time after the reduction [52, 64].

The reaction mechanism can be explained as a reduction of Au(III) to Au(I) by the added thiols. These ligands then stabilize Au(I) and promote the formation of Au(I):(SR)

5

intermediates [49, 56], whose structure reportedly can vary [65]. However, analysis of these species is complicated due to their strong dependence on the current conditions and their low solubility in most common solvents [50]. The subsequent reduction from Au(I) to Au(0), in most cases by addition of $NaBH_4$, is usually followed by a size focusing process, yielding the most stable cluster species [49, 55, 56, 64]. The obtained products can therefore vary depending on the exact reaction conditions [49, 50, 62]. Apart from the magic numbered clusters mentioned earlier, also kinetically stabilized clusters can be produced, which can only be converted into the thermodynamic products by core-etching through addition of excess thiols [62], which is visualized in Figure 1.4.
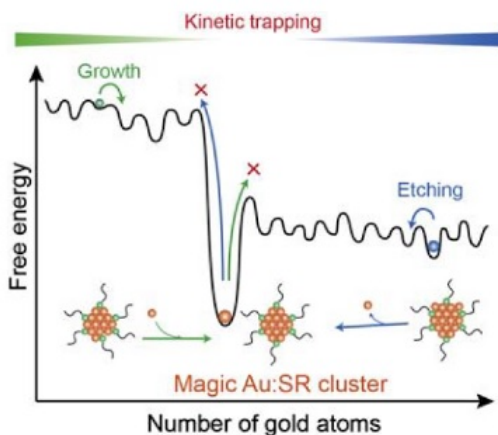
Figure 1.4.: Illustration of the formation of magic number and kinetically trapped $Au_m(SR)_n$ clusters. Adapted from [1].

Purification of the desired cluster can be achieved by washing with water and short chain alcohols (typically MeOH or EtOH) [64]. In cases when more than one cluster species has formed, extraction or size specific separation has to be performed afterwards. Size exclusion chromatography (SEC) and polyacrylamide gel electrophoresis (PAGE) are popular separation techniques for Au nanoclusters [62]. Characterization can be achieved using a variety of techniques, such as MS, NMR, IR and XPS. In particular, UV-Vis spectroscopy is often performed, as the spectral features can be seen as a fingerprint for certain cluster species, depending on the core size, the nature of the protecting ligand and the charge [66].

1.3.2. Synthesis of Phosphine Protected Au Nanoclusters

For the synthesis of phosphine protected Au nanoclusters, the protocol described above is slightly modified. The precursor material is usually a Au(I) complex of the general formula $AuX(PPh_3)$, which is dissolved in ethanol and subsequently reduced with $NaBH_4$. Again, formation of the product clusters occurs during a size focusing process. The chemical nature

of X was found to have big influence on the synthesis product, as neutral clusters stabilized by 10 ligands are obtained if strongly coordinating ligands, such as halides, thiolates or thiocyanates are used. Weaker coordinating species, for example nitrates, usually result in positively charged clusters, which are surrounded by 8 ligands [15].

As for the thiolate protected clusters, lots of parameters influence the formation of a specific product. For example, $Au_{11}(PPh_3)_7Cl_3$ is obtained when the reduction of $AuCl(PPh_3)$ is carried out in THF for 2 h, whereas reduction in CH_2Cl_2 with less than 1 eq. of $NaBH_4$ per eq. of $AuCl(PPh_3)$ for 24 h exclusively yields $[Au_{11}(PPh_3)_8Cl_2]Cl$ [31].

1.4. Ligand Exchange Reactions

Modification of the properties of Au nanoclusters, as well as post-synthetic functionalization are possible by ligand exchange reactions, which lead to replacement of cluster ligands with incoming new ones [67]. Steric factors, such as bulkyness and chain length, as well as the concentration of the exchange ligand and the solvent have profound influence on the reaction kinetics. Less electron density in the Au core is also known to increase the exchange rate. Moreover, the surface of the cluster exhibits a much higher reactivity than the center, which is explained by their difference in accessibility [68].

1.4.1. Thiol-to-Thiol Ligand Exchange

Thiol-to-thiol ligand exchange follows a S_N2 mechanism, with nucleophilic attack of an exchange thiol on a Au site leading to exchange. The reaction is associative, meaning that both bonding of the new and release of the old ligand happen at the same time [69, 70]. Theoretical calculations on the ligand exchange of $Au_{102}(SR)_{44}$ showed that the possible structure of the intermediate seems to be either $[Au_{102}(SR)_{44}(SR')]^*$ or $[Au_{102}(SR)_{44}(HSR')]^*$, with * indicating that the complex is transient and cannot be isolated [71]. This further confirms that the reaction is really associative. Figure 1.5 shows a possible pathway and the corresponding energy trend.

A broad variety of thiolates can be used for ligand exchange reactions, which includes both aliphtatic and aromatic ones, but also functionalized thiols. Moreover, bonding of chiral ligands introduces chirality to the cluster, which can be measured by circular dichroism (CD). Besides the commonly used monodentate thiols, bidentate ligands can also bind to the Au clusters [72].
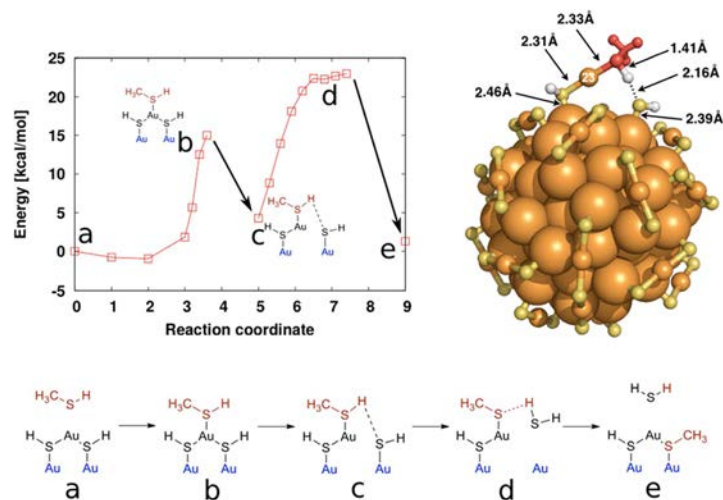
Figure 1.5.: Illustration of a second order thiol-to-thiol ligand exchange with methanethiol (lower panel) and corresponding energy diagram (top-left panel). An illustration of intermediate C is shown in the top-right panel. Reproduced from [71].

One example of that kind is the chiral ligand 1,1'-binaphthyl-2,2'-dithiol (BINAS), which binds to cluster with both of its sulfur atoms. Investigations of its reaction with $Au_{25}(2\text{-PET})_{18}$ and $Au_{38}(2\text{-PET})_{24}$ showed decrease in the spectral features of the starting material, which was attributed to loss of symmetry upon (incomplete) exchange [73, 74].

Further discussion of thiol-to-thiol ligand exchange can be found in Chapter 5.2.

1.4.2. Phosphine-to-Thiol Ligand Exchange

Ligand exchange on triphenylphosphine (TPP in short) protected Au_{11} clusters has already been studied intensively [31, 36, 75–78]. In 2002, Woehrle *et al.* first transferred the undecagold into thiolate protected clusters. They also stated that mixed ligand shell products will be obtained if the excess of exchange ligand is not large enough, though it cannot be scaled up infinitely high because of the instability of Au_{11} under these conditions [75].

Mechanistic studies of the ligand exchange on 1.5 nm PPh$_3$ protected Au nanoparticles with different thiol ligands were reported in 2005. The core of the precursor material was estimated to contain around 101 gold atoms. It was found that the reaction could be divided into three steps: First, a rapid exchange occurred, in which AuCl(PPh$_3$) was released and a part of the thiols attached to the Au core. This happened within the very first minutes after addition of the thiol ligands. Next, the residual TPP was released and immediately taken up by the AuCl(PPh$_3$), forming Au(I) complexes. This step is accompanied by addition

of further thiols onto the nanoparticle and is completed within approximately one hour. Finally, rearrangement of the new ligand shell gives a completely exchanged end product.

The proposed mechanism was found to be correct for both organic soluble and water soluble thiols, conducting standard ligand exchange protocols with one (DCM) or two phases (DCM/H$_2$O), respectively. The findings were based on a series of both ^{1}H and ^{31}P-NMR experiments, were no free PPh$_3$ was found in any step of the reaction except the very end (released from the Au(I) complexes in low amount) [79].

Similar experiments were then performed for thiol ligand exchange with undecagold. There, only release of PPh$_3$ was observed, being rapidly oxidized to PPh$_3$=O. Moreover, the ligand exchange was much slower than for the larger nanoparticles, indicating lower reactivity of Au$_{11}$. The rate was also shown to depend on the nature of the incoming thiol, with longer and bulkier ligands requiring significantly more time to react than shorter analogues [27].

Finally, Tsukuda and coworkers determined the product of the ligand exchange between Au$_{11}$ precursors and organic aliphatic thiol ligands to be [Au$_{25}$(PPh$_3$)$_{10}$(SC$_n$H$_{2n+1}$)$_5$Cl$_2$]$^{2+}$. Their structural investigations revealed two edge-fused icosahedrons, linked together by bridging thiol ligands. The TPP and chloride ligands were found to be attached to the external sites of the two Au$_{13}$ cores [78]. The structure without the organic framework is displayed in Figure 1.6.

The reported UV-Vis absorption profiles of ligand exchange products with organic thiols prior to the identification of [Au$_{25}$(PPh$_3$)$_{10}$(SR)$_5$Cl$_2$]$^{2+}$ strongly suggests that they were identical with it [27, 75, 78].
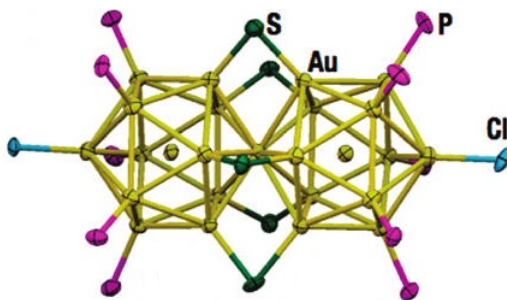
Figure 1.6.: Structure of [Au$_{25}$(PPh$_3$)$_{10}$(SR)$_5$Cl$_2$]$^{2+}$. The organic ligand framework is not shown. Yellow: Au; pink: P; green: S; blue: Cl. Adapted from [78].

In addition, [Au$_{25}$(PPh$_3$)$_{10}$(SR)$_5$Cl$_2$]$^{2+}$ was also obtained as the main product of the ligand exchange of 1-3.5 nm Au nanoparticles protected by TPP ligands and 2-phenylethanethiol [80]. A side product formed during the reaction could be identified as [Au$_2$(PPh$_3$)$_2$(SC$_2$H$_4$Ph)]$^{2+}$ [81]. Das *et al.* reported formation of [Au$_{24}$(PPh$_3$)$_{10}$(SC$_2$H$_4$Ph)$_5$X$_2$]$^+$, if a large excess of PPh$_3$ was added to [Au$_{25}$(PPh$_3$)$_{10}$(SC$_2$H$_4$Ph)$_5$X$_2$]$^{2+}$ [76].

Ligand exchange of Au_{11} clusters with L-glutathione (GSH) was investigated by Tsukuda and coworkers. They found complete exchange to only thiolate-protected $Au_{25}(SG)_{18}$ upon reaction at elevated temperatures in a biphasic reaction mixture ($CHCl_3/H_2O$). Within the first hour, the color was transferred to the aqueous layer, already showing typical UV-Vis absorption features of $Au_{25}(SG)_{18}$. Moreover, formation of insoluble material at the interface was reported, which dissolved upon reaction progress. TEM analysis showed that this compound was significantly larger than the Au_{25} clusters obtained in the end, suggesting rapid growth of the clusters, followed by a size focusing step [77]. Qian *et al.* obtained the same fully exchanged $Au_{25}(SG)_{18}$ clusters when reacting polydisperse TPP protected Au nanoparticles (size range 1-3.5 nm) with L-glutathione in a biphasic CH_2Cl_2/H_2O system at 55 °C [80].

Investigations of the ligand exchange with L-glutathione by Hutchison and coworkers with both forms of phosphine protected undecagold revealed that only $Au_{11}(PPh_3)_7Cl_3$ does react to $Au_{25}(SG)_{18}$. $[Au_{11}(PPh_3)_8Cl_2]Cl$ seems to maintain its core size, unless the reaction is conducted at higher temperature (55 °C) or with an extremely high excess of incoming thiol (> 400 eq. with respect to undecagold, reaction at 45 °C). Interestingly, also mixtures of both Au_{11} clusters mainly reacted to $Au_{25}(SG)_{18}$ clusters, even if only small amounts of $Au_{11}(PPh_3)_7Cl_3$ were present. It was assumed that the difference in reactivity can be attributed to the different stability of the two undecagold forms in halogenated solvents used for the ligand exchange. $Au_{11}(PPh_3)_7Cl_3$ seems to aggregate very fast, giving an Au_{25} cluster after size focusing. $[Au_{11}(PPh_3)_8Cl_2]Cl$, on the other hand, which is significantly more stable, exchanges to smaller thiolate protected Au nanoclusters. It should be noted that these smaller exchanged cluster are not very stable and decompose rapidly in aqueous solution [31].

2. Motivation of the Thesis

The aim of the work conducted within this thesis is to obtain better understanding of ligand exchange reactions of Au nanoclusters. Both phosphine-to-thiol and thiol-to-thiol ligand exchange were investigated in solution, which were accompanied by a change in the cluster core size.

In order to get further understanding of the interaction between Au nanoclusters and metal oxide support materials, ligand exchange reactions of dissolved (free) clusters and of clusters immobilized on oxides were compared. In order to be able to better follow the reaction, the exchange process between two very different kinds of ligands, phosphines and thiols, was examined. $Au_{11}(PPh_3)_7Cl_3$ was chosen as the starting material, due to the ease in synthesizing it in good yield and being a well studied cluster. The different systems are illustrated in Figure 2.1.
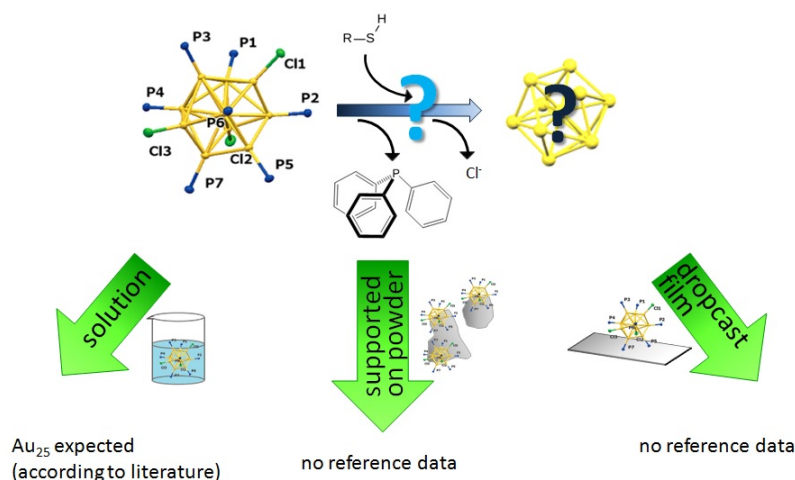
Figure 2.1.: Ligand exchange of $Au_{11}(PPh_3)_7Cl_3$ with thiols and the 3 different systems under investigation. Model of the structure of $Au_{11}(PPh_3)_7Cl_3$ adapted from [31], image of the Au_{11} core adapted from [7].

In addition, the possibility of post-functionalization of already immobilized clusters through ligand exchange was evaluated. This would allow to obtain catalytic surfaces with well-defined properties. One example is the introduction of chirality into the system by using chiral thiol ligands for the exchange reactions. With that, enantioselective catalysis with supported Au nanoclusters may become feasible.

3. Synthesis of Triphenylphosphine Protected Au$_{11}$ Nanoclusters

The starting material for the ligand exchange reactions, Au$_{11}$(PPh$_3$)$_7$Cl$_3$, was synthesized from HAuCl$_4 \cdot$ 3 H$_2$O, in contrast to the commonly used AuCl(PPh$_3$) [15]. 40 % yield of an 80:20 mixture of Au$_{11}$(PPh$_3$)$_7$Cl$_3$ and [Au$_{11}$(PPh$_3$)$_8$Cl$_2$]Cl could be achieved. Stability studies with Au$_{11}$(PPh$_3$)$_7$Cl$_3$ in THF showed formation of an unknown compound **A** after a few hours at RT.

3.1. Comparison to the Synthesis Published of Au$_{11}$(PPh$_3$)$_7$Cl$_3$

Au$_{11}$(PPh$_3$)$_7$Cl$_3$ is commonly synthesized by reduction of AuCl(PPh$_3$) with NaBH$_4$ in THF [31]. Further discussion can be found in the Chapters 1.2 and 1.3.2.
The starting material AuCl(PPh$_3$) is commercially available, or can be synthesized from HAuCl$_4 \cdot$ 3 H$_2$O in EtOH. The formation of the product is known to happen rapidly and yield white crystals precipitating from the reaction mixture [82, 83]. The yield varies from 67-80 % [82] up to 92 % [83], depending on the exact procedure. AuCl(PPh$_3$) is soluble in acetone, benzene [82], DCM, CHCl$_3$ and THF, but insoluble in hexane [83].

The presented synthesis, described in detail in Chapter 7.2, shows that Au$_{11}$(PPh$_3$)$_7$Cl$_3$ can be directly obtained from HAuCl$_4 \cdot$ 3 H$_2$O without isolation and cleaning of AuCl(PPh$_3$). In the first step, HAuCl$_4 \cdot$ 3 H$_2$O is reduced with triphenylphosphine (PPh$_3$ or TPP) in the presence of the phase-transfer catalyst tetraoctylammonium bromide (TOAB) to Au(I) species. This reaction step is very fast, as the color of the solution changes from bright orange to colorless immediately after addition of an excess of PPh$_3$. In the next step, an excess of NaBH$_4$ is added, which reduces Au(I) to Au(0). This is visible by a sudden color change to dark brown. The reaction mixtures is then stirred at high speed at RT for two days. This duration of the aging time is crucial, as will be discussed in later in this chapter.

3.2. Influence of Reaction Parameters

The design of the synthesis was strongly based on a published large-scale synthesis of Au$_{25}$(SR)$_{18}$. In that case, HAuCl$_4 \cdot$ 3 H$_2$O and TOAB are dissolved in THF and then the

chosen thiol is added in excess (5 eq. to $HAuCl_4 \cdot 3\,H_2O$) under low stirring. After the orange color has faded out completely, 10 eq. of $NaBH_4$ in ice-cold H_2O are added, which results in formation of dark brownish-black cluster species that are subsequently aged under high stirring for 4 days. This yields the stable Au_{25} cluster as the main product [53].

The presented synthesis of Au_{11} clusters follows the same protocol, with the only differences being the ligand added (PPh_3 instead of RSH) and the aging time after reduction (48 h instead of 96 h). However, as will be described in the next paragraphs, no phosphine protected Au_{25} nanoclusters could be obtained. Instead, the main product was found to be $Au_{11}(PPh_3)_7Cl_3$. This shows the big influence of the nature of the protecting ligand, as two different cluster species are obtained under otherwise identical conditions. It can be explained by different electronic and geometric configurations, leading to different structures of S- and P-protected Au nanoclusters (see Chapter 1.4.2).

In order to evaluate the influence of certain reaction parameters, the synthesis was carried out with different reaction times (14, 22, 30 and 48 h) and with different amounts of $NaBH_4$ (5 and 10 eq.). Table 3.1 summarizes the conditions, as well as the obtained products and their yield.

Table 3.1.: Reaction conditions and products of the synthesis of $Au_{11}(PPh_3)_7Cl_3$

Aging [h]	$NaBH_4$ [eq.]	Product Clusters	Yield [%]
14	5	$Au_{11}(PPh_3)_7Cl_3$ and $[Au_{11}(PPh_3)_8Cl_2]Cl$	10
14	10	$Au_{11}(PPh_3)_7Cl_3$ and $[Au_{11}(PPh_3)_8Cl_2]Cl$	25
22	10	mostly $Au_{11}(PPh_3)_7Cl_3$	23
30	10	mostly $Au_{11}(PPh_3)_7Cl_3$	35
48	10	mostly $Au_{11}(PPh_3)_7Cl_3$	40

A mixture of $Au_{11}(PPh_3)_7Cl_3$ and $[Au_{11}(PPh_3)_8Cl_2]Cl$ is formed in all the reactions. With increasing reaction time, the amount of $[Au_{11}(PPh_3)_8Cl_2]Cl$ decreases and mainly $Au_{11}(PPh_3)_7Cl_3$ is obtained. This is also demonstrated by the difference in the UV-Vis, NMR and MALDI-MS spectra (Figures 3.1, 3.2 and 3.3, respectively) recorded after 14 and 30 h of aging time.
This indicates that $[Au_{11}(PPh_3)_8Cl_2]Cl$ is the kinetic product, which transforms into $Au_{11}(PPh_3)_7Cl_3$ over time. Between 14 and 22 h of aging, the overall yield of Au_{11} clusters does not increase, but the amount of $Au_{11}(PPh_3)_7Cl_3$ in the product mixture rises significantly, confirming this assumption. Integration of the measured ^{1}H-NMR peaks showed that the relation $Au_{11}(PPh_3)_7Cl_3$ to $[Au_{11}(PPh_3)_8Cl_2]Cl$ changes from 55:45 (14 h) to 80:20 (30 h).

For the reaction with only 5 eq. of reducing agent NaBH$_4$, a very low yield of only 10 % was obtained. Thus, all further reactions were conducted with 10 eq.

Figure 3.1 shows the UV-Vis spectra, the Figures 3.2a and 3.2b the ^{1}H and ^{31}P-NMR spectra of the obtained product after 14 and 30 h, respectively. They are in good agreement with the spectra reported for single crystals of Au$_{11}$(PPh$_3$)$_7$Cl$_3$ and [Au$_{11}$(PPh$_3$)$_8$Cl$_2$]Cl [31]. As can be seen in the NMR spectra, in the case of only 14 h aging, another phosphine containing side product is formed, which could not be identified yet. This contaminant is not visible anymore when the reaction mixture is stirred for 30 h or longer.
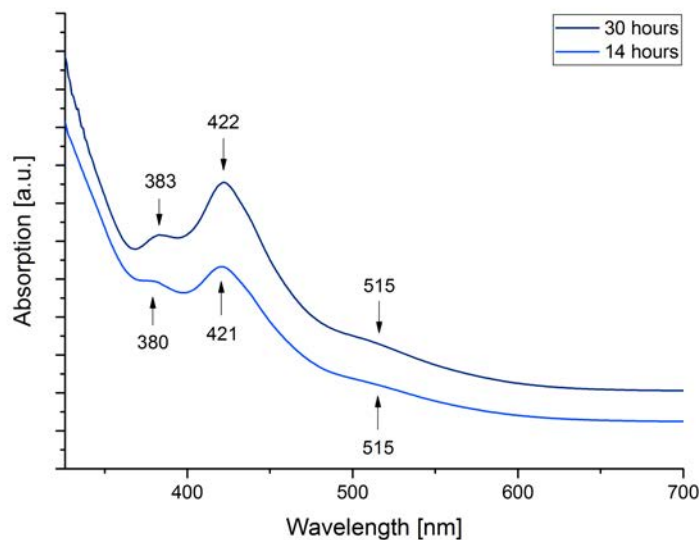

Figure 3.1.: UV-Vis spectrum of the reaction product after 14 and 30 h of aging. Spectra are stacked for clarity. The spectrum recorded after 14 h resembles that of an ≈ 1:1 mixture of Au$_{11}$(PPh$_3$)$_7$Cl$_3$ and [Au$_{11}$(PPh$_3$)$_8$Cl$_2$]Cl, whereas the one after 30 h is close to a spectrum of pure Au$_{11}$(PPh$_3$)$_7$Cl$_3$. Reference values from [31].

(a) ^{1}H-NMR
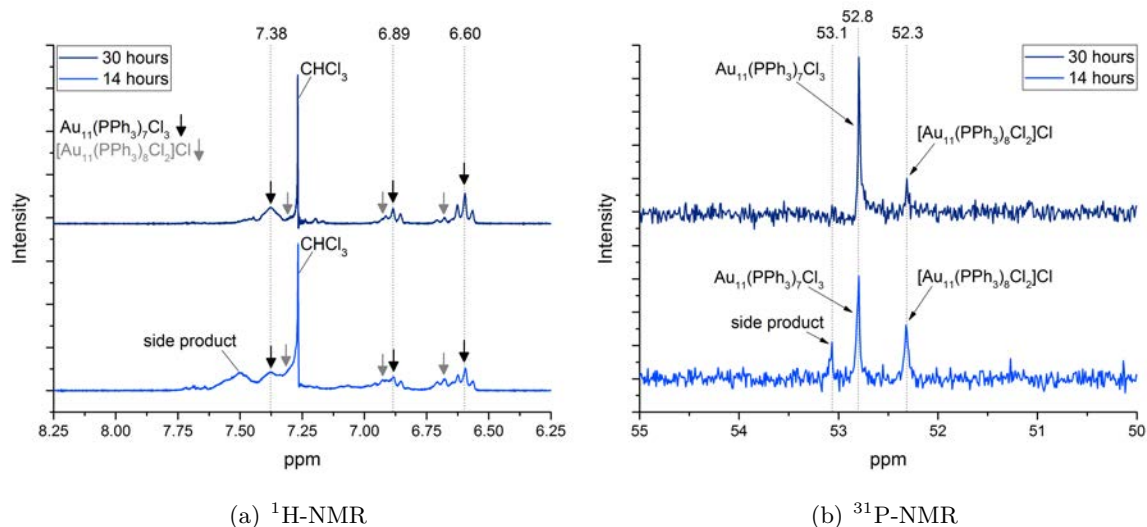
(b) ^{31}P-NMR

Figure 3.2.: (a) ^{1}H and (b) ^{31}P-NMR spectra after 14 and 30 h of aging. Spectra are stacked for clarity. For (b), only the ppm values of $Au_{11}(PPh_3)_7Cl_3$ are marked. The bold arrows mark the maxima of the peaks of $Au_{11}(PPh_3)_7Cl_3$ (black) and $[Au_{11}(PPh_3)_8Cl_2]Cl$ (grey). Reference values from [31].

The MALDI-MS spectra after 14 and 30 h of aging are displayed in Figure 3.3. Although different matrices were tried, fragmentation was observed in every spectrum. This is clearly not due to the presence of contaminants, as is proven by the UV-Vis and NMR spectra of the same samples. Sequential losses of PPh_3 ligands (m = 262 D) are visible, as is indicated in Figure 3.3. Moreover, peaks of $Au_{11}(PPh_3)_7Cl_2 \cdot CH_2Cl_2$ can be seen in both spectra, which are marked with green dashed lines in Figure 3.3. This is reasonable, as $Au_{11}(PPh_3)_7Cl_3$ is known to incorporate a solvent molecule in its crystal structure [84].

The contamination detected in the NMR spectra of the sample after 14 h aging is also observed in the MALDI-MS spectrum. Furthermore, the MS spectrum after 14 h contains significant amounts of bromide as a ligand instead of chloride, which results from the addition of the phase transfer catalyst tetraoctylammonium bromide. After 30 h, only small amounts are found, which is reasonable as there are four times more chloride than bromide ions present in the reaction mixture. In Figure 3.3, the most intense fragments are assigned. A more detailed list for $Au_{11}(PPh_3)_7Cl_3$ can be found in Chapter 7.2.
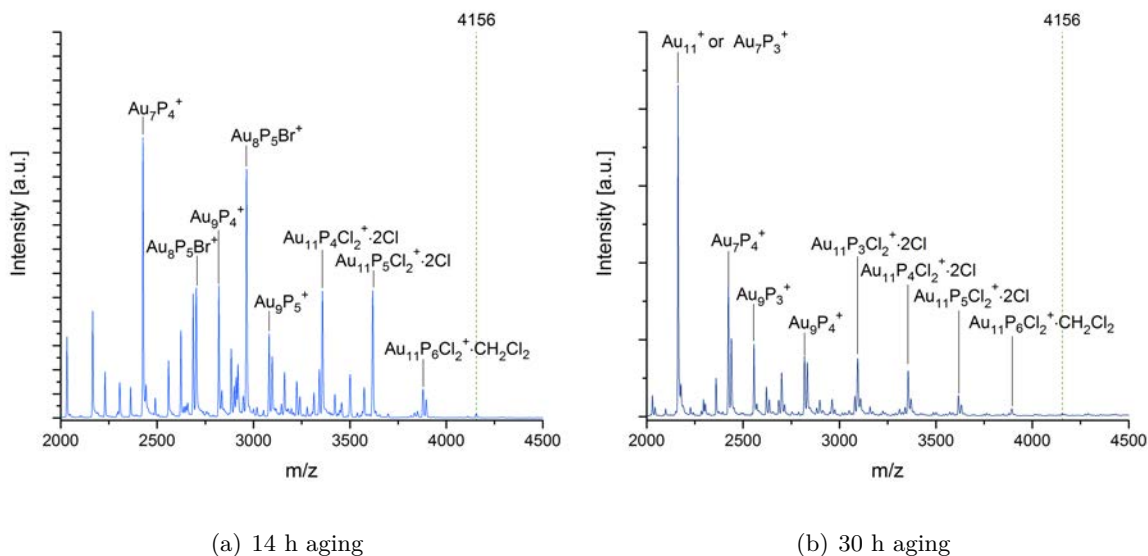
Figure 3.3.: MALDI-MS spectra of the product after (a) 14 h and (b) 30 h of aging. P is equal to PPh_3. The green dashed line marks the mass of $[Au_{11}(PPh_3)_7Cl_2 \cdot CH_2Cl_2]^+$.

In conclusion, an aging time of 48 h and reduction with 10 eq. of $NaBH_4$ were found to be the best of the tested parameters.

Longer stirring at RT was not tried due to instability of $Au_{11}(PPh_3)_7Cl_3$ in solvents like DCM [31, 36] or THF (see Chapter 3.5).

It should be noted that the two Au_{11} cluster species can be separated by size exclusion chromatography due their mass difference of 262 D. Moreover, it could be observed that $Au_{11}(PPh_3)_7Cl_3$ dissolves more readily in cold DCM, making separation by extraction possible.

For obtaining the samples for the ligand exchange reactions, the latter was used. The content of $Au_{11}(PPh_3)_7Cl_3$ was determined to be at least 95 % by integration of the ^{1}H-NMR peaks. As it was confirmed by Hutchison and coworkers that pure $Au_{11}(PPh_3)_7Cl_3$ as well as a 1:1 mixture of $Au_{11}(PPh_3)_7Cl_3$ and $[Au_{11}(PPh_3)_8Cl_2]Cl$ react to the same product upon ligand exchange with monodentate thiols [31], the minor quantities of the latter in the ligand exchange reaction samples were considered negligible.

In the next chapters about the ligand exchange procedures starting from Au_{11}, for simplification, only the term '$Au_{11}(PPh_3)_7Cl_3$' will be used for identification of the starting material. However, one should bear in mind that low amounts of $[Au_{11}(PPh_3)_8Cl_2]Cl$ ($< 5\%$) were also present.

3.3. Literature Procedures for Phosphine Protected Au Nanoclusters Starting from HAuCl$_4$ · 3 H$_2$O

Only a few procedures for synthesis of phosphine-protected Au nanoclusters starting from HAuCl$_4$ · 3 H$_2$O have been published so far, and none for Au$_{11}$. Shichibu *et al.* reported that [Au$_{13}$(POct$_3$)$_8$Cl$_4$]Cl (Oct = octyl) can be obtained when stirring HAuCl$_4$ · 3 H$_2$O and triphenylphosphine in a 1:1 mixture of H$_2$O and THF for only five minutes, followed by reduction with NaBH$_4$ over 3 h [85].

Teo *et al.* synthesized [Au$_{39}$(PPh$_3$)$_{14}$Cl$_6$]Cl$_2$ by mixing HAuCl$_4$ · 3 H$_2$O and PPh$_3$ in EtOH with subsequent 24 h reduction by NaBH$_4$ [86].

During the synthesis of [Au$_{24}$(PPh$_3$)$_{10}$(SC$_2$H$_4$Ph)$_5$Cl$_2$]$^+$, Das *et al.* isolated a reddish-brown intermediate. It was obtained after the transfer of HAuCl$_4$ · 3 H$_2$O to the toluene phase with the help of TOAB, followed by addition of PPh$_3$ under high stirring and reduction with NaBH$_4$ with a subsequent aging period of up to 16 h [76]. However, no characterization of the intermediate was published.

In Chapter 4.1 of this thesis, ligand exchange with Au$_{11}$(PPh$_3$)$_7$Cl$_3$ with an excess of 2-phenylethanethiol (2-PET) in solution is discussed, with yields [Au$_{25}$(PPh$_3$)$_{10}$(SC$_2$H$_4$Ph)$_5$Cl$_2$]$^{2+}$. Das *et al.* obtained the same mixed ligand shell Au$_{25}$ cluster as the initial product of the reaction with their reddish-brown crude and an excess of 2-PET. Only after addition of more PPh$_3$, an Au$_{24}$ cluster was isolated [76].

Therefore, it is speculated that this intermediate product after the reduction step could have contained significant amounts of Au$_{11}$(PPh$_3$)$_7$Cl$_3$ (and possibly also [Au$_{11}$(PPh$_3$)$_8$Cl$_2$]Cl). The conditions of the synthesis were similar to the one reported in this thesis, only the solvent (toluene instead of THF) and the stirring speed upon addition of PPh$_3$ was different. Moreover, the color of the crude product is reddish-brown in both cases and ligand exchange with an excess of 2-PET yields the same product. However, for the synthetic procedure discussed in this thesis, the reaction time had huge impact on nature and yield of the obtained products, as was shown earlier in this chapter. This was not the case for Das *et al.*, but could be due to the use of toluene instead of THF [76].

Hence, it seems that different phosphine protected cluster species are accessible by a direct one-pot synthesis from HAuCl$_4$ · 3 H$_2$O. This reduces the synthetic effort significantly, providing a good alternative to the common use of AuCl(PPh$_3$). Furthermore, due to different conditions, new phosphine protected cluster species might be accessible.

3.4. Formation of Compound A

In addition to the two different Au_{11} clusters, another product **A** was obtained by the discussed synthesis. It was extracted from the product mixture with cold THF and gave a brown powder after drying (see Chapter 7.2.1 for details). The product was found to be insoluble in water and hexane, and limited soluble in DCM and MeOH. Good solubility can be achieved in THF, toluene and EtOH. It was further noticed that **A** decomposes in alcoholic solutions under air over some days.

The stability experiments with $Au_{11}(PPh_3)_7Cl_3$ in THF (see Chapter 7.2.2) showed that **A** is also formed as the primary degradation product of Au_{11} clusters in this solvent. It was obtained when the cluster solution was left at RT even for only a few hours.

However, a clear trend is not observed when the yield of **A** is compared with the conditions of the synthesis: At an aging time of 14 h, already 80 mg are obtained if only 5 eq. of $NaBH_4$ are used. The yield then almost doubles for 10 eq. of reducing agent. At 22 h, it drops again to 80 mg, before it rises slightly for longer reaction times. This trend is illustrated in Figure 3.4. Clearly, some part of **A** must have decomposed or been converted to another species, as the yield decreased between 14 and 22 h.

It further seems that **A** is formed independently of the Au_{11} clusters, as the trend cannot be related. Moreover, its maximum amount is detected when a higher amount of $[Au_{11}(PPh_3)_8Cl_2]Cl$ is present in the product mixture, which reportedly is the more stable of the Au_{11} analogues and not prone to decomposition [31].
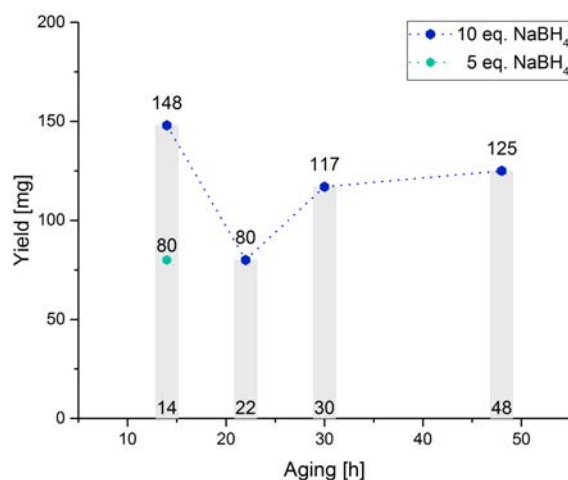
Figure 3.4.: Formation of compound **A** at different aging times

Compound **A** exhibits a well-defined UV-Vis spectrum with two maxima at 321 and 411 nm,

which is shown in Figure 3.5. As this suggested the presence of another phosphine-protected cluster species, further characterization was carried out. The ^{31}P-NMR spectrum in Figure 3.6 shows a peak at 29.1 ppm. This value is significantly smaller than the one of the Au$_{11}$ clusters and closer to that of AuCl(PPh$_3$) (33.7 ppm) [83] and O=P(PPh$_3$) (29.8 ppm) [87]. Hence, the electronic environment seems to differ from that of Au$_{11}$.

Figure 3.5.: UV-Vis spectrum of compound **A**

Figure 3.6.: ^{31}P-NMR spectrum of compound **A**. The inlet shows the entire spectrum; only the one singlet is observed.

MALDI-MS was measured to get an idea of the cluster size; the spectrum is shown in Figure 3.7. As for the Au_{11} clusters, loss of PPh_3 (262 D) is visible, but also loss of PPh_3O (278 D). This is interesting, as only one peak was found in ^{31}P-NMR. Due to the strong fragmentation, a clear mass peak could not be assigned. However, from the identified fragments, a core size of 11-12 gold atoms is suggested. The most important MALDI-MS fragments of **A** are assigned in Figure 3.7, a more detailed list is found in Chapter 7.2.1.
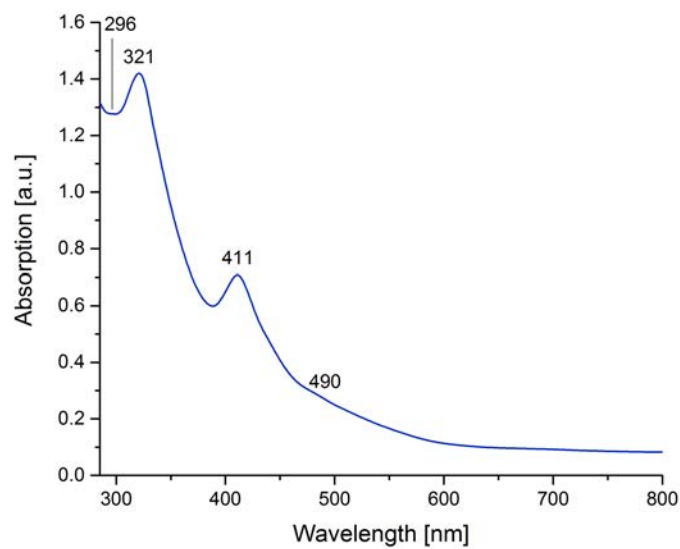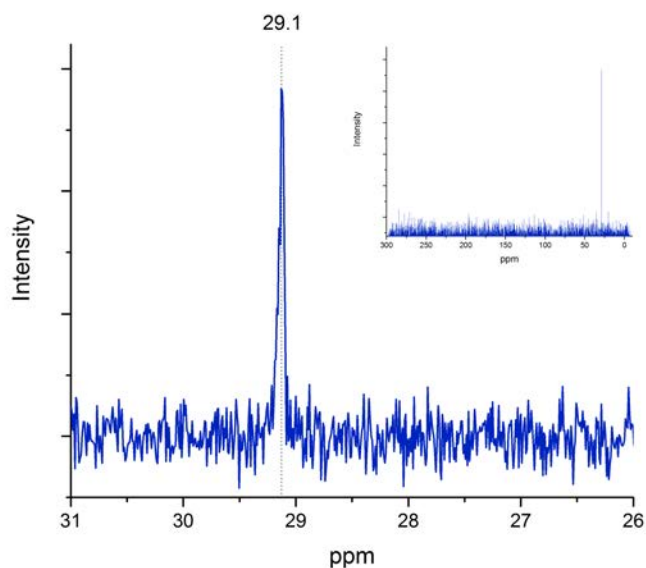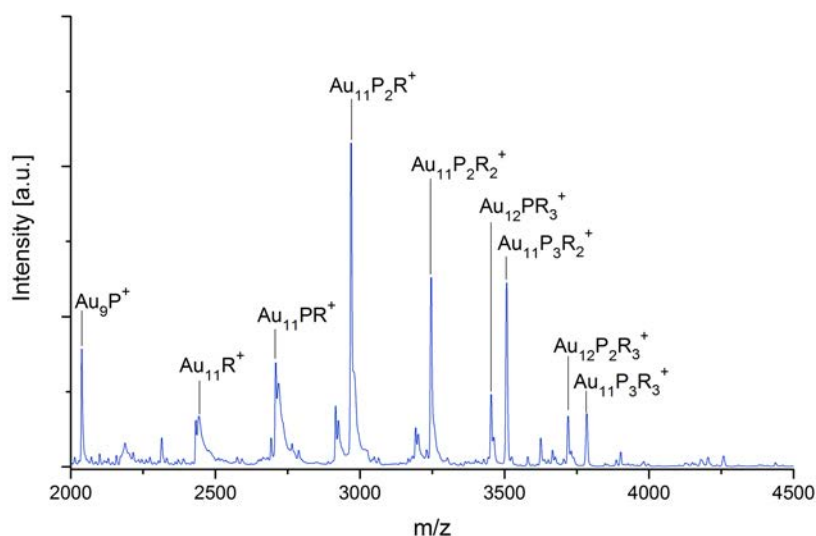

Figure 3.7.: MALDI-MS spectrum of compound **A**. P is equal to PPh_3, R to PPh_3O.

However, compound **A** could not be completely identified by the analysis methods used. Attempts to crystallize the compound have not been successful neither. Therefore, a complete assignment of the structure is currently not possible. Taken everything into account, it is likely that **A** represents another cluster species with 11-12 Au atoms according to MALDI-MS. This is in agreement with the UV-Vis spectral features, which are very similar to those of $Au_{11}(PPh_3)_7Cl_3$. Moreover, the mass spectral analysis suggests coordination of both PPh_3 and $PPh_3{=}O$. This is contrary to the results from ^{31}P-NMR, where only one peak was observed. Further studies will be necessary to fully reveal the structure of **A**.

3.5. Stability Study of $Au_{11}(PPh_3)_7Cl_3$

To test the stability of $Au_{11}(PPh_3)_7Cl_3$ in THF, a concentrated solution was exposed to air at RT for 6 d. This resulted in a very slow intensification of the dark yellow color of the solution. The defined spectrum of $Au_{11}(PPh_3)_7Cl_3$ changed even after only 1.5 h. After 3 h, it seemed to have been nearly completely converted into compound **A**. The spectrum did

not change significantly between 3 h and 4 d, indicating high stability of **A**. Only after 5 d, broadening of the peaks could be observed, which increased after 6 d. However, even then, the positions of the peak maxima were not affected.

The spectra are displayed in Figure 3.8, the values for the peak maxima are summarized in Chapter 7.2.2.

(a) first 24 hours   (b) 1-6 days
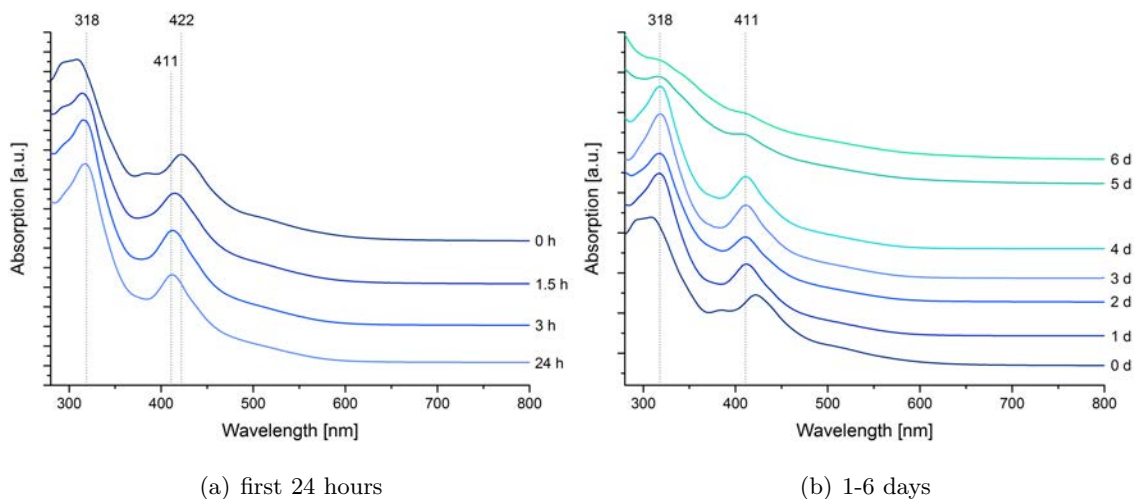
Figure 3.8.: UV-Vis spectra of the sample in THF over a duration of 6 d. Spectra are stacked for clarity.

Interestingly, a completely different behavior compared to the one described by McKenzie *et al.* for halogenated solvents [31] was observed. Instead of $AuCl(PPh_3)$, **A** was formed. This transformation also happened very quickly, as nearly complete conversion was observed in the UV-Vis spectrum after only 3 h.

It is therefore quite surprising that $Au_{11}(PPh_3)_7Cl_3$ could be synthesized in 40 % yield in the first place (see Chapter 7.2), concerning its low stability in THF. It is assumed that the presence of an excess of PPh_3 and/or the reducing conditions of the synthesis somewhat inhibited the formation of **A**. Further experiments will be required for confirmation.

3.6. Conclusions of Synthesis of Au$_{11}$(PPh$_3$)$_7$Cl$_3$

$Au_{11}(PPh_3)_7Cl_3$ was synthesized from $HAuCl_4 \cdot 3\,H_2O$ in THF in a one-step procedure, without isolation and cleaning of $AuCl(PPh_3)$. Optimization of the reaction conditions led to a yield of 48 % for 48 h of aging time. Extensive analysis of the reaction product by different techniques (UV-Vis, MALDI-MS, NMR, ATR-IR) showed that the obtained clusters were highly pure, containing an 80:20 mixture of $Au_{11}(PPh_3)_7Cl_3$ and $[Au_{11}(PPh_3)_8Cl_2]Cl$. Due

to their different chemical environment, separation by size exclusion chromatography or extraction can be achieved easily.

As the relative amount of the two Au_{11} cluster species shifted from 55:45 for 14 h of aging to 80:20 for 48 h of aging, $[Au_{11}(PPh_3)_8Cl_2]Cl$ seems to be the kinetic product, which is partially transformed into $Au_{11}(PPh_3)_7Cl_3$ upon longer reaction time.

Interestingly, a nearly similar protocol using the thiol ligand 2-PET instead of PPh_3 in the synthetic procedure [53] led to formation of Au_{25}. This further proves the dependence of the cluster properties on the nature of the protecting ligands.

Stability studies of $Au_{11}(PPh_3)_7Cl_3$ in THF showed that the cluster is transformed into an unidentified compound **A** even after only a few hours. The same compound was also isolated as a by product in the synthesis of $Au_{11}(PPh_3)_7Cl_3$. Further investigations will be carried out to determine its crystal structure.

4. Ligand Exchange Reactions of Au$_{11}$(PPh$_3$)$_7$Cl$_3$ with Thiol Ligands

The ligand exchange behavior of Au$_{11}$(PPh$_3$)$_7$Cl$_3$ was studied in three different systems: free clusters in solution, clusters immobilized on a high surface area (powder) metal oxide support, clusters as a dropcast film on planar support. For all three cases, for the ligand exchange, the cluster sample was exposed to a solution containing an excess of thiol. Figure 4.1 gives an overview of the reaction and the systems studied.
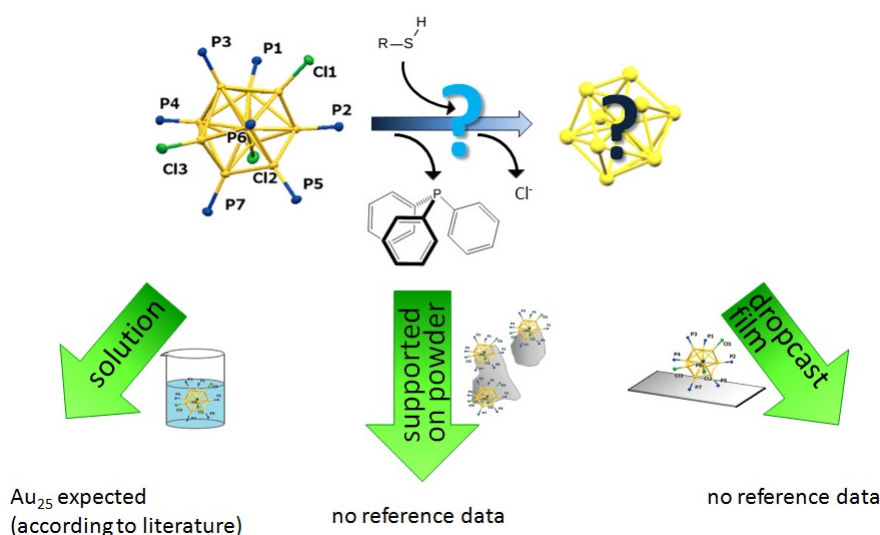
Figure 4.1.: Ligand exchange of Au$_{11}$(PPh$_3$)$_7$Cl$_3$ with thiols and the 3 different systems under investigation. Model of the structure of Au$_{11}$(PPh$_3$)$_7$Cl$_3$ adapted from [31], image of the Au$_{11}$ core adapted from [7].

Two different sulfur ligands, 2-phenylethanethiol (2-PET) and L-glutathione (GSH), were investigated, with the first one being soluble in organic solvents and the second one being soluble in water. They were chosen because of the existing literature on the ligand exchange of Au$_{11}$ with both of them [31, 36, 75–79], allowing better evaluation of the reactions conducted in this thesis.

For the first time, ligand exchange with immobilized Au$_{11}$ dropcast films upon exposure to a solution of exchange thiol can be reported. Moreover, significant differences of the products as compared to that of the reactions of free clusters in solution could be observed.

4.1. Ligand Exchange Reactions of $Au_{11}(PPh_3)_7Cl_3$ in Solution

The ligand exchange reactions in solution were conducted in both mono- and biphasic systems. Therefore, a solution of $Au_{11}(PPh_3)_7Cl_3$ was brought in contact with a solution of the exchange thiol (2-PET or GSH) and stirred for about a day. Different conditions were tested and the reaction was followed by *ex-situ* UV-Vis and MALDI-MS measurements.
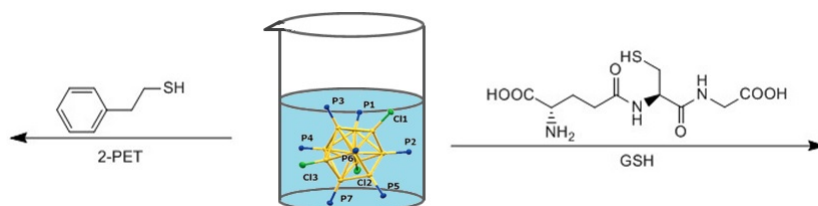
Figure 4.2.: Reactions of $Au_{11}(PPh_3)_7Cl_3$ in solution with thiol ligands (2-PET and GSH). Cluster structure adapted from [31].

4.1.1. Ligand Exchange with 2-Phenylethanethiol

Published ligand exchange procedures were considered for performing this reaction [36, 75, 76, 78, 79]. The reactions were carried out in chlorinated solvents with an excess of the exchange ligand 2-phenylethanethiol. Different conditions were tried, which are summarized in Table 4.1 and in Chapter 7.3.1. As is shown in Figure 4.3, a mixed ligand shell cluster $[Au_{25}(PPh_3)_{10}(SC_2H_4Ph)_5Cl_2]^{2+}$ was obtained as the product of the reaction, which is in good agreement with literature [36, 76, 78].

Figure 4.3.: Ligand Exchange from $Au_{11}(PPh_3)_7Cl_3$ to $[Au_{25}(PPh_3)_{10}(SC_2H_4Ph)_5Cl_2]^{2+}$

Table 4.1.: Conditions of the ligand exchange reactions of $Au_{11}(PPh_3)_7Cl_3$ and 2-PET in solution

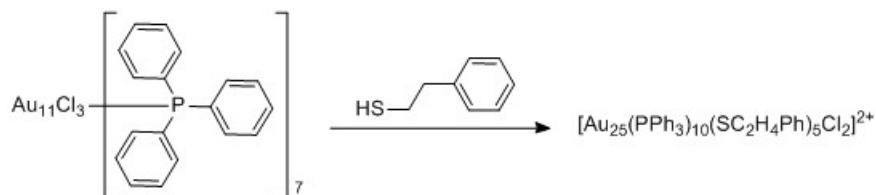| No.	eq. 2-PET	Solvent	Temp.	Product Formation
1	5	DCM	RT	90 min
2	10	DCM	RT	30 min
3	100	DCM	40 °C	<15 min
4.1	75	CHCl$_3$	50 °C	<15 min
4.2	75	CHCl$_3$	50 °C	[1]

[1] Reaction **4.2** started with the end product of reaction **4.1** (see also description in the text). No new product (e.g. completely exchanged Au_{25}(2-PET)$_{18}$) could be observed, but the product of reaction **4.1** was quite stable under the conditions of a second reaction; only minor decomposition occurred.

Ligand Exchange Reactions 1 and 2

In Figure 4.4, UV-Vis spectra of the first two conducted exchange reactions (no. **1** and **2** in Table 4.1) are displayed. It can be seen that the spectra change very fast. Even after 30 min, changes in shape and position of the peaks at 380 and 420 nm are visible. Although not visible in the UV-Vis spectrum, the clusters seem to grow quite fast, as indicated by the MALDI-MS spectra in Figure 4.5. The absence of peaks in the region between m/z = 2000-4000 can be attributed to the choice of THF as a solvent for the measurements. As described in Chapter 7.2, $Au_{11}(PPh_3)_7Cl_3$ is nearly insoluble in THF. This explains why it is not observed in the MS spectra, although the UV-Vis spectra indicate it is still the main component in the reaction mixture.

After 24 h, the color of the solution had changed from orange to greenish and the end product is determined to be $[Au_{25}(PPh_3)_{10}(SC_2H_4Ph)_5Cl_2]^{2+}$, which is obtained in high purity. This is proven by the good match of the UV-Vis and MALDI spectra of the 24 h samples and those of purified $[Au_{25}(PPh_3)_{10}(SC_2H_4Ph)_5Cl_2]^{2+}$ (see Figures 4.10 and 4.11).

When comparing the two reactions directly, it can be seen that higher amount of exchange ligand speeds up the exchange reaction, when all other parameters are kept constant. This is indicated in the MALDI-MS spectra. For reaction **1**, the cluster has already grown after 30 min, but not up to its final core size. At 90 min, it has already reached that size, but the fragmentation pattern stretches over a range of m/z = 4500-7500, indicating that the sample is not completely monodisperse. Then, a size focusing process seems to occur, yielding $[Au_{25}(PPh_3)_{10}(SC_2H_4Ph)_5Cl_2]^{2+}$ in high purity, as is suggested by the MALDI-MS spectrum for the 24 h sample. The presence of more than one peak can be attributed to fragmentation (see also the mass spectrum of purified $[Au_{25}(PPh_3)_{10}(SC_2H_4Ph)_5Cl_2]^{2+}$ in Figure 4.11).

For reaction **2**, a similar trend can be observed, but the reaction seems to be faster. The final core size is already reached after 30 min and the beginning of the size focusing can be

seen in the 90 min spectrum.

(a) 5 eq. of 2-PET (no. **1**) (b) 10 eq. of 2-PET (no. **2**)

Figure 4.4.: UV-Vis spectra of ligand exchange reaction **1** and **2**. Spectra are stacked for clarity.

(a) 5 eq. of 2-PET (no. **1**) (b) 10 eq. of 2-PET (no. **2**)

Figure 4.5.: MALDI-MS spectra of ligand exchange reaction **1** and **2**. Spectra are stacked for clarity. Matrix: DCTB, solvent: THF

Ligand Exchange Reactions 3 and 4

To test for complete ligand exchange, yielding solely thiolate-protected Au_{25} clusters, the reaction was repeated under harsher conditions (elevated temperature, higher excess of exchange ligand). However, the UV-Vis spectra of the reactions **3** and **4**, which are displayed in Figure 4.6 and 4.8, respectively, showed that this could not be achieved.

The reaction was significantly faster though, showing a rise of the typical Au_{25} plasmon band

26

[31] at around 680 nm even after only 15 min, accompanied by a very swift color change of the solution to green.

Ligand Exchange Reaction 3. The MALDI-MS spectrum of reaction **3** clearly shows the presence of a quite polydisperse product mixture after 15 min, with some clusters having already reached the final core size. After 180 min, most of the Au_{11} seems to have been converted to Au_{25}. After 24 h, the m/z area in the spectrum has narrowed significantly, indicating the presence of $[Au_{25}(PPh_3)_{10}(SC_2H_4Ph)_5Cl_2]^{2+}$ in high purity.

Also, smaller cluster species seem to be present at 180 min and 20 h, which have completely disappeared after 24 h. These species are also present in the 20 h spectrum of reaction **4.1** and the 3 h spectrum of reaction **4.2** (see Figure 4.9). They seem to arise from Au_{11} and Au_{13} cores with Cl and PPh_3 ligands, as splitting with m/z = 262 D is observed. This is reasonable, considering that $[Au_{25}(PPh_3)_{10}(SC_2H_4Ph)_5Cl_2]^{2+}$ is composed of two Au_{13} cores, sharing one edge Au atom [78].

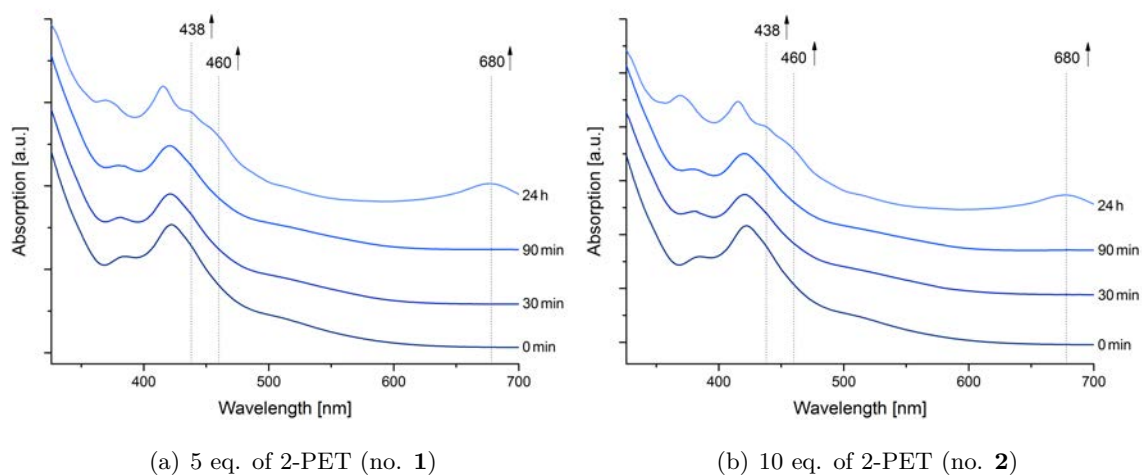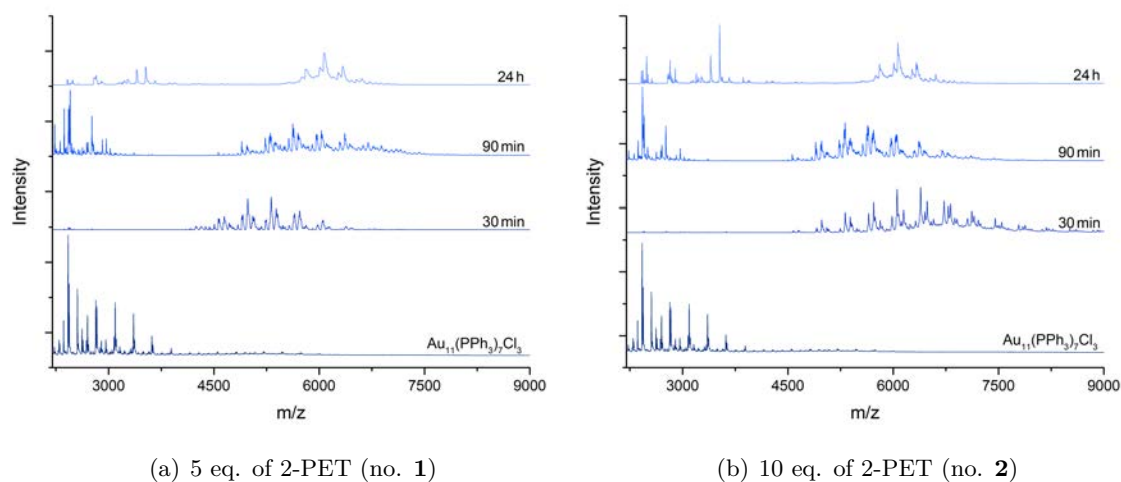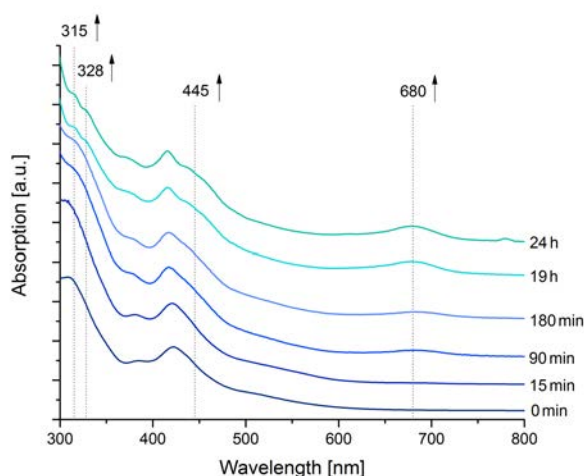**Figure 4.6.:** UV-Vis spectra of ligand exchange reaction **3**. Spectra are stacked for clarity.
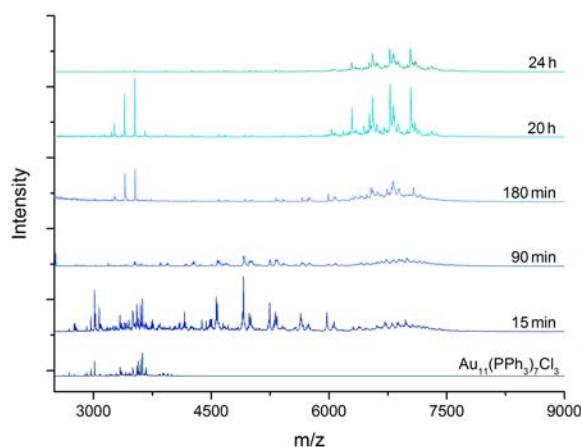
Figure 4.7.: MALDI-MS spectra of ligand exchange reaction **3**. Spectra are stacked for clarity. Matrix: DCTB, solvent: DCM

Ligand Exchange Reaction 4.1. When the temperature was increased from 40 to 50 °C for reaction **4.1**, the rate of the reaction increased further, showing product formation even earlier, as indicated by the UV-Vis spectra in Figure 4.8a. Interestingly, for **4.1**, the MALDI-MS spectrum in Figure 4.9a shows that the cluster size still seems to change between 20 and 24 h, indicating that 24 h of reaction time are really needed. The occurrence of a size focusing process is also clearly visible in the spectra.

Ligand Exchange Reaction 4.2. After 24 h, reaction **4.1** was stopped, the solvent evaporated and the greenish product cleaned with hexane to remove free TPP and 2-PET. Afterwards, it was redissolved in CHCl$_3$ and another 75 eq. of 2-PET were added (reaction no. **4.2**). As shown in Figure 4.8b, this led only to small changes in the UV-Vis spectra of the first three hours. After 24 h, broadening of the absorptions features is visible, but the primary absorption features remain. This might be related with beginning degradation of the clusters.

The MALDI-MS spectra (Figure 4.9) also show that the sample changed only slightly, with the pattern getting broader. This could very likely be due to thiol-to-thiol ligand exchange. The MS spectrum after 24 h looks again quite clean and resembles the one obtained for reaction **4.1** after 24 h. This is in contrast to the broadening of the UV-Vis, but can be explained by the fact that the samples were washed with hexane prior to the MALDI-MS measurements. Whatever side products had been formed, they seemed to be soluble in hexane and were therefore removed in this step.

It should be noted that contrary to Au$_{11}$(PPh$_3$)$_7$Cl$_3$, [Au$_{25}$(PPh$_3$)$_{10}$(SC$_2$H$_4$Ph)$_5$Cl$_2$]$^{2+}$ seems to be extraordinarily stable in halogenated solvents and in the presence of excess thiols, as

even after almost 48 h under this conditions at elevated temperatures, the main spectral features in the UV-Vis were maintained. The MALDI-MS spectrum confirmed the high purity of the sample.

(a) 1st LE (no. **4.1**)   (b) 2nd LE (no. **4.2**)
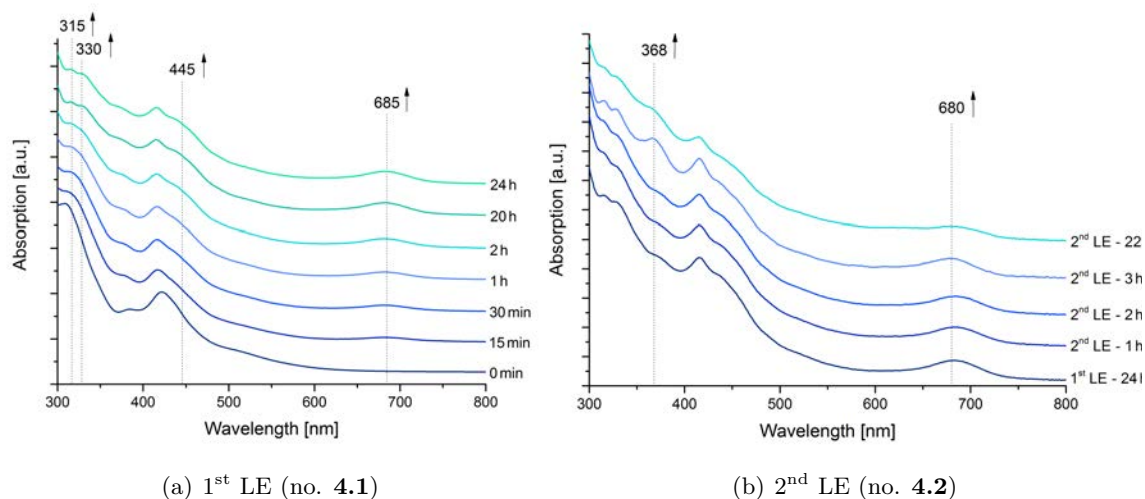
Figure 4.8.: UV-Vis spectra of ligand exchange reaction **4.1** and **4.2**. Spectra are stacked for clarity.

(a) 1st LE (no. **4.1**)   (b) 2nd LE (no. **4.2**)

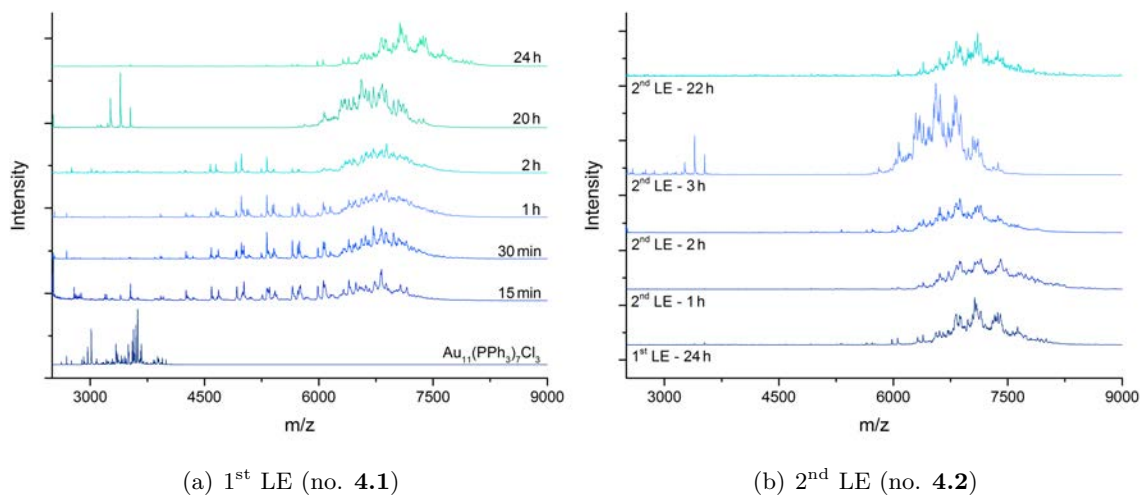**Figure 4.9.:** MALDI-MS spectra of ligand exchange reaction **4.1** and **4.2**. Spectra are stacked for clarity. Matrix: DCTB, solvent: $CHCl_3$

Characterization of $[Au_{25}(PPh_3)_{10}(SC_2H_4Ph)_5Cl_2]^{2+}$

The spectra of the purified end product $[Au_{25}(PPh_3)_{10}(SC_2H_4Ph)_5Cl_2]^{2+}$ are displayed in the Figures 4.10 and 4.11. The UV-Vis spectrum shows several well defined bands, which

are in perfect agreement with published spectra of this compound [36, 76, 81].

As was shown by Nobusada *et al.*, the HOMO–LUMO transition at around 680 nm is caused by participation of the whole cluster. However, the peaks at shorter wavelength seem to be due to contribution from one icosahedron only [88]. This corresponds very well to the 'cluster-of-clusters' model established by Teo *et al.* [89–91]. It was further investigated that cluster-solvent interactions have great influence on the absorption spectra, especially at low temperature [92].
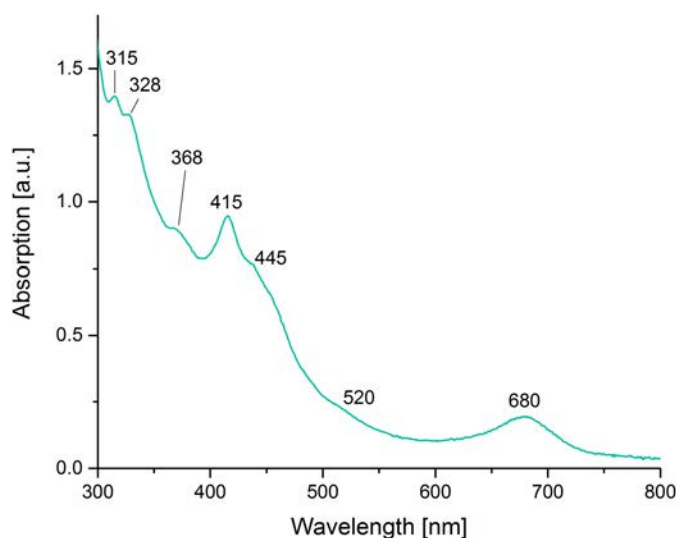
Figure 4.10.: UV-Vis spectrum of $[Au_{25}(PPh_3)_{10}(SC_2H_4Ph)_5Cl_2]^{2+}$ in MeOH

Fragmentation is observed in the MALDI-MS spectrum in Figure 4.11, which seems to be a problem for all phosphine protected Au nanoclusters described in this thesis. Maybe a different ionization technique (such as ESI) or using a matrix other than the popular DCTB for cluster measurements [93] might be beneficial. The most intense fragments were assigned in Figure 4.11, a more detailed list can be found in Chapter 7.3.1. All of them seem to have their origin in $[Au_{25}(PPh_3)_{10}(SC_2H_4Ph)_5Cl_2]X_2$, with X being a suitable counter ion, which could not be detected itself.
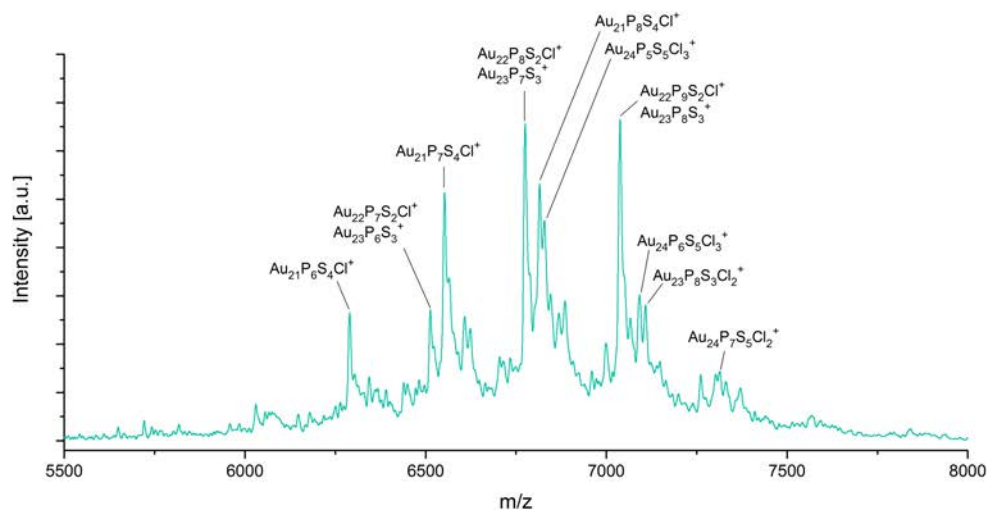
Figure 4.11.: MALDI-MS spectrum of $[\mathrm{Au}_{25}(\mathrm{PPh}_3)_{10}(\mathrm{SC}_2\mathrm{H}_4\mathrm{Ph})_5\mathrm{Cl}_2]^{2+}$. P is equal to PPh_3, S to $-\mathrm{SC}_2\mathrm{H}_4\mathrm{Ph}$.

As indicated by the experiments conducted as well as by literature [78, 80, 81], the mixed ligand shell cluster $[\mathrm{Au}_{25}(\mathrm{PPh}_3)_{10}(\mathrm{SC}_2\mathrm{H}_4\mathrm{Ph})_5\mathrm{Cl}_2]^{2+}$ appears to be quite stable. Latest experiments by Wang *et al.* also proved that selective one atom doping with Ag or Cu is possible, allowing controlled modification of the cluster properties [94]. Thus, the produced cluster is a promising candidate for further studies.

Stability in the Chosen Solvents (DCM and CHCl$_3$)

For ligand exchange with 1.5 nm TPP protected nanoparticles, decomposition was noticed when conducting the ligand exchange at elevated temperatures [79]. In the case of Au$_{11}$, different observations were made. Performing the exchange at 50 °C, Woehrle *et al.* reported decomposition in CHCl$_3$ and incomplete exchange in alcohol and similar solvents. The best results in their case were obtained with DMSO or a mixture of 1-chlorobutane and DCM [27]. However, Shichibu *et al.* used CHCl$_3$ as solvent for their ligand exchange and obtained the same product without notifying significant decomposition [78].

For the reactions **3** and **4**, formation of AuCl(PPh$_3$) in early stages of the reaction (in the 30 and 15 min sample) was noticed, indeed signaling slight degradation. This is shown in Figure 4.12 in the enlarged area of the UV-Vis spectra of reaction **3**, due to the presence of two small bands at 268 and 275 nm. These values are in perfect agreement with reported ones [79]. However, they did not seem to intensify much with progressing reaction. Only after 19 h of heating in solution, a slight increase is noticed. As no white solid could be seen in any of the samples, the quantity must have been very low.

Thus, chlorinated solvents seem to be a good choice for these specific ligand exchange reactions. It was even suggested that the relatively low stability of $Au_{11}(PPh_3)_7Cl_3$ in solution promotes the growth to Au_{25} upon addition of excess thiol, as the clusters agglomerate easily [31].
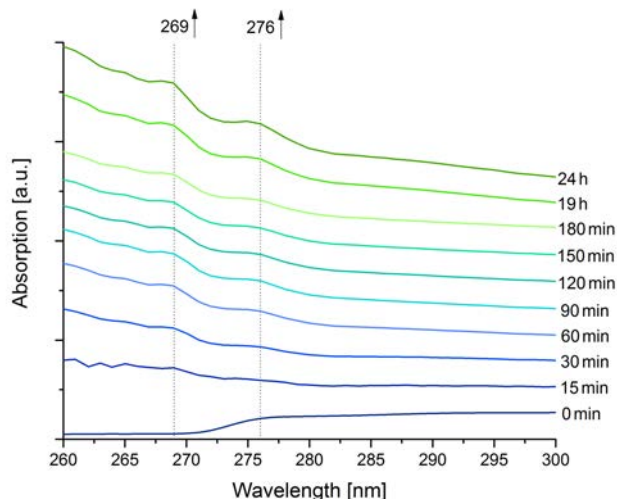

Figure 4.12.: Typical absorption maxima of $AuCl(PPh_3)$ during ligand exchange reaction **3**. Spectra are stacked for clarity.

Mechanistic Discussions

Concerning the reaction mechanism, Qian *et al.* suggested the presence of both PPh_3 and 2-PET in the DCM solution to be the reason for the formation of the mixed ligand shell Au_{25} clusters, due to a competition between the ligands [80]. However, this does not seem to be the case, as the formed $[Au_{25}(PPh_3)_{10}(SC_2H_4Ph)_5Cl_2]^{2+}$ does not react any further if the free PPh_3 ligands are completely removed and a fresh excess of thiol is added, as was done in reaction **4.2**. Moreover, the free PPh_3 is known to be rapidly oxidized to $PPh_3{=}O$, as was confirmed by trapping experiments [27, 31]. Thus, re-coordination of free TPP to the Au core in later steps of the reaction does not seem likely.

Later mechanistic studies suggested $[Au_2(PPh_3)_2(SC_2H_4Ph)]^{2+}$ to leave the cluster in the first step, followed by addition of 2-PET to the nanoparticle and size focusing to Au_{25} [81]. However, it should be noted that these studies were conducted starting from particles bigger than Au_{25}, making comparison with ligand exchanges starting from Au_{11} difficult.

Based on the results obtained for the reactions **1** to **4**, the transformation from Au_{11} to Au_{25} seems to progress in two steps: First, the clusters mainly grow, resulting in a polydisperse mixture, which is indicated in the MALDI spectra. Both larger and smaller

cluster species than Au_{25} seem to be present. Then, a size focusing process is apparent, with nearly only Au_{25} surviving. Similar behavior was also observed by Tsukuda and coworkers for the ligand exchange of Au_{11} with GSH [77].

As expected, the temperature clearly affects the rate of the reaction, with room temperature reaction taking more than a day for the size focusing process to be complete. This is indicated by the 24 h MALDI spectra of reaction **1** and **2**, where smaller fragments still seem to be present. However, $[Au_{25}(PPh_3)_{10}(SC_2H_4Ph)_5Cl_2]^{2+}$ is always the main end product.

Moreover, the excess of exchange ligand also influences the reaction rate, which is shown by comparison of reaction **1** and **2**. Higher amount of thiol is related with faster growth of the cluster, clearly indicating that the actual ligand exchange process is happening right in the beginning. This is in agreement with previous assumptions [27, 77, 81].

However, the influence of the temperature is greater than that of the amount of exchange thiol, which is obvious when comparing reaction **3** and **4**. Although only 75 % of 2-PET were used (compared to reaction **3**), reaction **4** was clearly faster, which is attributed to the higher temperature (50 °C instead of 40 °C).

To get better insight into the exact mechanism, further experiments with focus on the fate of the ligands need to be performed. This would allow to determine if the exchange leads to release of PPh_3 [27, 31] or any form of Au(I) complexes, such as $[Au_2(PPh_3)_2(SC_2H_4Ph)]^{2+}$ [81]. For example, this could be achieved by *in-situ* NMR or IR measurements and will be necessary for proper comparison with the ligand exchange reactions of immobilized clusters (see Chapter 4.2 and 4.3).

4.1.2. Attempted Ligand Exchange with L-Glutathione

Ligand exchange of $Au_{11}(PPh_3)_7Cl_3$ with L-glutathione (GSH) was attempted in a biphasic 1:1 system of DCM/H_2O under high stirring, following published procedures [31, 77]. Both temperature and amount of exchange ligand were varied, in order to find optimum conditions. The conducted reactions are summarized in Table 4.2.

Table 4.2.: Conditions of the ligand exchange reactions of $Au_{11}(PPh_3)_7Cl_3$ and GSH in solution

No.	product	eq. GSH	Temp.	Atmosphere
1	**S1**	430	35 °C	N_2
2	**S2**	200	RT	air
3	**S3**	50	40 °C	air

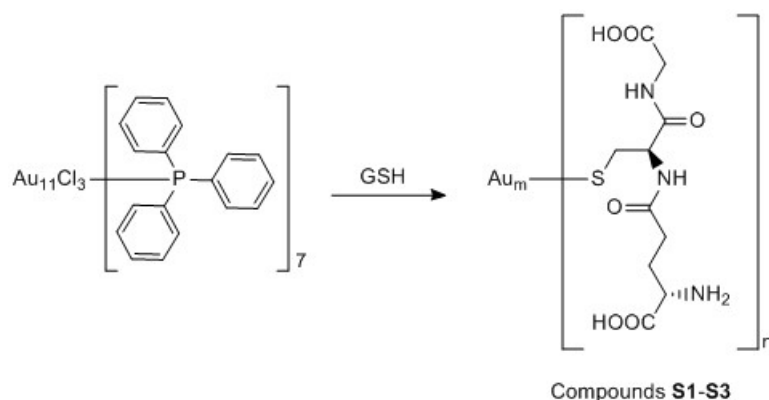**Figure 4.13.:** Ligand Exchange of $Au_{11}(PPh_3)_7Cl_3$ with GSH in solution

In contrast to literature, $Au_{25}(SG)_{18}$ could not be identified as the major reaction product. This is due to the absence of the typical spectral features of the compound in the UV-Vis spectra recorded for the crude products **S1**-**S3** after reaction (see Figure 4.14), where no peaks at 400, 450 and 680 nm [31, 77, 80] could be observed. In addition, the color of the aqueous phase was only slightly red instead of dark brown, and a lot of white precipitate had been formed at the interface.

The latter is a clear sign of decomposition [31, 75], very likely being Au(I) complexes [31]. Even reaction under inert atmosphere did not improve the reaction outcome. This is in agreement with observations by Shichibu *et al.*, who synthesized $Au_{25}(SG)_{18}$ through ligand exchange of a mainly Au_{11} containing precursor material regardless of the applied atmosphere (N_2 or under air) [77].

The UV-Vis spectra of the aqueous phases after the reaction (**S1**-**S3**), depicted in Figure 4.14, only show weak absorption features at 380 and 420 nm and an additional band at 470 nm. They are quite similar to the spectra of the ligand exchange from $[Au_{11}(PPh_3)_8Cl_2]Cl$ with GSH published by McKenzie *et al.* [31]. There, it is claimed that only small cluster species were formed, which were not stable in water for a long time and decomposed rapidly. This seems reasonable, as the characteristic spectral features of Au_{11} at 383 and 422 nm are maintained.

The difference in reactivity was related with the different Au_{11} species used as precursor material, with $Au_{11}(PPh_3)_7Cl_3$ growing to Au_{25}, whereas $[Au_{11}(PPh_3)_8Cl_2]Cl$ alone only exchanges its ligands without major modification of the core size [31]. This being true, it would suggest that the starting material used for the experiments within this thesis was actually $[Au_{11}(PPh_3)_8Cl_2]Cl$.

However, the presence of mainly $Au_{11}(PPh_3)_7Cl_3$ in the starting material could be confirmed by NMR measurements. Also, even pure $[Au_{11}(PPh_3)_8Cl_2]Cl$ could be reacted to $Au_{25}(SG)_{18}$ by McKenzie *et al.*, if temperature and excess of the thiol were high enough (45 °C and 430 eq.) [31]. This indicates that something else must be the reason for this different

reactivity, which cannot be explained by the nature of the undecagold starting material only.
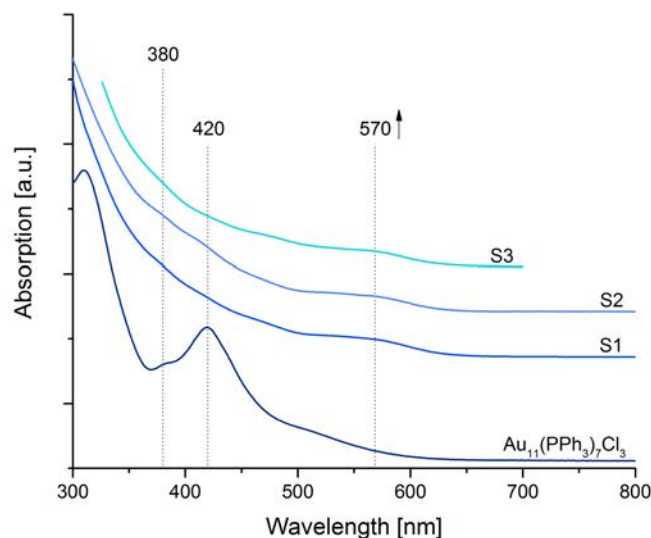

Figure 4.14.: UV-Vis spectra of the crude product mixtures **S1**-**S3** after ligand exchange with GSH (solvent: H_2O). The spectrum of the educt $Au_{11}(PPh_3)_7Cl_3$ in DCM is shown for comparison. Spectra are stacked for clarity. The spectrum of **S3** was recorded on a spectrometer with a smaller accessible wavelength range.

For reactions **2** and **3**, one possibility would be oxidation of GSH, as the reactions were carried out in air. However, this is contrary to observations by Shichibu *et al.*, who obtained even less side products when carrying out the reaction in air as compared to in N_2 atmosphere [77]. Another possibility is that the temperature was not high enough, as DCM was used instead of $CHCl_3$, preventing reaction at higher than $40\,°C$. Judging by the quite smooth profile of the UV-Vis spectrum, also McKenzie *et al.* did not obtain a lot of $Au_{25}(SG)_{18}$ when performing the ligand exchange with $Au_{11}(PPh_3)_7Cl_3$ and 430 eq. of GSH at only $30\,°C$. Moreover, they purified their products by gel filtration, assumably before recording the UV-Vis spectra, which was not possible for the experiments conducted within this thesis. Thus, formation of small amounts of $Au_{25}(SG)_{18}$ in the crude products **S1**-**S3** cannot be completely ruled out. However, it can be stated for sure that it was definitely not the only product formed in the reaction.

Concerning the reaction conditions, Woehrle *et al.* reported that the pH of the water phase needs to be in range between 5 and 8 to avoid decomposition of the Au:TPP precursor (at lower pH) and formation of disulfides (at higher pH). Moreover, for ligands with carboxylic acid functions such as in the used glutathione, they stressed that a slightly basic environment

is necessary to avoid formation of precipitate at the interface [27, 79]. This explains why the ligand exchange was not very successful under the tested conditions, as the pH of the aqueous GSH solution was found to be around 4-5. Hence, usage of a buffer system, as suggested by Woehrle *et al.* [27, 79], could be beneficial. If completely exchanged $Au_{25}(SG)_{18}$ can be obtained in that case still needs to be determined by further experiments.

4.1.3. Conclusions of Ligand Exchange Reactions in Solution

The reaction of $Au_{11}(PPh_3)_7Cl_3$ with 2-PET yielded $[Au_{25}(PPh_3)_{10}(SC_2H_4Ph)_5Cl_2]^{2+}$ in high purity. Changes in the reaction conditions (temperature, solvent, amount of exchange thiol) only lead to differences in the reaction kinetics, but not in the obtained product. Moreover, increasing the temperature seems to have greater influence than adding a higher amount of 2-PET to the solution.

According to the *ex-situ* UV-Vis and MALDI-MS measurements performed to follow the reaction, the Au_{11} cluster seems to grow quite fast at the beginning of the reaction, leading to a polydisperse reaction mixture. $[Au_{25}(PPh_3)_{10}(SC_2H_4Ph)_5Cl_2]^{2+}$ is then obtained after a size focusing process. This is in agreement with previous reports [77].

It was also shown that the mixed ligand shell cluster $[Au_{25}(PPh_3)_{10}(SC_2H_4Ph)_5Cl_2]^{2+}$ does not react further, if it is stirred in a solution of 75 eq. of 2-PET at 55 °C for a day. In addition, no major degradation was observed, indicating high stability of the Au_{25} cluster.

Ligand exchange with GSH to $Au_{25}(SG)_{18}$ could not be accomplished when following published protocols [31, 77]. This was possibly due to the low pH of the aqueous phase, leading to decomposition of the $Au_{11}(PPh_3)_7Cl_3$ cluster [27, 79]. New approaches will be tested with the aid of a buffer system.

For both cases, the ligand exchange should be followed *in-situ* by a method sensitive to the chemical nature of the ligands, such as NMR or IR. This would allow to determine at which stage of the reaction the actual ligand exchange takes place. Moreover, a new method for mass spectroscopic analysis needs to be developed, leading to less fragmentation.

4.2. Ligand Exchange Reactions with Dropcast Films of $Au_{11}(PPh_3)_7Cl_3$ on Planar Surfaces

Within this chapter, ligand exchange with dropcast films of $Au_{11}(PPh_3)_7Cl_3$ on planar surfaces (Al_2O_3 or ZnSe) are discussed. *Ex-situ* PM-IRRAS and *in-situ* ATR-IR spectroscopic studies were performed, aiming to get insights in the ligand exchange reaction behavior of clusters immobilized on surfaces. Therefore, the clusters were dropcasted on an Al_2O_3 plate or a ZnSe crystal, which were subsequently exposed to a solution containing the exchange

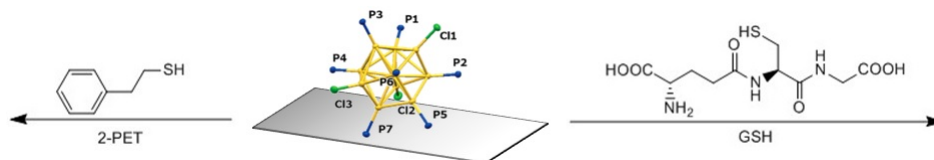thiol (2-PET or GSH), without dissolving the cluster films.

Figure 4.15.: Reactions of $Au_{11}(PPh_3)_7Cl_3$ dropcast films on Al_2O_3 and ZnSe surfaces with thiol ligands. Cluster structure adapted from [31].

4.2.1. Reaction of a Dropcast Film of $Au_{11}(PPh_3)_7Cl_3$ on Al_2O_3 with 2-PET

The reactions **1** and **2** were conducted in three steps, as described in Chapter 7.4.1. The solutions containing the exchange ligand were renewed after each step and defined amounts of $CHCl_3$ were added to create a more suitable chemical environment for the ligand exchange. This was based on the results obtained for the ligand exchange in solution (see Chapter 4.1.1). Table 4.3 gives an overview of the conditions tested.

Table 4.3.: Conditions of the reactions of $Au_{11}(PPh_3)_7Cl_3$ on Al_2O_3 with 2-PET

No.	product	1st step	2nd step	3rd step
1	F1	toluene	8:2 toluene/CHCl$_3$	7:3 toluene/CHCl$_3$
2	F2	hexane	8:2 hexane/CHCl$_3$	6:4 hexane/CHCl$_3$

Reaction 1

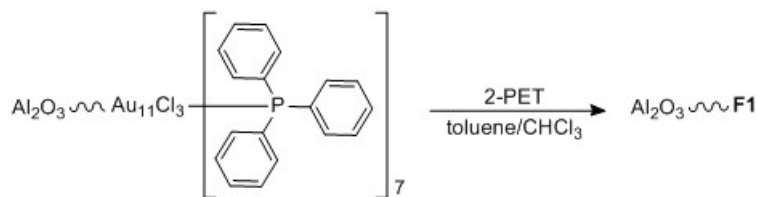**Figure 4.16.:** Reaction **1** of $Au_{11}(PPh_3)_7Cl_3$ on Al_2O_3 with 2-PET

For ligand exchange reaction **1**, toluene was chosen as a solvent. As $Au_{11}(PPh_3)_7Cl_3$ does not dissolve therein, the cluster should stay in solid phase and remain attached to the plate. After step 1, the solution had turned slightly yellow, suggesting that a small amount of cluster or another Au containing species (e.g. Au(I) complexes) was present in the solution phase. However, judging on the weak color and the state of the film on the plate, this amount

seemed to be rather small.

After the first 22 h, some changes were already visible in the PM-IRRAS spectrum, as shown in Figure 4.17. New spectral features started to evolve at 1495, 1179, 1067, 1056 and 983 cm^{-1}, which are marked by dashed lines. As no color change of the cluster film was noticed, unlike during the exchange with both cluster and 2-PET in solution (see Chapter 7.3.1), the product of step 1 was assumed to be different to $[Au_{25}(PPh_3)_{10}(2\text{-PET})_5Cl_2]^{2+}$. Moreover, the clusters were found to stay attached to the Al_2O_3 plate, even when rinsed with DCM. Therefore, significant interaction between Au_{11} and alumina was assumed. As a result, it was decided to add 20 % of $CHCl_3$ to the solvent in step 2, to achieve better interaction between the cluster and the solution phase. This time, the solution stayed clear over a period of at least 22 h (longer times not tested), indicating that the cluster did not dissolve. The PM-IRRAS recorded after this step again showed some changes, with the new spectral features getting more intense.

For step 3, the amount of $CHCl_3$ was again increased to 30 %. This time, spectra were recorded after 6, 24 and 50 h. However, as shown in Figure 4.17, the reaction was already complete after the first 6 h, as no changes could be observed afterwards. No significant broadening was observed after 50 h, indicating that the clusters were stable under the present conditions.
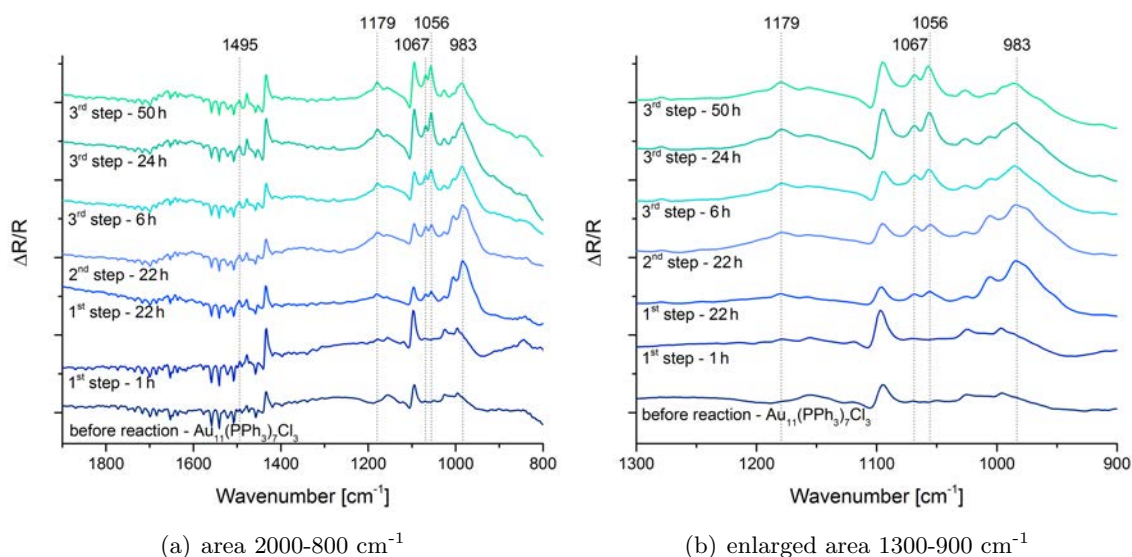

(a) area 2000-800 cm^{-1} (b) enlarged area 1300-900 cm^{-1}

Figure 4.17.: PM-IRRAS of reaction **1**. Newly evolving bands are marked by dashed lines. Spectra are stacked for clarity.

In Figure 4.18, the PM-IRRAS of the end product **F1** is shown. The spectral features were assigned by comparison with literature IR spectra of PPh_3 and 2-PET (see spectra in Chapter A.2) and published assignments [95–99]. A list of the bands of **F1** is shown in

Chapter 7.4.1. It can be seen that the majority of them can be attributed to the PPh₃ ligands (black assignments). Thus, no complete ligand exchange was achieved. However, the bands assigned in green can be clearly related with 2-PET, indicating that some ligands did indeed attach to the cluster. The features at 1495 and $1057\,cm^{-1}$ were also emerging and gaining intensity over the progress of the reaction, as shown in Figure 4.17.

It should be further noted that it was not possible to assign all bands. Also, some changes in the spectral features originating from the PPh₃ ligands were noticed (both shifts in the maximum wavenumber and intensity). The maxima of the bands related to 2-PET also shifted slightly over the duration of the reaction. However, it could not be identified if this was due to a change in the cluster structure or inaccuracies in the measurement process. In addition, it was not possible to determine if the incoming thiol was definitely bound to the Au core, as the Au-S and Au-P vibrations can only be seen in the FIR region below $800\,cm^{-1}$ [100].
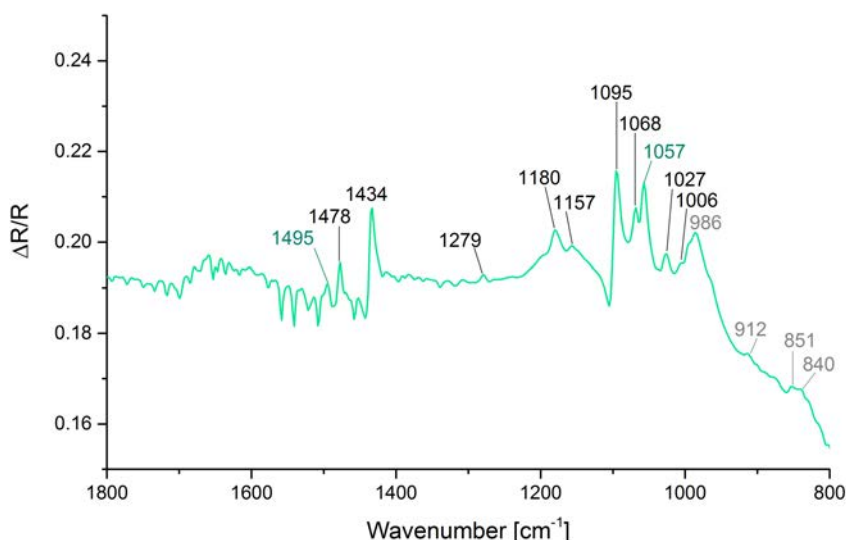

Figure 4.18.: PM-IRRAS of **F1**. Black: PPh₃, green: 2-PET, grey: not assigned.

To estimate the cluster size after the reaction, MALDI-MS spectra were measured by scratching a small amount of clusters off the plate and dissolving them again. As shown in Figure 4.19, a lot of fragmentation was observed, where the most intense peaks could all be assigned to fragments without any 2-PET in the ligand shell. Sulfur containing fragments were only found for some of the less intense features. This indicates that not a lot of ligands got exchanged during the reaction. It is likely that only the clusters on the film surface are reacting, with the ones within the film remaining unchanged. However, the sample for the MS measurement was taken over the whole film thickness and therefore contained much more 'inner clusters' than 'surface clusters', thus explaining why no intense peaks of fragments containing 2-PET could be found.

The core size seems to be maintained, as the observed fragments are similar to that of $Au_{11}(PPh_3)_7Cl_3$.

Table 4.4.: Assignment of the PM-IRRAS bands of **1**

Ligand	Band [cm^{-1}]	Assignment[1]
2-PET	1495	$CH_{aliph.}$ bend./scis.
	1057	-
PPh$_3$	1478	$HCC_{arom.}$ ip-bend.
	1434	$CC_{arom.}$ stretch.
	1279	$HC_{arom.}$ ip-bend./$CC_{arom.}$ stretch.
	1180	$HCC_{arom.}$ ip-bend.
	1157	$HCC_{arom.}$ ip-bend.
	1095	PC stretch.
	1068	$CC_{arom.}$ stretch./$HCC_{arom.}$ ip-bend.
	1027	$HC_{arom.}$ op-bend.
	1006	$CC_{arom.}$ stretch./$HCC_{arom.}$ ip-bend.

[1] Assignment according to reference data for PPh$_3$ [95–99] and the reference spectra in Chapter A.2. Only the most important additions (>15 %) to a vibration are listed.
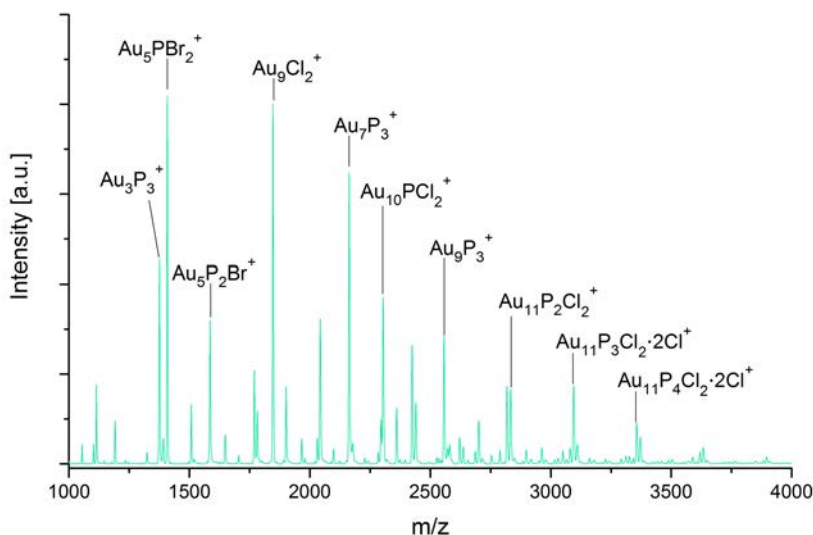
Figure 4.19.: MALDI-MS spectrum of **F1**. P is equal to PPh$_3$.
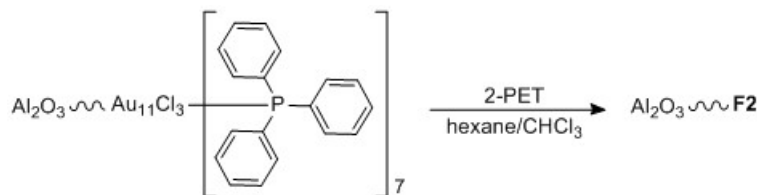
Reaction 2

Figure 4.20.: Reaction **2** of $Au_{11}(PPh_3)_7Cl_3$ on Al_2O_3 with 2-PET

The protocol for reaction **2** was identical to the one for reaction **1**, with the only difference being the use of hexane instead of toluene as the main solvent. In the first step, the solution remained completely clear, meaning the cluster did not dissolve. In the second step, a solution with 20 % of $CHCl_3$ was used to enhance the possibility of interaction between cluster and ligand. After 22 h, the solution was slightly colored, indicating that small amounts of Au containing species were present in the solution. For the third step, the amount of $CHCl_3$ was increased up to 40 %. This time, the solution was still clear after 24 h and only gained a little bit of yellow color after 50 h.
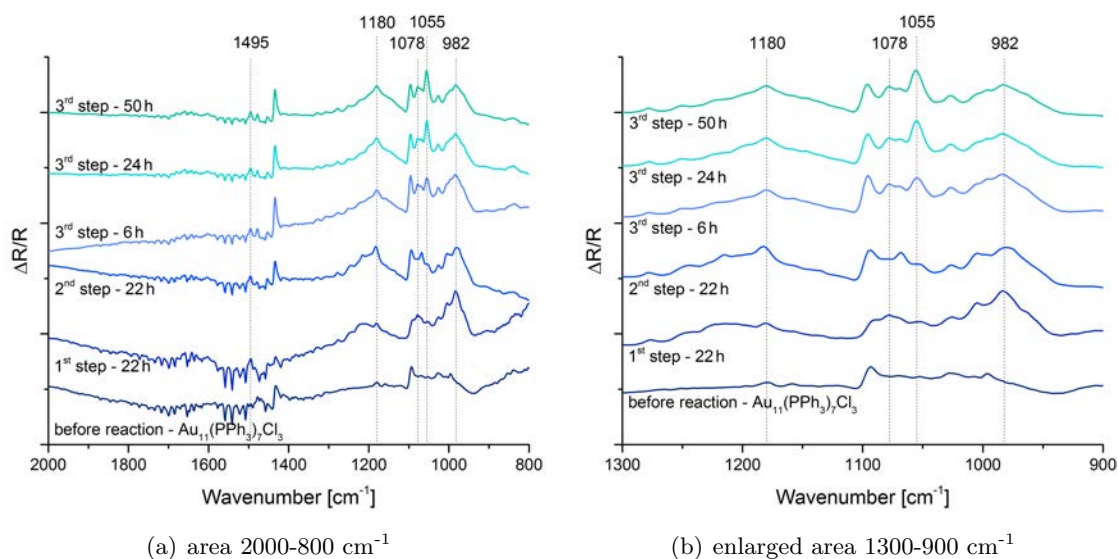

(a) area 2000-800 cm^{-1}

(b) enlarged area 1300-900 cm^{-1}

Figure 4.21.: PM-IRRAS of reaction **2**. Newly evolving bands are marked by dashed lines. Spectra are stacked for clarity.

The spectra recorded with PM-IRRAS at defined reaction times are shown in Figure 4.21. Even after the first step only, changes are clearly visible with new bands evolving at 1495, 1078, 1055 and 982 cm^{-1}. With step 2 and 3, the spectrum gets more defined

and the new features gain intensity. After the 24 h of step 3, no more changes can be observed, showing the reaction had already been complete by then under the present conditions.

The spectrum of the end product **F2** is displayed in Figure 4.22. Again, assignment was achieved by comparison with literature data [95–99] and reference spectra (Chapter A.2). Most of the features could be related to PPh_3, but also some of 2-PET could be found, which emerged over the duration of the reaction (1495 and $1056\,cm^{-1}$). As for reaction **1**, the ligand exchange was clearly not complete, but some kind of reaction with the cluster must have occurred. This is shown by the shifts and intensity changes of the PPh_3 bands. Again, it remains unclear where the thiol ligand really binds, as the FIR region was inaccessible in this experiment.
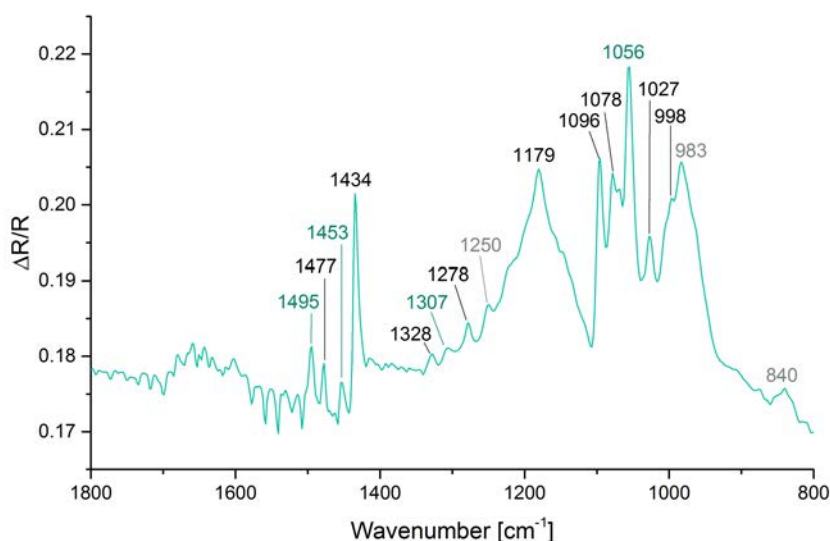

Figure 4.22.: PM-IRRAS of **F2**. Black: PPh_3, green: 2-PET, grey: not assigned.

Table 4.5.: Assignment of the PM-IRRAS bands of **2**

Ligand	Band [cm^{-1}]	Assignment[1]
2-PET	1495	$CH_{aliph.}$ bend./scis.
	1453	$CH_{aliph.}$ bend./scis.
	1307	-
	1056	-
PPh$_3$	1477	$HCC_{arom.}$ ip-bend.
	1434	$CC_{arom.}$ stretch.
	1328	$CH_{arom.}$ ip-bend./HCP ip-bend.
	1278	$HC_{arom.}$ ip-bend./$CC_{arom.}$ stretch.
	1179	$HCC_{arom.}$ ip-bend.
	1096	PC stretch.
	1078	$CC_{arom.}$ stretch./$HCC_{arom.}$ ip-bend.
	1027	$HC_{arom.}$ op-bend.
	998	$CC_{arom.}$ stretch./$HCC_{arom.}$ ip-bend.

[1] Assignment according to reference data for PPh$_3$ [95–99] and the reference spectra in Chapter A.2. Only the most important additions (>15 %) to a vibration are listed.
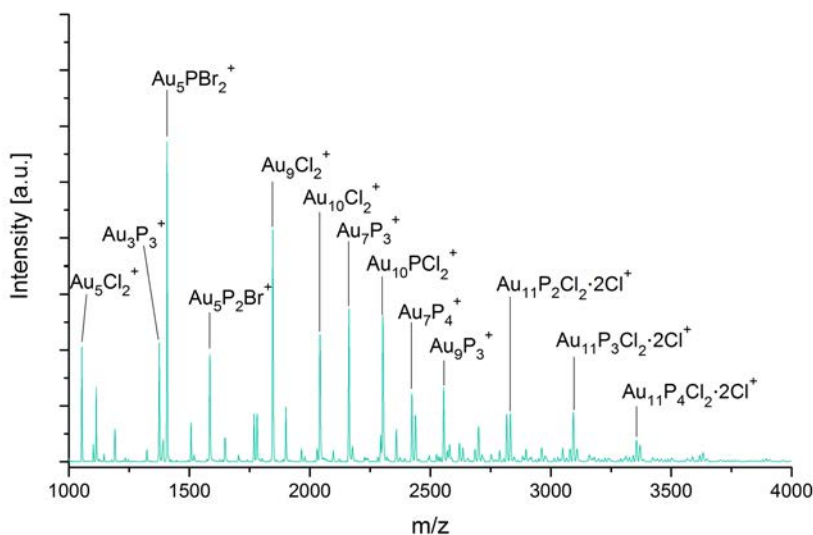
Figure 4.23.: MALDI-MS spectrum of **F2**. P is equal to PPh$_3$.

The MALDI-MS spectrum of **F2** in Figure 4.23 shows pronounced fragmentation. In

addition, the most intense peaks all correspond to fragments which do not contain any 2-PET ligands. Thus, not a lot of ligands were exchanged during the reaction. This might be due to only the ligands on the film surface reacting, whereas the Au_{11} clusters below remain unchanged. However, the core size seems to remain stable, as the observed fragments are similar to that of $Au_{11}(PPh_3)_7Cl_3$. Also, the MS spectra of **1** and **2** are very similar.

Comparison of Reaction 1 and 2

As was shown by the PM-IRRAS measurements, the results of both ligand exchange attempts are quite similar. The main new bands evolving are the same, as are the spectra of the end products **F1** and **F2**. However, it seems that the reaction progressed further when toluene/$CHCl_3$ was used as a solvent, as the intensities of the new features are higher. Also, the addition of chloroform to the reaction mixture apparently increased the reactivity with the exchange thiol, without dissolving significant amount of the cluster. Thus, the interaction between the Au cluster and the Al_2O_3 surface is considerable. Its nature remains to be unraveled in future work.

4.2.2. Reaction of a Dropcast Film of $Au_{11}(PPh_3)_7Cl_3$ on Al_2O_3 with GSH

The ligand exchange protocol is described in Chapter 7.4.2. In this case, a mixture of 20 % of MeOH in water was used as solvent due to the polar nature of the GSH ligands. MeOH was added to increase the contact between clusters and liquid phase, as well as to enhance the solubility of the freed PPh_3 ligands upon exchange.
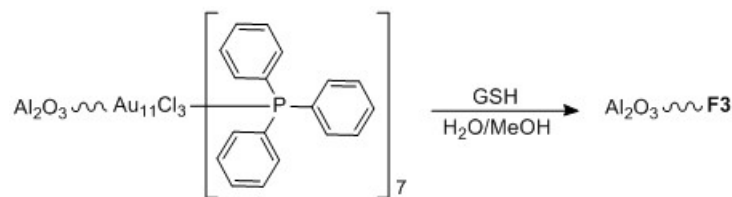

Figure 4.24.: Reaction of $Au_{11}(PPh_3)_7Cl_3$ on Al_2O_3 with GSH

The PM-IRRAS spectra are displayed in Figure 4.25. Already after 18 h, the spectrum has changed drastically, with the characteristic bands of the cluster disappearing and other broad features evolving at the same time (marked with dashed lines). The spectra then only varied slightly between 18 and 66 h, indicating that the reaction was complete. The resulting end spectrum of the obtained product **F3** resembles the one of a glutathione film on Al_2O_3. A red-shift of the spectral features is visible, which can be explained by differences between free and bound GSH, respectively.
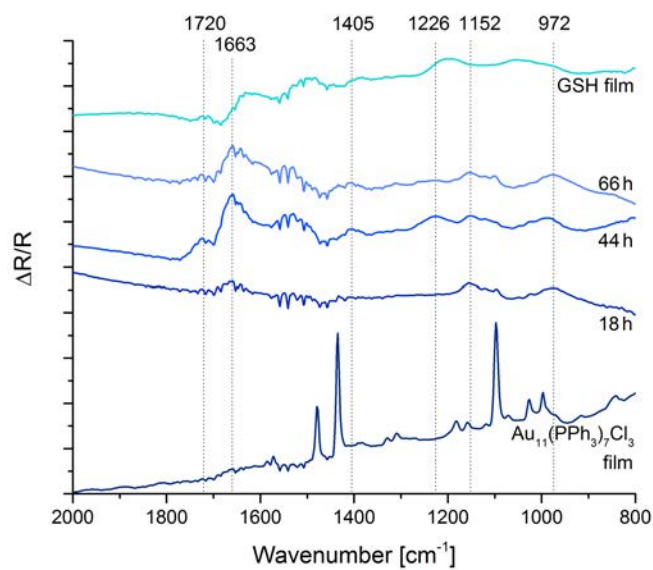
Figure 4.25.: PM-IRRAS of reaction **3**. Newly evolving bands are marked by dashed lines. Spectra are stacked for clarity.
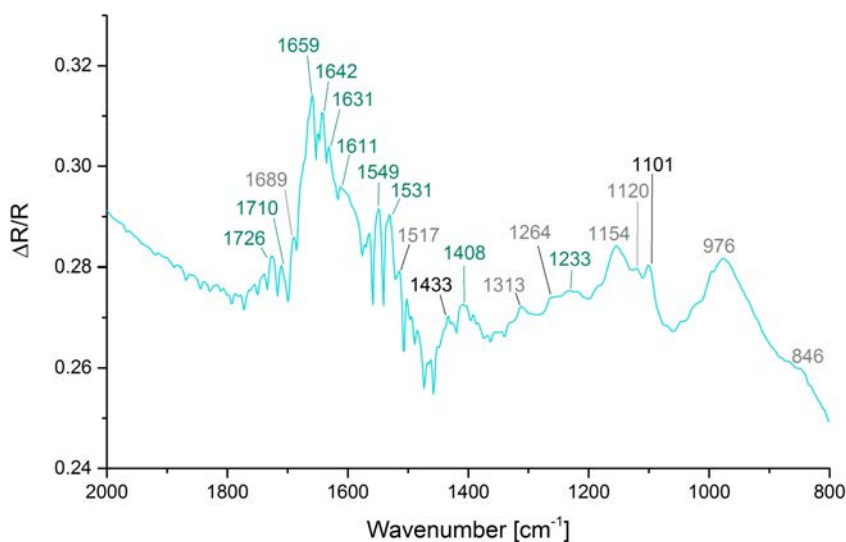

Figure 4.26.: PM-IRRAS of **F3**. Black: PPh$_3$, green: GSH, grey: not assigned.

The PM-IRRAS of the product **F3** after 66 h is shown in Figure 4.26. Identification of the bands was done based on literature spectra of PPh$_3$ [95–99] and glutathione [101]. Most of the features can be assigned to GSH (marked in green), which indicates that some

exchange did indeed occur. Only the most intense bands of PPh$_3$ can still be seen at 1433 and 1101 cm^{-1}. Moreover, also a distinct increase in the polarity of the film was noticed when rinsing the plate with solvents prior to the PM-IRRAS measurements to remove free ligands. This further assures the presence of the polar GSH ligand in the sample.

Table 4.6.: Assignment of the PM-IRRAS bands of **3**

Ligand	Band [cm^{-1}]	Assignment[1]
GSH	1726	CO stretch.
	1710	CO stretch.
	1659	amide I
	1642	amide I/H$_2$O def.
	1631	amide I/H$_2$O def.
	1611	NH$_3^+$ def.
	1549	amide II
	1531	amide II
	1408	S(COO$^-$) stretch.
	1233	amide III
PPh$_3$	1433	CC$_{arom.}$ stretch.
	1001	PC stretch.

[1] Assignment according to reference data for PPh$_3$ [95–99] and GSH [101], as well as the reference spectra in Chapter A.2. Only the most important additions (>15 %) to a vibration are listed.

For determining the approximate size of the cluster after exchange and getting an idea of the number of exchanged ligands, MALDI-MS was measured. As can be seen, a maximum of two exchanged ligands can be found in the cluster after the reaction. Also, it seems that the PPh$_3$ ligands are reacting, and not the chloride. Therefore, a change in the electronic and also geometric structure is expected, as the coordination of these two types of ligands is quite different, as discussed in Chapter 1.1. In addition, the core size seems to be stable, with similar fragments having been observed for the precursor Au$_{11}$(PPh$_3$)$_7$Cl$_3$.
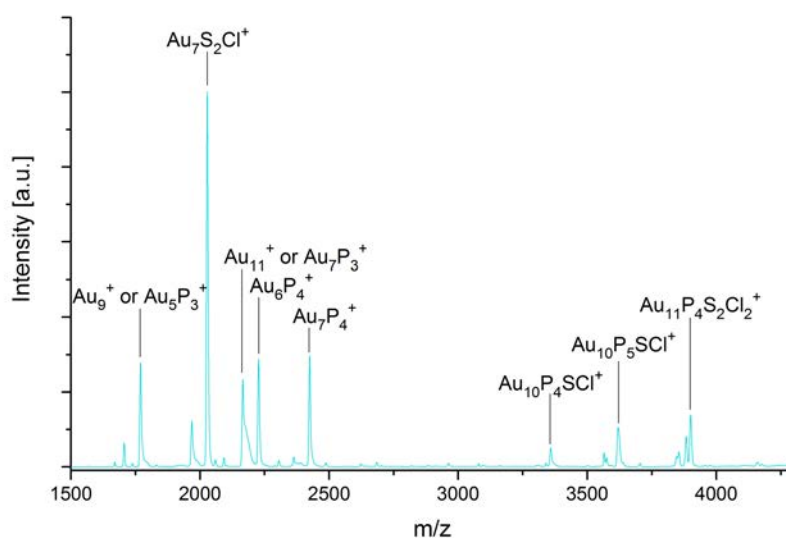
Figure 4.27.: MALDI-MS of **F3**. P is equal to PPh$_3$ and S to -SG.

4.2.3. Attempted Ligand Exchange Reaction of Au$_{11}$(PPh$_3$)$_7$Cl$_3$ with a Dropcast Film of GSH on Al$_2$O$_3$

For this reaction, the concept was reversed: A film of glutathione was prepared on an Al$_2$O$_3$ plate and then exposed to a solution of Au$_{11}$(PPh$_3$)$_7$Cl$_3$ in CHCl$_3$. The exact procedure is described in Chapter 7.4.3. Once the plates were removed from the solution, deposition of red material over the whole area could be observed. To determine its nature, PM-IRRAS was measured on two spots as is shown in Figure 4.28; one on the film (blue cross) and one on the side (green cross).

Figure 4.28.: PM-IRRAS measurement positions. Blue cross: on GSH film, green cross: on the Al$_2$O$_3$ surface on the side.

As is shown in the spectra evolution over time, it seems that the cluster did deposit on the plate, but did not react with the GSH film. This is concluded from the PM-IRRAS signals being the same for both positions (see Figure 4.29). The bands can all be attributed to signals of the PPh$_3$ ligands [95–99]. As it was not possible to wash away the immobilized clusters with different solvents, the interaction between Au$_{11}$ and alumina seems to be significantly strong.

(a) on the GSH film (blue cross)

(b) on the Al_2O_3 surface (green cross)
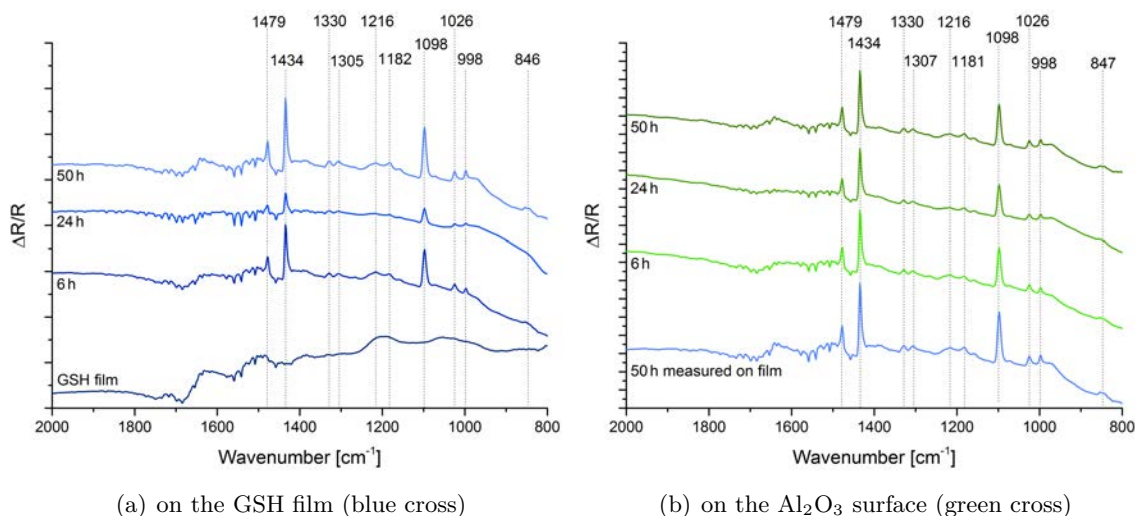
Figure 4.29.: PM-IRRAS of the attempted reaction between $Au_{11}(PPh_3)_7Cl_3$ in solution and a GSH film on Al_2O_3. Newly evolving bands are marked by dashed lines. Spectra are stacked for clarity.

One possible explanation for the failure of this reaction is that the active site of the GSH ligand, which is the -SH group, was not available for bonding to Au because it was interacting with the Al_2O_3. This is visualized in Figure 4.30. Another possibility would be a lack of contact between the ligand film and the solution phase due to bad choice of solvent. Thus, no further reactions with immobilized ligands were attempted.
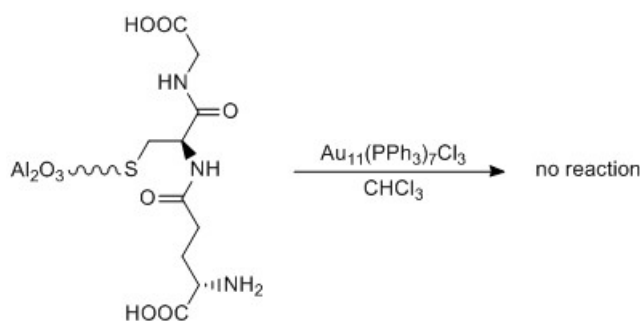
Figure 4.30.: Attempted Reaction of $Au_{11}(PPh_3)_7Cl_3$ in solution with GSH on Al_2O_3

4.2.4. Reaction of a Dropcast Film of $Au_{11}(PPh_3)_7Cl_3$ on ZnSe with GSH

The reaction of a dropcast film of $Au_{11}(PPh_3)_7Cl_3$ on a ZnSe ATR crystal with GSH was monitored by *in-situ* ATR-IR spectroscopy. Therefore, a $0.01\,M$ solution of GSH in 8:2 H_2O/EtOH was flowed through the ATR cell at low speed for $30\,h$, interacting with the cluster film inside the cell. Further details are provided in Chapter 7.4.4.
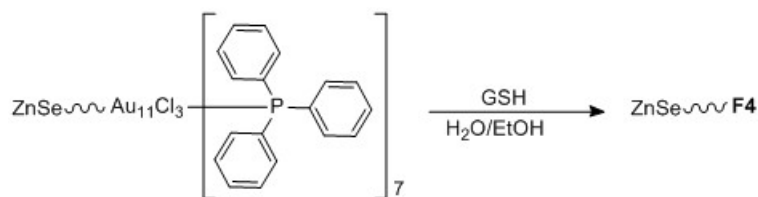
Figure 4.31.: Reaction of $Au_{11}(PPh_3)_7Cl_3$ on ZnSe with GSH

Within the first two hours, changes in the ATR-IR spectra were observed. Figure 4.32 shows the CH-stretching region, where band shifts and broadening are apparent. This indicates changes in the geometric and electronic structure of the clusters. After the first two hours, no further changes could be observed by *in-situ* measurements. However, it is not clear if this was due to the reaction being already complete, or the absorption of the solution flowed through prevented detection the slight changes.
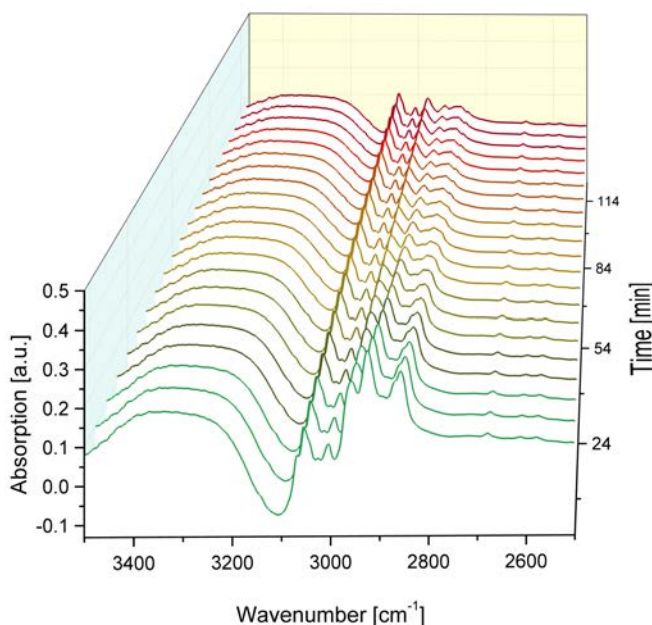
Figure 4.32.: CH-stretching region of the *in-situ* ATR-IR measurements of the reaction of $Au_{11}(PPh_3)_7Cl_3$ on ZnSe with GSH over the first 120 min

The spectra of the dry cluster film recorded before and after the reaction (**F4**) are shown in Figure 4.33. Identification of the peaks was done based on literature data of PPh_3 [95–99] and glutathione [101], as well as by comparison to a recorded GSH reference spectrum (see Chapter A.2). Peaks of the C=O stretching vibration ($1725\,\mathrm{cm^{-1}}$ and the amide regions I and II (1643, 1548 and $1530\,\mathrm{cm^{-1}}$ are visible, proving the presence of GSH in the sample. Moreover, several bands appear shifted, indicating a different bonding situation in the cluster,

and thus, successful ligand exchange. **F4** is assumed to be a mixed-ligand shell cluster, as vibrations of both PPh_3 and GSH were assigned (see also Chapter 7.4.4) The broad OH stretching vibration at $3300 \, cm^{-1}$ can be attributed the incorporation of solvent molecules into the cluster [84].
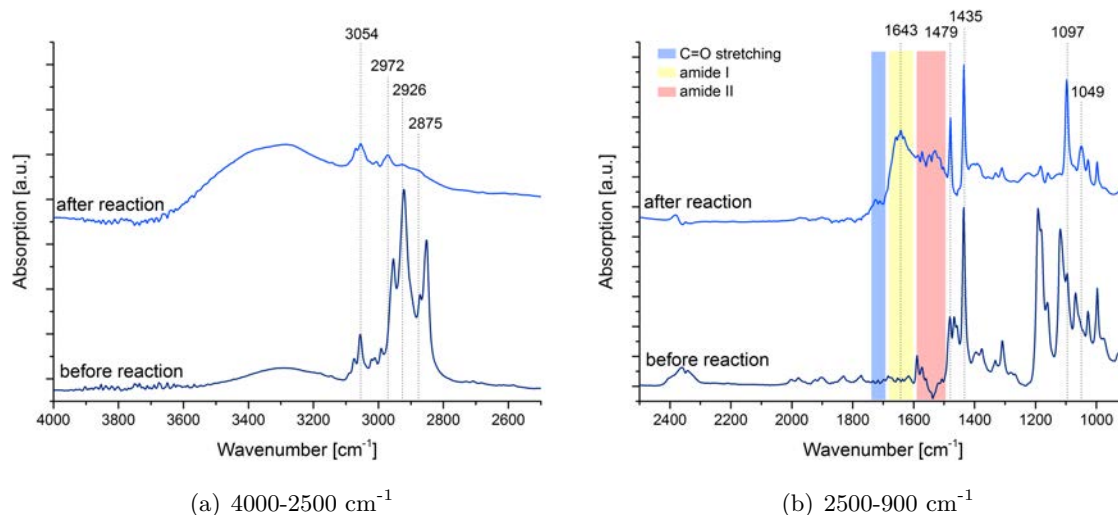

(a) 4000-2500 cm^{-1} (b) 2500-900 cm^{-1}

Figure 4.33.: ATR-IR spectra of $Au_{11}(PPh_3)_7Cl_3$ (before reaction) and **F4** (after reaction) on ZnSe

4.2.5. Conclusions of Ligand Exchange Reactions of Cluster Films on Al_2O_3 and ZnSe

First approaches of ligand exchange reactions for immobilized dropcast films of $Au_{11}(PPh_3)_7Cl_3$ were conducted. Analysis with PM-IRRAS and MALDI-MS revealed that incomplete ligand exchange took place for $Au_{11}(PPh_3)_7Cl_3$ on Al_2O_3 plates with both 2-PET and GSH. Core-size evaluation by MALDI-MS gave an estimate of 9-11 Au atoms. Due to fragmentation of the cluster during the measurement, a more exact determination was not possible. For more detailed studies on this process, optimization of the MS analysis, with a possible change of the ionization technique to electrospray, will be necessary.

Attempts to achieve a ligand exchange with an immobilized GSH film on Al_2O_3 and $Au_{11}(PPh_3)_7Cl_3$ in solution (reversed system) were not successful.

In-situ ATR-IR measurements of the ligand exchange between $Au_{11}(PPh_3)_7Cl_3$ film on a ZnSe crystal and a solution of GSH showed significant changes in the CH stretching region of the spectrum. After the reaction, peaks for the C=O stretching vibration and the amide regions I and II were observed, indicating bonding of GSH to the cluster.. This confirms the results obtained for the system on Al_2O_3.

4.3. Ligand Exchange Reactions of Au$_{11}$(PPh$_3$)$_7$Cl$_3$ Supported on Metal Oxide Materials

Within this Chapter, first approaches of ligand exchange reactions of Au$_{11}$(PPh$_3$)$_7$Cl$_3$ supported on metal oxide materials (SiO$_2$ and Al$_2$O$_3$ powders) will be discussed. The clusters were immobilized on the powders by wet impregnation, meaning stirring the support suspended in an Au$_{11}$ solution for 24 h and additional cleaning and drying [102]. Afterwards, the samples were stirred in a solution of the exchange ligand (2-PET or GSH) under air for 20 h. UV-Vis spectra and STEM images were used to analyze both educts and products. However, only preliminary results can be presented within this thesis, as the characterization was not yet finished.
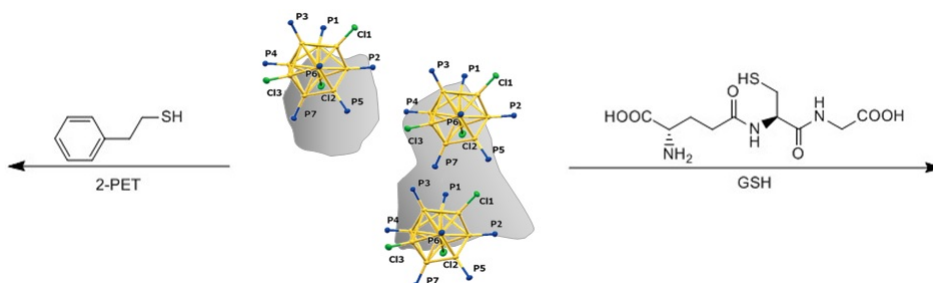
Figure 4.34.: Reactions of Au$_{11}$(PPh$_3$)$_7$Cl$_3$ supported on metal oxides (SiO$_2$ and Al$_2$O$_3$) with thiol ligands. Cluster structure adapted from [31].

4.3.1. Supporting Process and Loading

2 wt% Au were chosen as loading for these experiments. For catalytic applications, the loading is usually even lower [42]. However, in order to be able to analyze the samples accurately, deposition of a higher amount of Au$_{11}$ clusters was used.

The originally bright red solution containing the cluster turned (nearly) colorless over the 24 h of stirring with the support material, with the color being transferred to the solid phase. Thus, significant interaction between Au$_{11}$ and the metal oxides is assumed. Even rinsing the filtered slurries with small amounts of MeOH did not lead to washing out of the clusters. This is in contrast to previous reports of supported Au$_{11}$ [39], but might be related to the use of different Au$_{11}$ analogues, as suggested by comparison of the UV-Vis spectra. The impregnation was performed under N$_2$ atmosphere, which can be be seen more like a precaution and not a necessity. The choice of MeOH as solvent is attributed to the low stability of Au$_{11}$(PPh$_3$)$_7$Cl$_3$ in halogenated solvents [31] and THF (see Chapter 3.5). In addition, it was shown that alcoholic solutions lead to better dispersion of Au$_{11}$ clusters on the support material [39].

Figure 4.35 displays the UV-Vis spectra of the dry powders after supporting. Defined

spectral transitions can be seen, with most of them appearing for both support materials (marked with dashed lines). This indicates that the cluster was stable during the supporting procedure. The spectral features appear red-shifted compared to the spectrum of pure $Au_{11}(PPh_3)_7Cl_3$, which was observed previously [39]. Reference spectra of the support powders can be found in Chapter A.3.

Interestingly, the absorption continuously increases from $\approx 480\,nm$ upwards. This might be due to the interaction between the ligand shell of the cluster with the support material, as no similar behavior could be observed for exposed Au_{11} gold cores [39, 40]. This is further affirmed by the fact that it does not show any correlation with the size of the supported clusters, as visualized in Figure 4.36, in which the sample with $5\,wt\%$ Au exhibits increased particle sizes due to aggregation.
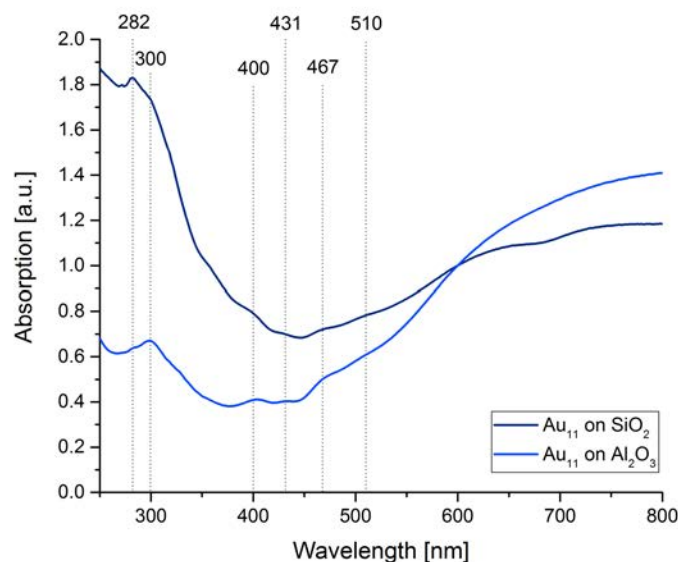
Figure 4.35.: UV-Vis spectra of $Au_{11}(PPh_3)_7Cl_3$ supported on metal oxides (SiO_2 and Al_2O_3)

When the Au loading on SiO_2 was increased to $5\,wt\%$, the sample turned bright pink upon drying at $65\,°C$. The UV-Vis spectrum recorded of the dry powder was broader and more featureless than the one with $2\,wt\%$ Au, which is shown in Figure 4.36.
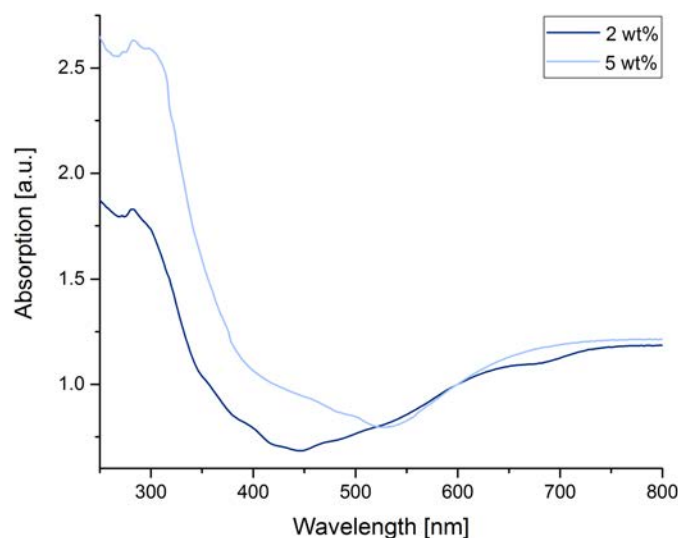
Figure 4.36.: UV-Vis spectra of SiO$_2$ supported Au$_{11}$(PPh$_3$)$_7$Cl$_3$ with loading of 2 wt% and 5 wt% Au

To get better information on loading and core size of the supported clusters, STEM images were obtained. As the measurements were still ongoing upon completion of this thesis, only the images of the samples with SiO$_2$ support can be presented. However, as the UV-Vis spectra after the wet impregnation look alike, it is assumed that the results for the unreacted Al$_2$O$_3$ sample will be similar.

The HAADF images for the unreacted clusters on SiO$_2$ are shown in the Figures 4.37 and 4.37. For a loading of 2 wt % Au, particles between 0.7 and 2.0 nm are observed, with most of them being around 1.2 nm in diameter. Published data for Au$_{11}$ report the core size without ligand shell to be 0.8 nm [39], which is significantly smaller than the value reported here. However, one needs to take into account that for the samples analyzed within this thesis, the ligands were not removed, resulting in larger particles.
For 2 wt % Au, the cluster seems to be well dispersed on the support material, which is shown in the overview image in Figure 4.38a. For loading of 5 wt % Au, this is not the case anymore, which is indicated in Figure 4.38b. The particles are aggregating, leading to larger particles being formed and inhomogeneous distribution. The size is then between 1.5-4.5 nm, with a modulus of 3.0 nm. It is therefore concluded that higher loading is not beneficial for this system.

(a) 2 wt% Au

(b) 5 wt% Au
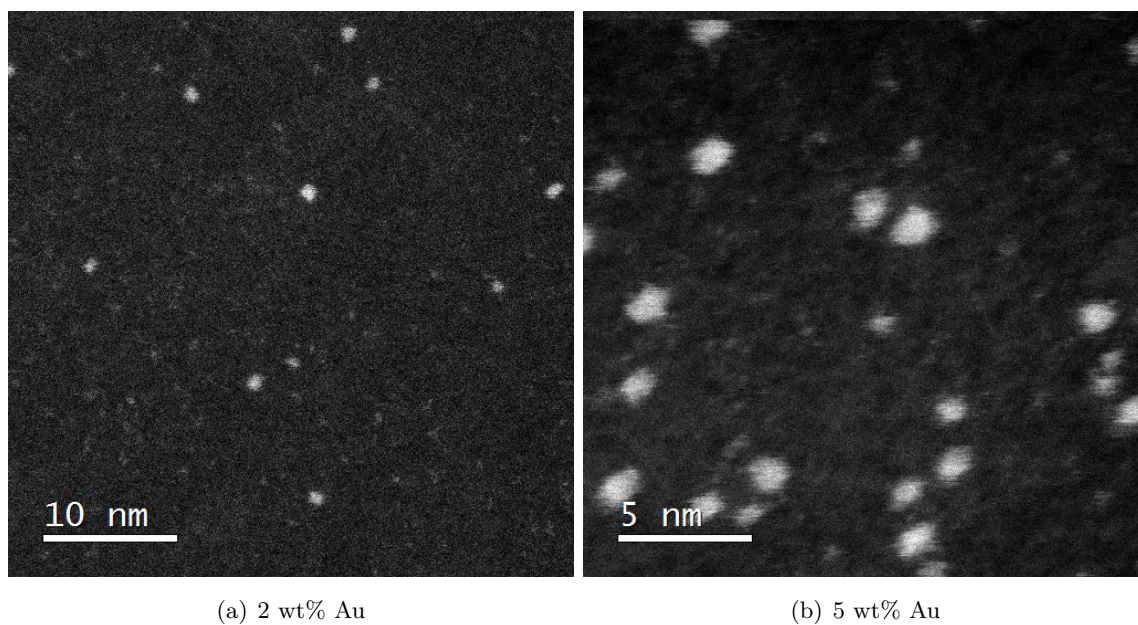
Figure 4.37.: HAADF-STEM images of the clusters supported on SiO_2

(a) 2 wt% Au

(b) 5 wt% Au
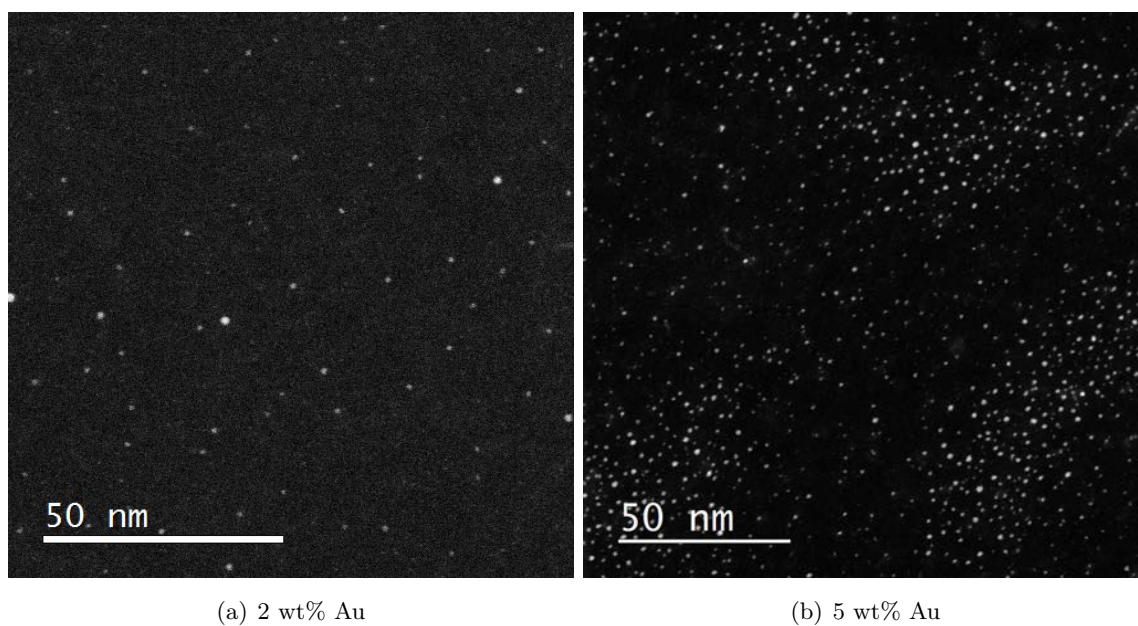
Figure 4.38.: HAADF-STEM images of the clusters supported on SiO_2 (overview)

4.3.2. Reactions of SiO$_2$ supported Au$_{11}$(PPh$_3$)$_7$Cl$_3$ with Thiol Ligands

The conditions of the attempted ligand exchang were chosen based on the results of the reactions in solution and with films on Al_2O_3 (see Chapters 4.1 and 4.2). The procedure

is described in Chapter 7.5.4. Toluene was chosen as solvent for the ligand exchange with 2-PET instead of the typically used halogenated solvents due to its higher boiling point (less evaporation) and more inert nature. DCM or CHCl$_3$ might interact with the support materials and therefore interfere with the tested reactions.
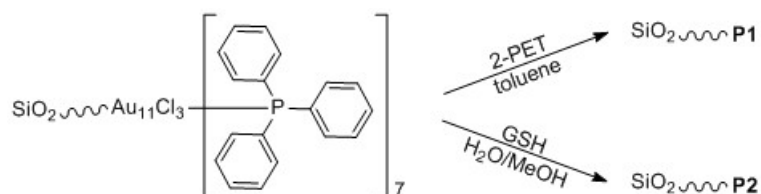
Figure 4.39.: Reaction of SiO$_2$ supported Au$_{11}$(PPh$_3$)$_7$Cl$_3$ with thiol ligands (2-PET and GSH)

The liquid phase, removed after the reactions, was nearly clear for both ligands. It was collected and the solvent phase removed under reduced pressure, yielding only small amounts of a dark brown (reaction with 2-PET) and dark green (reaction with GSH) residue. As the mass of these side products was below 2 mg, further characterization was not carried out. However, it can be concluded that the clusters did not leave the support during reaction, which indicates strong interaction.
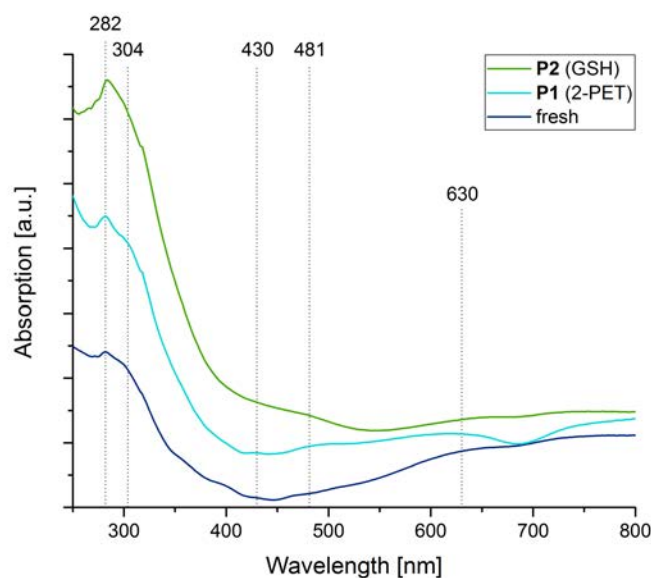
Figure 4.40.: UV-Vis spectra of SiO$_2$ supported Au$_{11}$(PPh$_3$)$_7$Cl$_3$ before and after reaction with exchange thiol (2-PET ot GSH). Spectra are stacked for clarity.

UV-Vis spectra were measured for the dry powder samples before ('fresh') and after

the attempted exchange reactions (**P1** and **P2**). They are depicted in Figure 4.40. The spectra seem to broaden, but especially for sample **P1**, defined transitions are still observed. Moreover, no significant rise of a plasmon band can be seen, indicating that after the reactions, the cluster core size was still quite small (below 25 Au atoms).

To gain more insight into the reaction process and the nature of the samples, STEM measurements were performed. The images after the reactions with 2-PET and GSH are shown in Figure 4.41 and 4.42, respectively.

For sample **3** of the reaction with 2-PET, the particle size was determined to be between 0.9-1.9 nm, with the majority of the clusters having a size around 1.1 nm. This suggests that the cluster core did not change upon addition of excess thiol, in contrast to what happened for the reaction in solution 4.1. Moreover, the sample still seemed well dispersed after the reaction.

(a) ABF image   (b) HAADF image
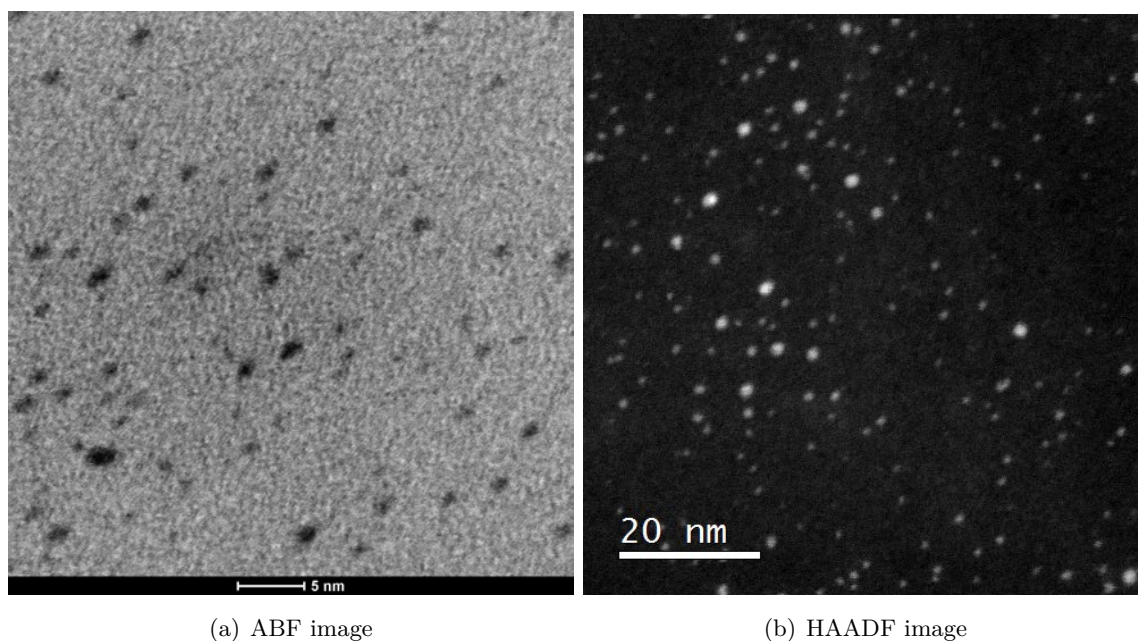
Figure 4.41.: STEM images of sample **P1**

For sample **4** of the reaction with GSH, the images seem of low quality, preventing clear identification of particles smaller than 1 nm. From the current image, it seems that the clusters were not stable upon reaction conditions. However, better images are required for confirmation.
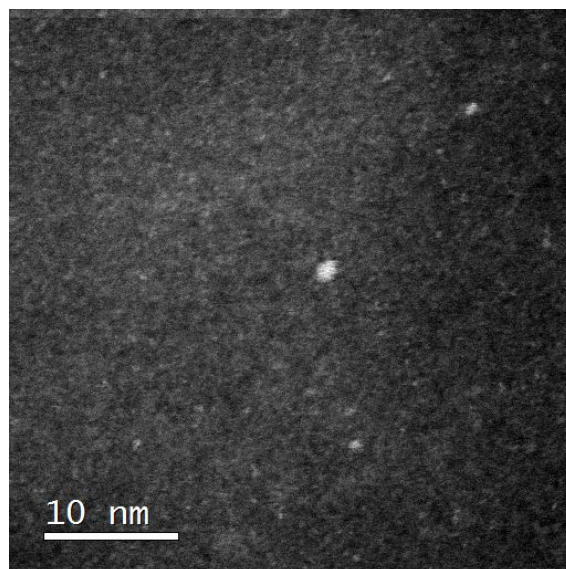
Figure 4.42.: HAADF-STEM image of sample **P2**

As the conducted sample analysis did not yield information about differences in the ligand shell before and after reaction, ICP-OES and ICP-MS will be carried out for determination. The optimization of the measurement process was still ongoing when the work on this thesis was finished, so no final result can be presented here. In addition, XPS measurements are performed in order to get information about the oxidation state of the Au atoms in the clusters. A more detailed discussion about the ligand exchange reactions on supported Au_{11} nanoclusters will thus be realized in future work.

4.3.3. Reactions of Al_2O_3 supported $Au_{11}(PPh_3)_7Cl_3$ with Thiol Ligands

For these reactions, the conditions were chosen according to the ligand exchange reactions in solution and with dropcast films on Al_2O_3 (see Chapters 4.1 and 4.2). The procedures are further described in Chapter 7.5.4.
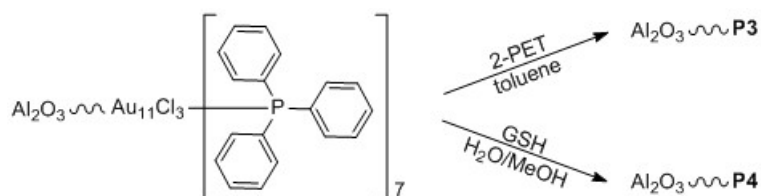
Figure 4.43.: Reaction of Al_2O_3 supported $Au_{11}(PPh_3)_7Cl_3$ with thiol ligands (2-PET and GSH)

The liquid phase, which was removed by filtration after stirring in the thiol solutions, was

collected for both reactions. In the case of addition of 2-PET, it was found to be completely clear and removal of toluene only gave minimum amounts of a white residue, indicating that the clusters remained on the support during reaction.

For the GSH sample, the solution phase was murky beige, obviously containing some fine solid parts. Thus, stability of the clusters upon reaction cannot be guaranteed for sample **P4**.

UV-Vis spectra of the dry powder samples were recorded before ('fresh') and after the reaction (**P3** and **P4**) and are shown in Figure 4.43. It can be seen that for both tested exchanges, the spectra seem to broaden and the observed features shift. This suggests that a polydisperse mixture might have been formed during reaction.
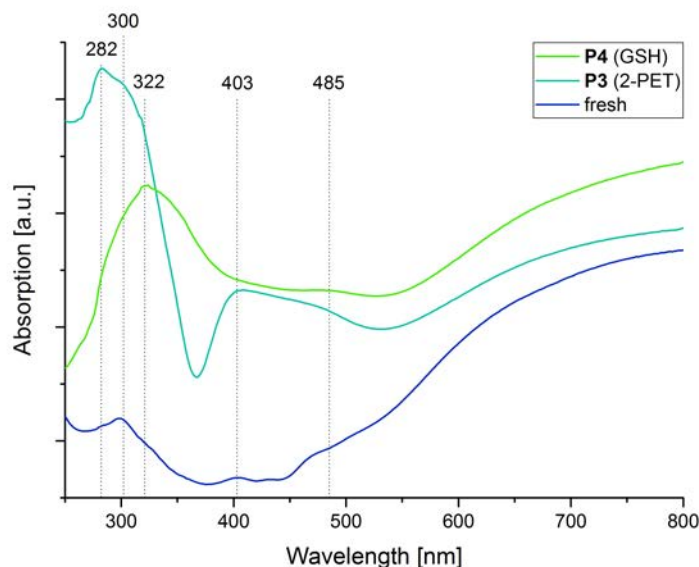
Figure 4.44.: UV-Vis spectra of Al_2O_3 supported $Au_{11}(PPh_3)_7Cl_3$ before and after reaction with exchange thiol (2-PET or GSH). Spectra are stacked for clarity.

However, based only on the UV-Vis spectra, it is difficult to evaluate what has really happened during the attempted ligand exchange. Thus, further analysis of the samples will be performed. This includes TEM and XPS measurements, as well as ICP-OES and ICP-MS. As the data collection was not finished when this thesis was completed, no definite results can be presented here. Therefore, the exact nature of the samples **P3** and **P4** will be discussed in future work.

4.3.4. Conclusions of First Attempts of Ligand Exchange Reactions of SiO$_2$ and Al$_2$O$_3$ Supported Clusters

Au$_{11}$(PPh$_3$)$_7$Cl$_3$ was successfully immobilized on two different metal oxide support materials (SiO$_2$ or Al$_2$O$_3$) by wet impregnation [102]. Characterization of the powder samples by UV-Vis and STEM assured that no aggregation had occurred.

First attempts of ligand exchange reactions were performed by stirring a suspension of the supported cluster with a solution of exchange thiol (2-PET or GSH). Distinct color changes were observed for all samples, indicating that some reaction must have happened. To get a better understanding of the process and products, further analysis will be carried out, including STEM, XPS, ICP-OES and ICP-MS. Preliminary evaluation of the STEM images of the samples on SiO$_2$ shows that the Au core size is preserved upon ligand exchange.

4.4. Conclusions of Ligand Exchanges of Au$_{11}$(PPh$_3$)$_7$Cl$_3$ with Thiol Ligands

Ligand exchange reactions of Au$_{11}$(PPh$_3$)$_7$Cl$_3$ with thiols were carried out in three different systems: dissolved clusters in solution, dropcast films on surfaces (Al$_2$O$_3$ or ZnSe) and clusters supported on powder metal oxides (SiO$_2$ or Al$_2$O$_3$). Two different kinds of thiol ligands were used, with one being soluble in organic solvents (2-PET) and one being soluble in H$_2$O (GSH).

For all tested systems, only partial ligand exchange was obtained. However, it could be shown that contrary to results for the solution system, when the cluster core size increased from Au$_{11}$ to Au$_{25}$, no major change in cluster size was observed for immobilized clusters. This might be due to the hindered mobility of Au$_{11}$ once it interacts with the support material. The reactions performed with the clusters in solid phase represent the first report of ligand exchange reactions with immobilized clusters.

5. Ligand Exchange from Au$_{15}$(SG)$_{13}$ to Au$_{20}$(SC$_2$H$_4$Ph)$_{16}$

During the ligand exchange of Au$_{15}$(SG)$_{13}$ with 2-phenylethanethiol, Au$_{20}$(SC$_2$H$_4$Ph)$_{16}$ was formed in high yield. This presents a novel, facile approach for synthesizing thiolate protected Au$_{20}$ nanoclusters. Characterization and structural investigations on Au$_{20}$(SC$_2$H$_4$Ph)$_{16}$ were carried out by UV-Vis, MALDI-MS and EXAFS.

5.1. Synthesis of Au$_{15}$(SG)$_{13}$

The synthetic procedure was equivalent to the one reported in [58]. Details can be found in Chapter 7.6.1.

Due to the fact that no column or electrophoresis system for the separation of H$_2$O soluble Au nanoclusters was available, the crude product could not be further purified. However, the recorded UV-Vis spectrum depicted in Figure 5.1 shows a band at 375 nm and a shoulder at 410 nm. These are in good agreement with spectral data published for Au$_{15}$(SG)$_{13}$ [58, 59, 103]. The absorption features are rather weak, which can be attributed to the presence of impurities in the crude product.
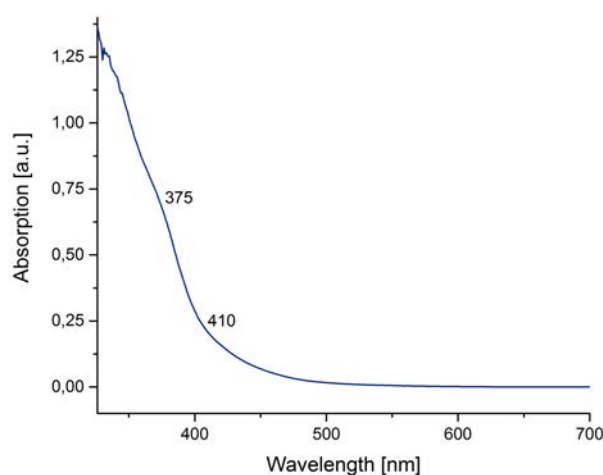
Figure 5.1.: UV-Vis spectrum of crude Au$_{15}$(SG)$_{13}$

5.2. Ligand Exchange to $Au_{20}(SC_2H_4Ph)_{16}$

For the ligand exchange, published protocols were considered [73, 104]. An excess of 2-phenyl-ethanethiol in a mixture of MeOH and DCM was used; the whole procedure can be found in Chapter 7.6.2.
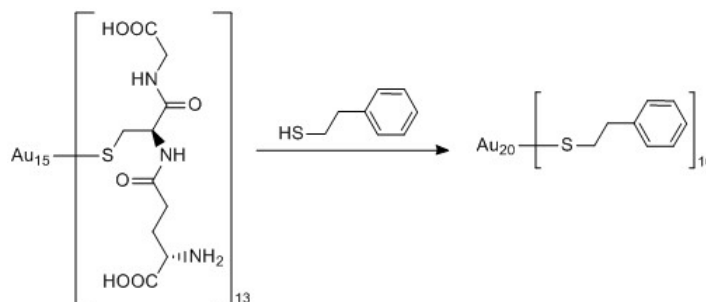
Figure 5.2.: Ligand exchange from $Au_{15}(SG)_{13}$ to $Au_{20}(SC_2H_4Ph)_{16}$

As can be seen in Figure 5.2, the core size was not maintained during the ligand exchange. It was reported previously that the obtained $Au_{20}(SC_2H_4Ph)_{16}$ is very stable under addition of an excess of thiol [61], whereas $Au_{15}(SG)_{13}$ is not [105]. Thus, it can be assumed that the reaction conditions were too harsh for Au_{15}, as 150 eq. of 2-PET, with reference to the molar amount of $Au_{15}(SG)_{13}$, were added. During the etching, a size-focusing process must have occurred, which yielded Au_{20}.

Figure 5.3 shows the UV-Vis spectra of the starting material and the obtained product after the reaction. A clear shift in the absorption features can be seen.
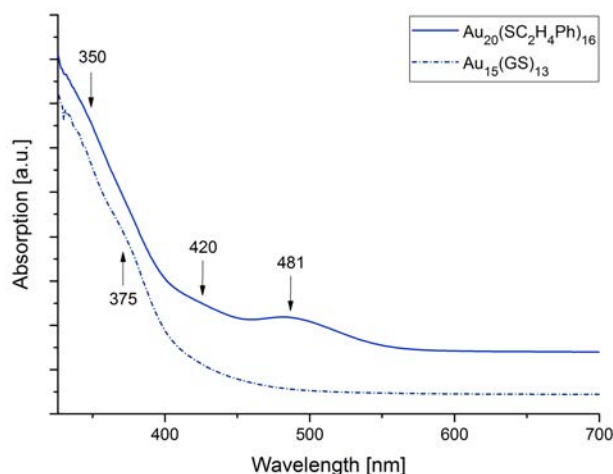
Figure 5.3.: UV-Vis spectra of starting material (Au_{15}) and product (Au_{20})

No ligand exchange from Au_{15} to Au_{20} has been reported in literature so far, therefore the mechanism of the reaction is not known. However, similar results (ligand exchange accompanied by growth of the cluster core) are obtained when reacting some triphenylphosphine-protected Au nanoclusters with excess thiols: $Au_{11}(PPh_3)_7Cl_3$ is known to yield Au_{25} clusters [31, 77, 78] (see also Chapter 4.1) and $Au_{55}(PPh_3)_{12}Cl_6$ reacts to Au_{75} [106]. Moreover, even a polydisperse mixture of Au nanoparticles protected by PPh_3 (size range 1–3.5 nm) forms the mixed ligand shell $[Au_{25}(PPh_3)_{10}(SC_2H_4Ph)_5Cl_2]^{2+}$ cluster [80, 81]. Different mechanisms have been suggested for ligand exchange reactions between PPh_3 and thiols, which are in detail discussed in Chapter 1.4.2 and 4.1. According to Tsukuda and coworkers, first a polydisperse mixture of different cluster sizes is formed [105], whereas Hutchison and Pintauer & Jin claim presence of Au(I)-species [79, 81]. However, it can be agreed on that a size focusing process occurs due to core etching, which gives the most stable cluster species under the present conditions as the main product [79, 81, 105].

Whether or not this concept is applicable to thiolate protected Au nanoclusters as well, still needs to be investigated. Gautier and Bürgi reported thiolate-for-thiolate exchange for Au_{15} nanoclusters, with no major influence on the core size being observed when carrying out the reaction under inert atmosphere. However, in the presence of O_2, drastic changes were detected. Therefore, a 2 step mechanism was proposed, with the first step being a rapid exchange of the ligands by radicals. This is followed by a core etching step, which may lead to alterations of the nanocluster size [107]. The second process is suggested to occur only under aerobic conditions and involve an Au(I)-(SR) species [107, 108].

It was also discovered that the cluster core sizes can decrease during ligand exchange. One possible synthesis of $Au_{20}(SPh\text{-}t\text{-}Bu)_{16}$ clusters is starting from Au_{25}^-, with a large excess of HSPh-t-Bu added and the mixture stirred at slightly elevated temperatures [63]. Similar proceedings were also observed for Au_{38} and HSPh-t-Bu, in that case yielding $Au_{36}(SPh\text{-}t\text{-}Bu)_{24}$. For the latter, the mechanism consists of four steps, with the first step being incomplete ligand exchange while maintaining the core size and the last one being size focusing through core-etching [109], in agreement with what was suggested by Gautier and Bürgi [107]. In between, distortion of the original Au_{38} core followed by a disproportion to Au_{36} and Au_{40} can be seen. At the end of the reaction, no Au_{40} clusters are left [109].

The proposed steps of rapid exchange followed by core etching seem reasonable for the present reaction too. First, a change in the color of the reaction mixture, paired with the formation of a yellow precipitate, was noticed even after 10 minutes. This suggests that the reaction was very fast in the beginning. After 8 hours, the solution appeared colorless again, but an orange precipitate had been formed. The latter is explained by the bad solubility of $Au_{20}(SC_2H_4Ph)_{16}$ in MeOH (the reaction was carried out in 1:1 mixture of MeOH:DCM). It is clearly indicated that the initially formed product was not the one obtained at the end of the reaction. However, as the yellow precipitate formed in the beginning was not isolated, it

remains unclear whether the surface ligands had already been completely exchanged at that time. The formation of $Au_{20}(SC_2H_4Ph)_{16}$ during the following core etching is explained by its extraordinary robustness in the presence of excess thiol [61].

When extracting the Au_{20} clusters out of the crude with DCM, small amounts of white precipitate remained, which could not be dissolved in MeOH, DCM or toluene. Thus, it is obvious that another Au species was present in the reaction mixture, as possible residual GSH had been washed out before. Further reaction studies need to be performed in order to identify the side product and get insight into mechanistic details and kinetics.

It should be noted that the presented ligand exchange reaction exhibits a valuable synthetic pathway for $Au_{20}(SC_2H_4Ph)_{16}$. Although Au_{20} clusters can be synthesized from $HAuCl_4 \cdot 3\,H_2O$ by reduction, it requires very precise control of the reaction conditions for the Au_{20} clusters to be formed preferential to the more stable Au_{25} analogues [61, 63]. As previously mentioned, a ligand exchange protocol starting with $Au_{25}(SC_2H_4Ph)_{18}^-$ has also been published, but is suffering from low yield (about $10\,\%$) [110].

The ligand exchange from $Au_{15}(SG)_{13}$ is therefore a quite attractive pathway, as the synthesis of the starting cluster is quite facile with about $40\,\%$ yield [58]. Purification of $Au_{15}(SG)_{13}$ is not necessary, as the crude product can be directly used for the following conversion to Au_{20}. Moreover, this next step requires no elaborate synthetic techniques, but just a large excess of exchange thiol (approximately $150\,$eq.) and moderate stirring at RT. After a short cleaning procedure, about $65\,\%$ of $Au_{20}(SC_2H_4Ph)_{16}$ can be obtained in high purity.

5.3. Characterization of $Au_{20}(SC_2H_4Ph)_{16}$

Figure 5.4a shows the UV-Vis spectrum of $Au_{20}(SC_2H_4Ph)_{16}$ after purification with SEC. A prominent feature at $481\,$nm and two shoulders at 350 and $420\,$nm are visible, which correspond well with reported data [61, 63].

To determine the optical energy gap of the compound, the spectrum was converted into a photon energy plot[a]. The intersection of the fitted asymptote after absorption onset (red dashed line in Figure 5.4b) with the abscissa indicates a band gap of $2.21\,$eV. This value is close to the $2.15\,$eV observed by Jin and coworkers [61]. It should be noted that the units of their ordinate were different due to the application of a Jacobinian factor, which could be responsible for the slight difference. Compared to $Au_{25}(SC_2H_4Ph)_{18}$ or $Au_{15}(SG)_n$ clusters encapsulated in cyclodextrin, which exhibit a HOMO–LUMO gap of $1.33\,$eV [114] and $1.75\,$eV [111], respectively, the value for $Au_{20}(SC_2H_4Ph)_{16}$ is significantly larger.

---

[a]Although it seems common practice in literature to correct the absorption values with a Jacobinian factor [61, 111, 112], this was objected due to mathematical incorrectness when concerning absorption spectra [113].
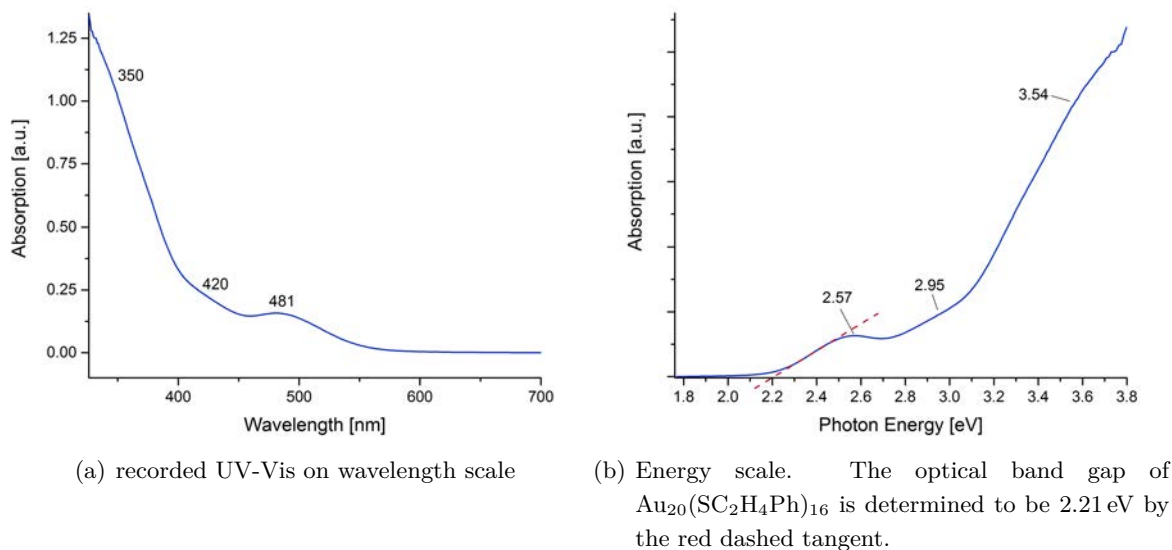
(a) recorded UV-Vis on wavelength scale

(b) Energy scale. The optical band gap of $Au_{20}(SC_2H_4Ph)_{16}$ is determined to be $2.21\,eV$ by the red dashed tangent.

Figure 5.4.: Optical spectra of $Au_{20}(SC_2H_4Ph)_{16}$

As a result, a highly symmetrical structure for the Au_{20} cluster is indicated. According to calculations by Li *et al.*, the unstabilized Au_{20} core adapts a tetrahedral geometry, which is close to the one of a small bulk gold fragment. Furthermore, their photoelectron spectroscopic studies also revealed a big HOMO–LUMO gap of $1.77\,eV$ [115]. Recently, the crystal structure of $Au_{20}(TBBT)_{16}$ (with TBBT standing for *tert*-butylbenzothiol, -SPh-*t*-Bu) was reported, indeed confirming that the inner Au_7 core is built out of two tetrahedra, sharing one gold atom. The kernel is protected by two monomeric staples (S(R)-Au-S(R); R standing for -Ph-*t*-Bu) and one trimeric staple (S(R)-Au-S(R)-Au-S(R)-Au-S(R)), and furthermore by a $[Au\text{-}S(R)]_8$ ring connected with the core through Au-Au bonds [110]. The structure is displayed in Figure 5.5.
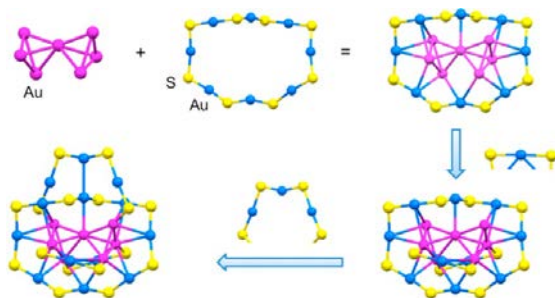
Figure 5.5.: Structure of $Au_{20}(TBBT)_{16}$. The cluster is built out of a Au_7 core, a $[Au\text{-}S(R)]_8$ ring, two monomeric staples and one trimeric staple. Reproduced from [110].

Previously, calculations of Pei *et al.* predicted a prolate structured Au_8 kernel, consisting out of two Au_4 tetrahedra connected on the edges. Moreover, they also prognosticated the

existence of four trimeric staple motives (S(R)-Au-S(R)-Au-S(R)-Au-S(R)) in the structure of Au_{20} clusters [116], which is displayed in Figure 5.6. Their structures showed good agreement with the spectral data obtained by Jin and coworkers [61, 116]. A prolate-structured Au_8 fcc core, protected by four level-3 staples was also independently predicted by Jiang *et al.* [117].
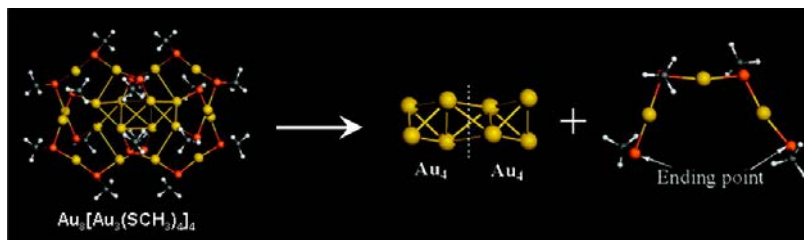
Figure 5.6.: Predicted structure of $Au_{20}(SCH_3)_{16}$. The cluster is built out of an Au_8 core protected by four trimeric staples. Yellow: Au; red: S; black: C; white: H. Adapted from [116].

As these two types of structures are quite different, Dimuthu *et al.* very recently performed computations to study the influence of the ligand (aliphatic vs. aromatic) on the structure of $Au_{20}(SR)_{16}$. According to their results, it is likely that $Au_{20}(SC_2H_4Ph)_{16}$ will have a very similar geometry as $Au_{20}(TBBT)_{16}$ [118]. It should be noted that no crystal structure of $Au_{20}(SC_2H_4Ph)_{16}$ has been published so far.

In order to get some more insight into the structure of the synthesized Au_{20} cluster, extended X-ray absorption fine structure (EXAFS) spectra were measured at the SuperXAS beamline of the Swiss Light Source (SLS) synchrotron at Au L3-edge. XAFS is a valuable tool for structure determination, as information about e.g. bond lengths, oxidation state, coordination number and surrounding atoms can be obtained [119]. It has been used for characterization of Au nanoclusters by several groups, for example to study influences on the structure of $Au_{25}(SR)_{18}$ [120] and $Au_{19}(SR)_{13}$ [121] or the effects of the removal of the thiol ligands from Au_{38} [13]. As the data treatment and fitting process is still ongoing, no final result can be presented here. The preliminary evaluation presented in Figure 5.7a shows quite high resolution, which assures the purity of the sample. Moreover, the spectrum shows features comparable to those of Au nanoclusters of similar size [121]; see Figure 5.7b and c.
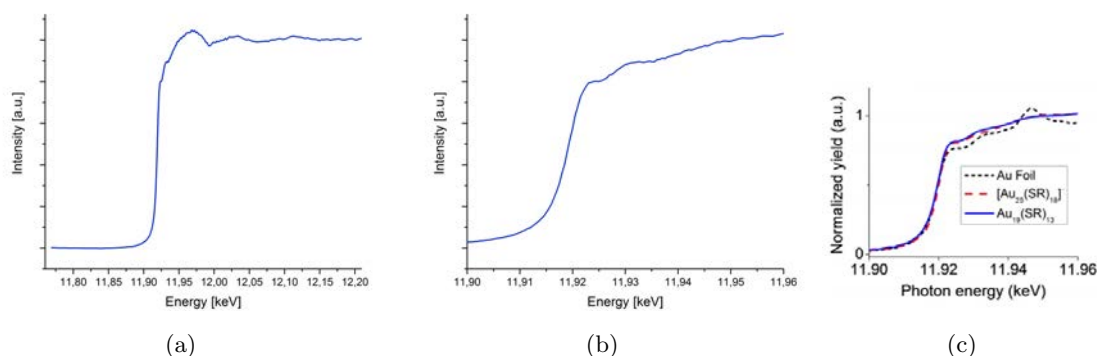
Figure 5.7.: (a) Preliminary evaluated EXAFS spectrum of $Au_{20}(SC_2H_4Ph)_{16}$ (b) Enlarged EX-AFS spectrum in the area from 11.90 to 11.96 keV for better comparison with the literature spectra (c) XANES spectra of $[Au_{25}(SR)_{18}]^-$ (blue), $Au_{19}(SR)_{13}$ (red) and gold foil (black). Reproduced from Chevrier *et al.* [121].

The MALDI-MS spectrum in Figure 5.8 proves that complete ligand exchange from GSH to 2-PET occurred, as no peaks of clusters containing GSH can be observed. The fragments which give rise to the most intense features are shown; a more detailed list can be found in Chapter 7.6.2. Loss of $Au(SC_2H_4Ph)$ (334 Da) is observed, which is a common feature of thiolate-protected Au nanoclusters [93].
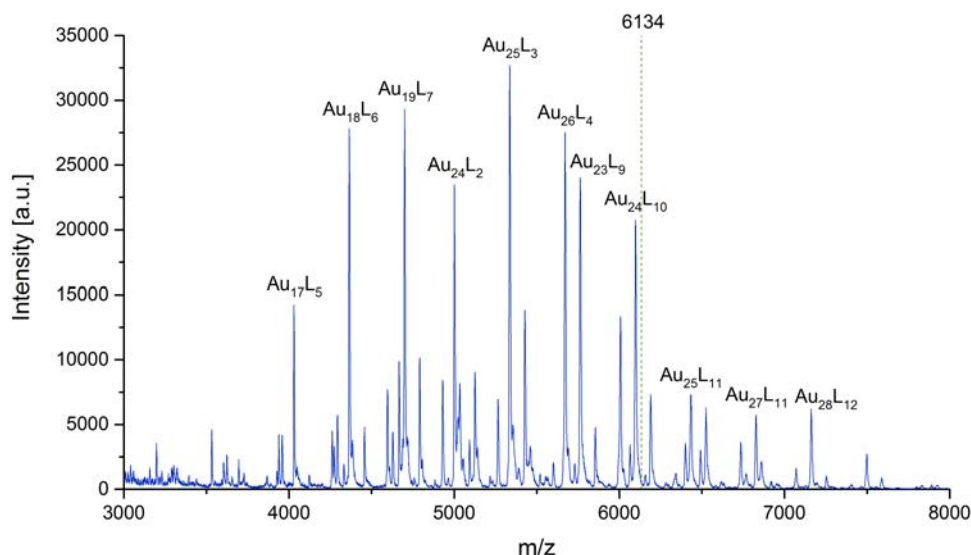
Figure 5.8.: MALDI-MS spectrum of $Au_{20}(SC_2H_4Ph)_{16}$. L is equal to $-SC_2H_4Ph$. The dashed green vertical line marks the molecular weight of $Au_{20}(SC_2H_4Ph)_{16}$ (6134 Da).

However, the mass peak of $Au_{20}(SC_2H_4Ph)_{16}$ cannot be identified, as indicated in Figure

5.8. Moreover, the spectrum shows a lot of both fragmentation and aggregation. It is therefore likely that the sample degrades during the ionization process. This assumption is supported by the EXAFS spectra from the very same sample recorded at SLS synchrotron, which showed high resolution. Thus, it can be stated that the $Au_{20}(SC_2H_4Ph)_{16}$ was quite pure. The same is suggested by the well defined UV-Vis features visible in Figure 5.4.

It should also be noted that the only published ESI-MS spectrum of $Au_{20}(SC_2H_4Ph)_{16}$ also showed both fragmentation and aggregation. However, in that case it was possible to detect an intense $[M+Cs]^+$ adduct [61].

Hence, it is concluded that the conditions of the MS measurements were not suitable for the sample. A particularly soft ionization process seems to be necessary to detect stable Au_{20} cluster ions. Using another MALDI matrix than the commonly used DCTB for thiolate-protected Au nanoclusters [93] might give a better result.

5.4. Conclusions of Ligand Exchange to $Au_{20}(SC_2H_4Ph)_{16}$

$Au_{20}(SC_2H_4Ph)_{16}$ could be synthesized from crude $Au_{15}(SG)_{13}$ in a ligand exchange reaction. The large excess of 150 eq. of added exchange ligand, 2-phenylethanethiol, yielded Au_{20} clusters through core etching. $Au_{20}(SC_2H_4Ph)_{16}$ is reported to be very stable under such conditions [61]. UV-Vis and MALDI-MS analysis assured the presence of complete ligand exchanged Au_{20}. The ligand exchange procedure described within this thesis is therefore a useful pathway to synthesize $Au_{20}(SC_2H_4Ph)_{16}$, as published procedures are quite demanding [61, 63].

Further studies need to be done to investigate mechanism and kinetics of the ligand exchange process. *In-* and *ex-situ* spectroscopic methods (UV-Vis, MS, FTIR, NMR) will be used. Furthermore, the structure of Au_{20} has been studied by EXAFS spectroscopy, with preliminary data being already available and showing high resolution. In addition, the conditions of the MALDI-MS analysis need to be optimized in order to obtain spectra with less fragmentation.

6. Conclusions and Outlook

In this thesis, new and optimized protocols for the synthesis of $Au_{11}(PPh_3)_7Cl_3$ were developed, leading to cluster samples of high purity. Stability studies of Au_{11} in THF showed rapid conversion to an unidentified compound **A**, which was also identified as a by-product during the synthesis of Au_{11}. Preliminary analysis suggests a Au_{11} nanocluster with $O=PPh_3$ ligands as the most likely structure of compound **A**.

Reaction of $Au_{11}(PPh_3)_7Cl_3$ in solution with an excess of 2-phenylethanethiol led to partial ligand exchange and formation of the mixed ligand shell cluster $[Au_{25}(PPh_3)_{10}(SC_2H_4Ph)_5Cl_2]^{2+}$. No fully thiolate protected clusters could be obtained upon varying the conditions, indicating high stability of the Au_{25} cluster structure.

Ligand exchange reactions with $Au_{11}(PPh_3)_7Cl_3$ immobilized on planar Al_2O_3 and ZnSe surfaces represent the great challenge of the current work. Different routes were designed and analyzed, using spectroscopic techniques to evaluate the reaction pathways and to get preliminary mechanistic insights. It has been observed that parameters such as the chemical nature of the surface, the type of exchange ligand and the solvent strongly affect the reactions of immobilized clusters. Better performance has been achieved using the water soluble thiol L-glutathione, as compared to reactions in organic media.

A first analysis by PM-IRRAS indicated modifications of the structure of $Au_{11}(PPh_3)_7Cl_3$, as clear changes in the spectral features were observed. This included the detection of characteristic vibrations of the exchange thiol ligand, as well as shifts of the triphenylphosphine bands. Corresponding results were obtained by *in-situ* ATR-IR measurements acquired during the ligand exchange, with significant changes in the CH-stretching region being visible within the first two hours.
MALDI-MS confirmed maintenance of the number of Au atoms in the cluster core and exchange of 1-2 ligands for glutathione. This is very different to the reactions in solution, which led to formation of $[Au_{25}(PPh_3)_{10}(SR)_5Cl_2]^{2+}$.

The reaction studies of immobilized Au nanoclusters present a breakthrough in studies of ligand exchange properties of Au nanoclusters, as previous research has mainly focused on solution systems with dissolved clusters. This work is the first one focusing on ligand exchange of clusters in solid state and provides the basis for further in-depth investigations.

Future studies are planned to focus on the reaction mechanism and the optimization of the reaction parameters, in order to obtain a fundamental understanding of the nature of the interaction between Au clusters and support materials. Therefore, specific reaction design and complex characterization techniques will be required to monitor the reactions. A first step was already achieved herein by examining ligand exchange for clusters immobilized on high surface area metal oxide powders.

This may finally lead to a rational design of monodisperse clusters with defined catalytic surfaces and properties. A fascinating route would be control of chirality via chiral (thiol) ligands, enabling enantioselective catalysis by Au nanocluster catalysts.

7. Experimental Section

7.1. General Remarks

7.1.1. Usage of Chemicals and Glassware

When the purity of the reagents and solvents could be ensured, they were used without further treatment. If this was not the case, solvents were distilled and solid compounds recrystallized prior to use. A Merck Simplicity system was available for producing nanopure water ($18.2\,M\Omega$). Laboratory glassware was rinsed thoroughly with aqua regia, Milli-Q water and acetone before usage to avoid contamination.

7.1.2. Chromatographic Methods

Size-exclusion chromatography (SEC) was done in glass columns filled with Bio-Beads S-X1 Support (company Bio-Rad). THF or toluene were used as solvents.

7.1.3. Methods of Analysis

For recording UV-Vis spectra in liquid phase, a PerkinElmer 750 Lambda and a Varian Cary 50 Bio spectrometer were used. Measurements were done in quartz glass cuvettes with a path length of $1\,cm$. The solvent varied depending on the nature of the sample; DCM, toluene, THF, MeOH and chloroform were all used.

Measurements in solid phase were done with a PerkinElmer 750 Lambda spectrometer with an integrating sphere with an inner diameter of $60\,mm$. Spectra were collected in diffuse transmittance mode at an angle of $0\,°$. Quartz glass cuvettes with a path length of $1\,cm$ or $0.5\,cm$ were used.

In both cases, the spectra were collected at room temperature between wavelengths of 250 and $800\,nm$.

Matrix-assisted laser desorption ionization mass spectra (MALDI-MS) were recorded on a prototype Axima MALDI TOF^2 (time-of-flight (TOF)/reflectron time-of-flight (RTOF)) MS (company Shimadzu, Kratos Analytical) and a Bruker Autoflex mass spectrometer. Both spectrometer were equipped with a nitrogen laser and measurements were accomplished operating at near treshold laser irradiances in positive linear mode. The matrices used were *trans*-2-[3-(4-*tert*-Butylphenyl)-2-methyl-2-propenylidene]malononitrile (DCTB) and 2',4',6'-Trihydroxyacetophenone Monohydrate (THAP). The ratio of analyte:matrix was

between 1:10 and 1:100 and various solvents (DCM, chloroform, methanol) were used depending on the nature of the sample. The spectra were recorded in raster mode with single laser pulses ($\lambda = 337\,nm$ at $50\,Hz$) and later averaged (between 300 and 600 spectra) to give the MS spectra displayed within this thesis. All measurements were performed through collaborations with Dr. Ernst Pittenauer (Institute of Chemical Technologies and Analytics, TU Wien) or the SMS forum (UniGe).

Nuclear magnetic resonance (NMR) spectra were measured on a Bruker Avance-250 spectrometer at $250\,MHz$ (^{1}H) or at $101.20\,MHz$ (^{31}P). For ^{1}H, the chemical shift is reported in parts per million from the standard tetramethylsilane (TMS), when using the protio-solvent peak as a internal reference. For ^{31}P, the shift is given in parts per million from $85\,\%$ phosphoric acid. Data treatment was done with TopSpin (company Bruker). The solvent used was deuterated chloroform (CDCl$_3$).

Attenuated total reflection infrared spectra (ATR-IR) were recorded on a Bruker Vertex 70 FTIR spectrometer equipped with a liquid nitrogen cooled MCT detector. A commercially available ATR flow cell (company Specac) was used, which is depicted in Figure 7.10. A ZnSe crystal (52(48) mm x 20 mm x 2 mm) was used, where the sample was dropcasted on with EtOH or H$_2$O. All spectra were recorded at room temperature with a resolution of $4\,cm^{-1}$. The covered spectral range was from 4000 to $450\,cm^{-1}$. For the *in-situ* measurements of the ligand exchange, a solution of GSH in 8:2 H$_2$O/EtOH was flowed through the cell at low speed (0.05 ml/min) over a period of 8 h using a peristaltic pump.

Polarization-modulation infrared reflection-absorption spectroscopy (PM-IRRAS) was performed at the Department of Physical Chemistry in the research group of Prof. Bürgi (UniGe), using a Bruker Tensor 27 FT-IR spectrometer, which external beam port was connected to a Bruker PMA 50 unit. Modulation of the polarized light was achieved with a photoelastic modulator (PEM) PEM 90 (company Hinds) at $50\,Hz$. For the demodulation of the polarization modulation (PM) signal, a Stanford Research SR830 DSP lock-in amplifier (LIA) was used. The spectrometer was equipped with a liquid nitrogen cooled D313/Q MCT detector. The samples were mounted with an IRRAS sample holder in the sample compartment within the Bruker PMA 50 unit. A High Pass Filter with a cut-off at $3800\,cm^{-1}$ was used for the measurements. All spectra were recorded at room temperature with a resolution of $4\,cm^{-1}$ and an angle of $80°$ between sample and detector. Data treatment was done in OPUS (company Bruker).
Small alumina plates were used as sample holders. To remove any contamination and obtain a clean and smooth surface, the plates were polished with Metadi Diamond Polishing Compound (1 and 1/4 micron, company Buehler) on a 10" Buehler microcloth. The plates were then rinsed with EtOH before usage. A plain alumina plate was used as reference for all measurements. The samples were later dropcasted (solvent DCM) centrally on the plates and let dry for at least 5 h before PM-IRRAS was recorded. The same position on the plate

was chosen for all measurements.

High-angle annular dark-field (HAADF) and annular bright field (ABF) imaging was done at the University Service Center for Transmission Electron Microscopy (USTEM) of TU Wien with help of Dr. Michael Stöger-Pollach. A FEI Tecnai F20 S-TWIN analytical (scanning) transmission electron microscopy [(S)TEM] instrument at an accelerating voltage of 200 kV was used. An energy resolution of approximately 1 eV and a spatial resolution of approximately 0.5 nm could be achieved. The sample was dispersed in a small amount of EtOH and one drop placed on the copper grid of the sample holder. Analysis of the particle size was done with ImageJ.

Extended X-ray absorption fine structure (EXAFS) spectra were recorded at the Super XAS beamline at the Swiss Light Source (SLS) synchrotron. The intensity of the x-ray beam provided by a Super Bend magnet (2.9 T) was around $6 \cdot 10^{11}$ photons per second. Spectra were measured at Au L3-edge (11.919 keV) using a Si(111) channel-cut monochromator. A collimating mirror coated with silicon and a toroidal mirror coated with rhodium, both installed at 2.8 mrad, were used for focusing and elimination of higher harmonics. The incident x-rays then had a spot size of 0.3 x 0.3 mm. Collection of the fluorescence signal was achieved by a five-element SDD detector (SGX). The sample was dropcasted on Kapton tape (polyimide) and cooled to liquid N_2 temperature with a cryo-gun. The Ifeffit software is used for data treatment [122].

7.2. Synthesis of Au$_{11}$(PPh$_3$)$_7$Cl$_3$

$$HAuCl_4 \cdot 3\,H_2O + exs.\ PPh_3 \xrightarrow[\text{2. NABH}_4]{\text{1. TOAB}} Au_{11}(PPh_3)_7Cl_3$$
$$393.83 \qquad\qquad\qquad\qquad\qquad\qquad 4109.05$$
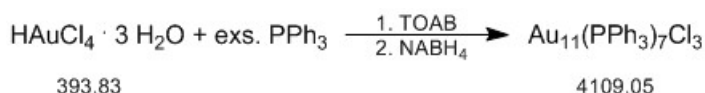
Figure 7.1.: Synthesis of Au$_{11}$(PPh$_3$)$_7$Cl$_3$

The synthesis of Au$_{11}$(PPh$_3$)$_7$Cl$_3$ nanoclusters was based on previously reported procedures [31, 53, 123]. 1 eq. of HAuCl$_4$ $\cdot$ 3 H$_2$O (500 mg, 1.27 mmol) and 1.2 eq. of tetraoctylammonium bromide (TOAB) (833 mg, 1.52 mmol) were dissolved in 50 ml of THF, resulting in an orange solution. While the reaction mixture was stirred at RT at slow speed, 5 eq. of triphenylphosphine (TPP or PPh$_3$) (1165 mg, 6.35 mmol) were added, giving a clear colorless solution after just a few seconds. Low speed stirring at RT was continued for another hour. Then, the speed was increased to around 500 rpm and 10 eq. of NaBH$_4$ (480 mg, 12.70 mmol) were added in 10 ml ice-cold H$_2$O. This resulted in a color change to brown and the evolution of H$_2$ gas, visible through bubbling at the beginning of the reduction process. The mixture was then stirred at RT at high speed for 48 h. During that time, the solution

turned reddish-brown and white precipitate (phase transfer catalyst and/or residues from NaBH$_4$) was formed.

The solvent was removed by rotavapory evaporation at 20 °C and the reddish-brown precipitate washed with H$_2$O three times. Afterwards, the crude mixture was extracted with cold THF (fridge temperature, around 5 °C) to remove the formed by-product and the phase-transfer catalyst. As Au$_{11}$(PPh$_3$)$_7$Cl$_3$ is not stable in solution for a long time, even at RT [31], cleaning with cold solvents is crucial. The extraction progress was followed by measuring UV-Vis, with the brown side-product showing a prominent band at 411 nm. Once the absorption shifted to 420 nm, marking beginning elution of Au$_{11}$(PPh$_3$)$_7$Cl$_3$, fridge-cold DCM was used for further extraction. Again, the process was followed by UV-Vis (bands at 383 and 422 nm). The solvent was then removed by rotary evaporation at 20 °C, which yielded around 195 mg (40 % of the theoretical yield) of Au$_{11}$(PPh$_3$)$_7$Cl$_3$ as a red solid.

The compound was stored at -20 °C. Characterization was done by UV-Vis, ATR-IR, MALDI-MS, ^{1}H and ^{31}P-NMR. Details of the optimization and analysis of the synthetic procedure is given in Chapter 3. The UV-Vis and ATR-IR spectra are displayed in A.1, the other spectra can be found in Chapter 3.

^{1}H-NMR (250 MHz, CDCl$_3$): δ [ppm] = 7.38 (br t, 2H, CH, H^{ortho}), 6.89 (t, J$_3$ = 7.2 Hz, 1H, CH, H^{para}), 6.60 (t, J$_3$ = 7.6 Hz, 2H, CH, H^{meta})

^{31}P-NMR (101.20 MHz, CDCl$_3$): δ [ppm] = 52.8 (s, 1P)

UV-Vis (CH$_2$Cl$_2$): λ$_{max}$ [nm] = 293 (shoulder), 309, 383, 422, 515 (shoulder)

MALDI-MS (matrix: DCTB, solvent: DCM): m/z = 3894 [Au$_{11}$P$_6$Cl$_2$·CH$_2$Cl$_2$]$^+$, 3632 [Au$_{11}$P$_5$Cl$_2$·CH$_2$Cl$_2$]$^+$, 3617 [Au$_{11}$P$_5$Cl$_2$·2Cl]$^+$, 3370 [Au$_{11}$P$_4$Cl$_2$·CH$_2$Cl$_2$]$^+$, 3356 [Au$_{11}$P$_4$Cl$_2$·2Cl]$^+$, 3109 [Au$_{11}$P$_3$Cl$_2$·CH$_2$Cl$_2$]$^+$, 3094 [Au$_{11}$P$_3$Cl$_2$·2Cl]$^+$, 3080 [Au$_9$P$_5$]$^+$, 2961 [Au$_8$P$_5$Br]$^+$, 2897 [Au$_9$P$_4$Br]$^+$, 2833 [Au$_{11}$P$_2$Cl$_2$ · 2Cl]$^+$, 2818 [Au$_9$P$_4$]$^+$, 2700 [Au$_8$P$_4$Br]$^+$, 2621 [Au$_8$P$_4$]$^+$, 2556 [Au$_9$P$_3$]$^+$, 2439 [Au$_8$P$_3$Br]$^+$, 2424 [Au$_7$P$_4$]$^+$, 2360 Au$_{12}$$^+$ core or [Au$_8$P$_3$]$^+$, 2304 [Au$_{10}$PCl$_2$]$^+$, 2294 [Au$_9$P$_3$]$^+$, 2178 [Au$_8$P$_2$Br]$^+$, 2163 Au$_{11}$$^+$ core or [Au$_7$P$_3$]$^+$, 2030 [Au$_5$P$_4$]$^+$; with P = PPh$_3$

ATR-IR (ZnSe crystal): $\tilde{\nu}_{max}$ [cm^{-1}] = 3090 (w) CH$_{arom}$ stretch., 3075 (m) CH$_{arom}$ stretch., 3056 (m) CH$_{arom}$ stretch., 3021 (w) CH$_{arom}$ stretch., 3010 (w) CH$_{arom}$ stretch., 2991 (w) CH$_{arom}$ stretch., 2954 (s) CH$_{arom}$ stretch., 2921 (s) CH$_{arom}$ stretch., 2871 (m) CH$_{arom}$ stretch., 2851 (s) CH$_{arom}$ stretch., 1598 (w) n.a., 1572 (w) n.a., 1482 (m) CC$_{arom}$, 1467 (m) n.a., 1459 (w) n.a., 1435 (s) CC$_{arom}$ stretch., 1398 (w, br) n.a., 1376 (w) n.a., 1332 (w) CH$_{arom.}$ ip-bend./HCP ip-bend., 1308 (m) n.a., 1192 (s) HCC$_{arom.}$ ip-bend., 1162 (m) HCC$_{arom.}$ ip-bend., 1097 (m) PC stretch., 1068 (m) CC$_{arom.}$ stretch./HCC$_{arom.}$ ip-bend., 1028 (m) CH$_{arom.}$ op-bend, 997 (m) CC$_{arom.}$ stretch./HCCH$_{arom.}$ tors., 976 (m) n.a.

(a) solid (b) DCM solution
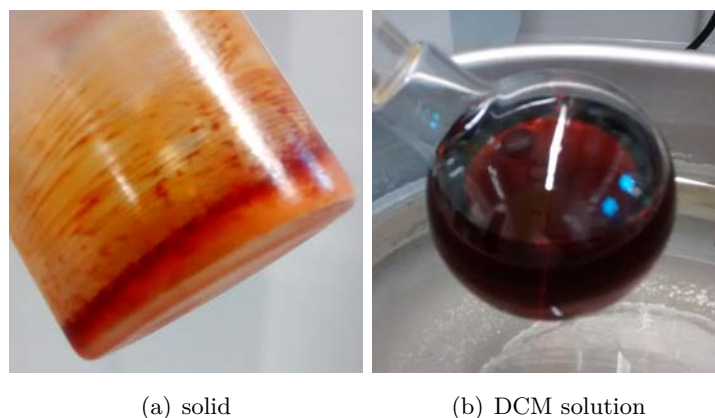
Figure 7.2.: Colors of $Au_{11}(PPh_3)_7Cl_3$

7.2.1. Isolation of Compound A
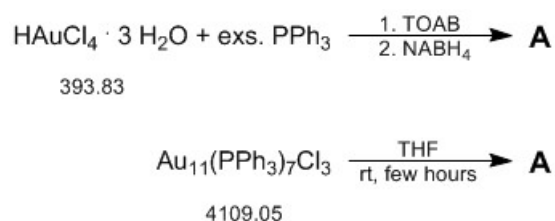
Figure 7.3.: Formation Pathways of Compound **A**

Compound **A** was isolated as another product in the synthesis of $Au_{11}(PPh_3)_7Cl_3$ (see Chapter above). It was extracted from the crude product mixture with cold THF. As the phase-transfer catalyst was also dissolving in this step, further purification was necessary. One possibility would be size exclusion chromatography, as the elution of the brown product is easily visible. Another option is dissolving the crude in a minimum amount of MeOH at $60\,°C$. Brown precipitate is formed after two days in the fridge and can be separated by filtration and washing with cold MeOH.

It was also shown that **A** is formed when a concentrated solution of $Au_{11}(PPh_3)_7Cl_3$ in THF is kept at RT for a few hours.

Characterization was done with UV-Vis, ^{31}P-NMR and MALDI-MS. The spectra are shown in Chapter 3.4, a brief summary is given here.

UV-Vis (THF): λ_{max} [nm] = 296 (small shoulder), 321, 411, 490 (shoulder)

^{31}P-NMR (101.20 MHz, CDCl$_3$): δ [ppm] = 29.1 (s, 1P)

MALDI-MS (matrix: DCTB, solvent: THF): m/z = 3784 [Au$_{11}$P$_3$R$_3$]$^+$, 3719 [Au$_{12}$P$_2$R$_3$]$^+$, 3625 [Au$_{13}$P$_3$R]$^+$, 3507 [Au$_{11}$P$_3$R$_2$]$^+$, 3454 [Au$_{12}$PR$_3$]$^+$, 3246 [Au$_{11}$P$_2$R$_2$]$^+$, 3193 [Au$_{12}$R$_3$]$^+$, 2969 [Au$_{11}$P$_2$R$_1$]$^+$, 2915 [Au$_{12}$PR]$^+$, 2719 [Au$_{11}$R$_2$]$^+$, 2709 [Au$_{11}$PR]$^+$, 2443 [Au$_{11}$R]$^+$, 2432 [Au$_{11}$P]$^+$, 2038 [Au$_9$P]$^+$; with P = PPh$_3$ and R = PPh$_3$O

7.2.2. Stability Test of Au$_{11}$(PPh$_3$)$_7$Cl$_3$ in THF

To obtain information about the stability of Au$_{11}$(PPh$_3$)$_7$Cl$_3$ in THF, a concentrated solution was prepared. It was left in air at RT for 6 d and UV-Vis spectra were measured after 1.5, 3 and 24 h, and then after every additional 24 h. The spectra are displayed in Chapter 3.5. The color intensified during the experiment, which is shown in Figure 7.4.

UV-Vis (THF, 0 h): λ_{max} [nm] = 293 (shoulder), 309, 383, 422, 515 (shoulder)
UV-Vis (THF, 1.5 h): λ_{max} [nm] = 293 (shoulder), 315, 415, 510 (shoulder)
UV-Vis (THF, 3 h): λ_{max} [nm] = 293 (small shoulder), 316, 412, 510 (shoulder)
UV-Vis (THF, 1-4 d): λ_{max} [nm] = 295 (small shoulder), 318, 411, 490 (shoulder)
UV-Vis (THF, 5-6 d): λ_{max} [nm] = 318 (broad), 411 (broad)

(a) 0 h   (b) 6 d
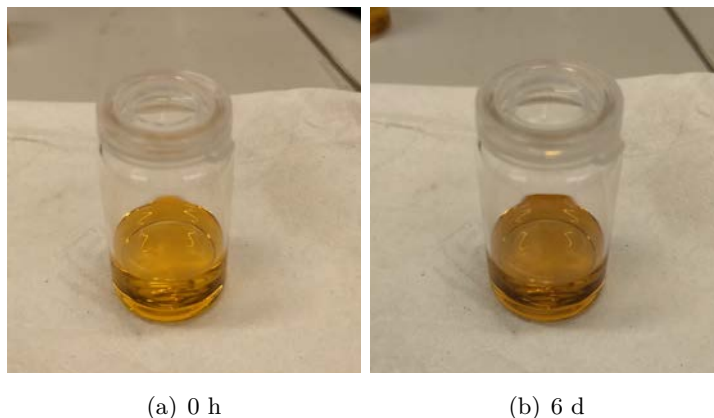
Figure 7.4.: Color change during the stability test of Au$_{11}$(PPh$_3$)$_7$Cl$_3$ in THF

7.3. Ligand Exchange of Au$_{11}$(PPh$_3$)$_7$Cl$_3$ in Solution

7.3.1. Ligand Exchange with 2-PET to [Au$_{25}$(PPh$_3$)$_{10}$(SC$_2$H$_4$Ph)$_5$Cl$_2$]$^{2+}$
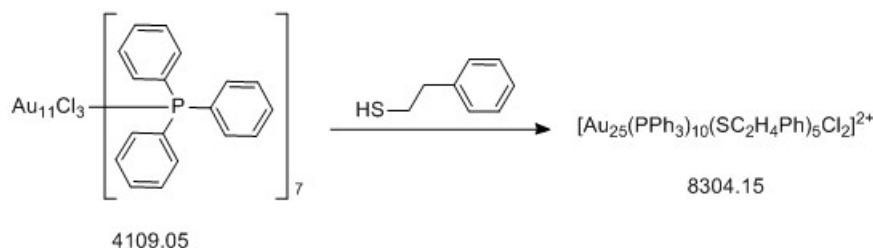
Figure 7.5.: Ligand Exchange of Au$_{11}$(PPh$_3$)$_7$Cl$_3$ with 2-PET in solution

The ligand exchange was conducted similarly to previously reported procedures [36, 75, 76, 78, 79]. Different conditions were tried (solvents, temperature, amount of 2-PET, reaction time), however, the same product was obtained for all reactions. The protocol described in the following was the one for reaction **4**, the parameters for all conducted reactions are summarized in Table 7.1. The other reactions were conducted analogously (except no reflux for reaction **1** and **2**). Reaction **3** and **4** were conducted during a scientific stay in the research group of Prof. Bürgi (UniGe).

Table 7.1.: Conditions of the ligand exchange reactions with Au(PPh$_3$)$_7$Cl$_3$ and 2-PET in solution

No.	mg Cluster	eq. 2-PET	Solvent	Temp.
1	10	5	20 ml DCM	RT
2	10	10	20 ml DCM	RT
3	12	100	15 ml DCM	40 °C
4.1	15	75	15 ml CHCl$_3$	50 °C
4.2	*	75	15 ml CHCl$_3$	50 °C

*Reaction **4.2** started with the end product of reaction **4.1** (see also description in the text).

In a typical ligand exchange procedure, 1 eq. of Au(PPh$_3$)$_7$Cl$_3$ (14.7 mg, 3.6 · 10^{-3} mmol) was dissolved in 15 ml of CHCl$_3$ and the mixture was heated up to 50 °C. Then, 75 eq. of 2-PET (36 μl, 0.27 mmol) were added and the reaction stirred for 24 h under reflux. Even after only 15 min, a color change to green was visible.

After the 24 h, the reaction was stopped by cooling down and evaporation of the solvent. The precipitate was washed with hexane three times to remove free ligands (PPh$_3$ and

2-PET). It was then redissolved in 15 ml of CHCl$_3$ and heated up to 50 °C again. Further 75 eq. of 2-PET (36 µl, 0.27 mmol) were added and the reaction pursued for 22 h. However, this step was found to be unnecessary, as no change in the obtained product was noticed, which means that the reaction had already been complete after the first 24 h. The produced [Au$_{25}$(PPh$_3$)$_{10}$(SC$_2$H$_4$Ph)$_5$Cl$_2$]$^{2+}$ was found to be quite stable, as the UV-Vis spectrum changed only little and MALDI-MS confirmed its purity even after the second day of heating in CHCl$_3$.

300 µl aliquots were taken at defined times and UV-Vis spectra recorded immediately in DCM (same solvent for all tried reactions). The solvent was then evaporated and the precipitate washed three times with hexane to remove excess thiol. The crude mixture was then extracted with toluene and in addition with MeOH. The toluene fraction was also purified with SEC. The main product [Au$_{25}$(PPh$_3$)$_{10}$(SC$_2$H$_4$Ph)$_5$Cl$_2$]$^{2+}$ was found to be in the MeOH fraction, which did not contain any other impurities (see MALDI-MS).

UV-Vis and MALDI-MS spectra were measured of all samples to determine the reaction progress. The spectra and a detailed discussion can be found in Chapter 4.1.1, the values for the final product [Au$_{25}$(PPh$_3$)$_{10}$(SC$_2$H$_4$Ph)$_5$Cl$_2$]$^{2+}$ are given below.

UV-Vis (MeOH or CH$_2$Cl$_2$): $\lambda_{\max}$ [nm] = 315, 328 (shoulder), 368 (shoulder), 415, 445 (shoulder), 520 (weak shoulder), 680

MALDI-MS (matrix: DCTB, solvent: DCM): m/z = 7313 [Au$_{24}$P$_7$S$_5$Cl$_2$]$^+$, 7302 [Au$_{23}$P$_9$S$_3$]$^+$ or [Au$_{22}$P$_{10}$S$_2$Cl$_2$]$^+$, 7108 [Au$_{24}$P$_7$S$_4$]$^+$ or [Au$_{23}$P$_8$S$_3$Cl$_2$]$^+$, 7092 [Au$_{24}$P$_6$S$_5$Cl$_3$]$^+$, 7038 [Au$_{23}$P$_8$S$_3$]$^+$ or [Au$_{22}$P$_9$S$_2$Cl$_2$]$^+$, 6886 [Au$_{22}$P$_7$S$_5$Cl]$^+$, 6868 [Au$_{20}$P$_{10}$S$_2$Cl]$^+$, 6828 [Au$_{24}$P$_5$S$_5$Cl$_3$]$^+$, 6815 [Au$_{21}$P$_8$S$_4$Cl]$^+$, 6775 [Au$_{23}$P$_7$S$_3$]$^+$ or [Au$_{22}$P$_8$S$_2$Cl$_2$]$^+$, 6623 [Au$_{22}$P$_6$S$_5$Cl]$^+$, 6607 [Au$_{20}$P$_9$S$_2$Cl]$^+$, 6552 [Au$_{21}$P$_7$S$_4$Cl]$^+$, 6513 [Au$_{23}$P$_6$S$_3$]$^+$ or [Au$_{21}$P$_7$S$_2$Cl$_2$]$^+$, 6289 [Au$_{21}$P$_6$S$_4$Cl]$^+$, 6030 [Au$_{21}$P$_5$S$_4$Cl]$^+$; with P = PPh$_3$ and S = -SC$_2$H$_4$Ph

(a) start   (b) end
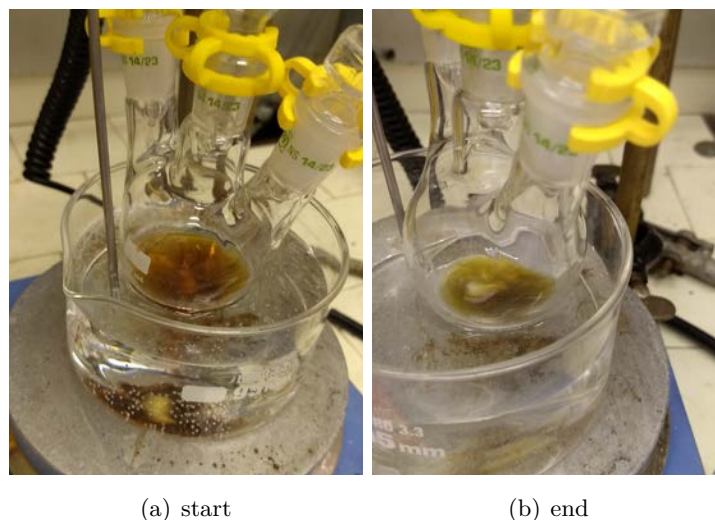
Figure 7.6.: Color change from orange to green during the ligand exchange reaction

7.3.2. Attempted Ligand Exchange with GSH
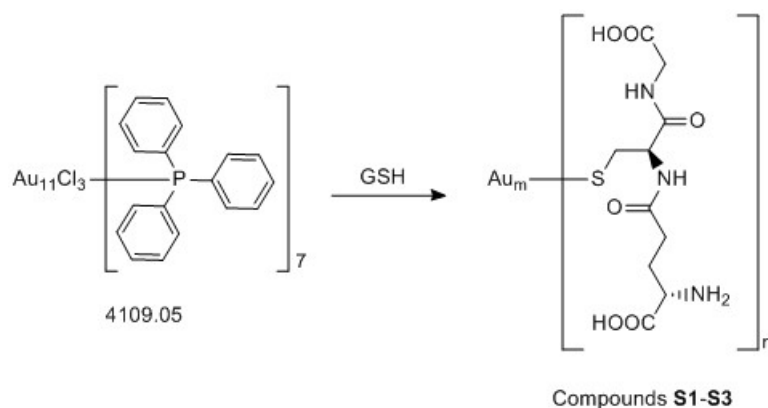
Figure 7.7.: Ligand Exchange of $Au_{11}(PPh_3)_7Cl_3$ with GSH in solution

The ligand exchange was conducted according published procedures [31, 77]. Different conditions were tested, which are summarized in Table 7.2. In the following, only one procedure is described, with the other two having been conducted analogously.

1 eq. of $Au_{11}(PPh_3)_7Cl_3$ (6 mg, 0.0015 mmol) were dissolved in 10 ml of DCM (orange colored solution) and a solution of 430 eq. of L-Glutathione (GSH) (193 mg, $1.5 \cdot 10^{-3}$ mmol) in 10 ml H_2O (clear solution) was added. The reaction mixture was heated up to 30 °C and left at high stirring for 18 h. By then, the organic layer was completely colorless. However, only a light reddish color could be observed in the organic phase, and a lot of white precipitate had been formed at the interphase.

Next, phases were separated and the reddish aqueous layer washed three times with DCM.

78

Table 7.2.: Conditions of the ligand exchange reactions of $Au_{11}(PPh_3)_7Cl_3$ and GSH in solution

No.	mg Cluster	eq. GSH	Solvents	Temp.	Atmosphere
1	6	430	$10\,ml$ DCM/$10\,ml$ H_2O	$35\,°C$	N_2
2	2	200	$2\,ml$ DCM/$2\,ml$ H_2O	RT	air
3	10	50	$10\,ml$ DCM/$10\,ml$ H_2O	$40\,°C$	air

The precipitate was removed by filtration. As no further separation method for water-soluble clusters (e.g. PAGE) was available, characterization was done with UV-Vis of the crude product mixtures **S1**-**S3** only. The spectra can be found in Chapter 4.1.

UV-Vis (H_2O): λ_{max} [nm] = 380 (shoulder), 420 (shoulder), 570

7.4. First Approach of Ligand Exchange Reactions of $Au_{11}(PPh_3)_7Cl_3$ Dropcast Films on Surfaces

The reactions were conducted in two steps: First, $Au_{11}(PPh_3)_7Cl_3$ was dropcasted on the chosen surface (Al_2O_3 plate or ZnSe crystal). Next, the sample was exposed to a solution of the exchange ligand (2-PET or GSH) at RT. In one attempt, the roles were also reversed, with the ligand immobilized on the surface and the Au cluster in solution. The exact procedures are described in the following. The reactions with the Al_2O_3 plates and the PM-IRRAS measurements were done during a scientific stay in the research group of Prof. Bürgi (UniGe).

7.4.1. Ligand Exchange of a Dropcast Film of $Au_{11}(PPh_3)_7Cl_3$ on Al_2O_3 with 2-PET

The Al_2O_3 plates were polished and cleaned according to the procedure described in Chapter 7.1.3. Then, 1 eq. of $Au_{11}(PPh_3)_7Cl_3$ (3 mg, $7.3 \cdot 10^{-4}$ mmol) was dissolved in a small amount of DCM and dropcasted onto an Al_2O_3 plate. After the cluster had completely dried up, a PM-IRRAS spectrum was recorded.

The plates were then placed in a solution of 200 eq. of 2-PET (20 μl, 0.15 mmol) in 10 ml of toluene (no. **1**) or hexane (no. **2**). After leaving them at RT for 22 h, the plates were taken out and rinsed with hexane and small amounts of DCM to remove excess ligands, dried and analyzed again with PM-IRRAS. For reaction **1**, the toluene solution had turned slightly yellowish, whereas the hexane of reaction **2** was still clear.

After measuring, new solutions with 200 eq. of 2-PET in 10 ml of an 8:2 solution of toluene/$CHCl_3$ (no. **1**) or hexane/$CHCl_3$ (no. **2**), were prepared an the plates put in for another 22 h. The washing steps were repeated and another spectrum recorded for each

plate.

In a third step, the plates were put into a solution of 200 eq. of 2-PET in 10 ml of a 7:3 toluene/CHCl$_3$ (no. **1**) or 6:4 hexane/CHCl$_3$ (no. **2**). They were left at RT for 50 h, with PM-IRRAS spectra recorded after 6, 24 and 50 h. After the second and third step, the toluene solution of reaction **1** was completely clear, but the hexane solution of reaction **2** showed a light yellow color. Figure 7.8 visualizes the whole procedure.
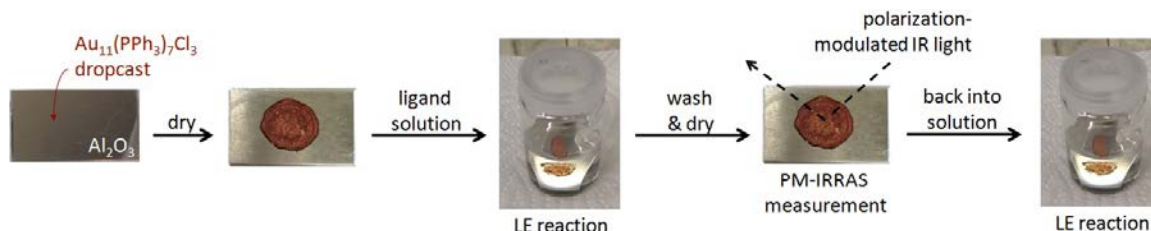
Figure 7.8.: Steps of a ligand exchange reaction of Au$_{11}$(PPh$_3$)$_7$Cl$_3$ on Al$_2$O$_3$, followed by PM-IRRAS

The PM-IRRAS and MALDI-MS spectra of the products **F1** and **F2** for reaction **1** and **2**, respectively, are shown in Chapter 4.2.1. For the MS measurements, a small amount of sample was scratched off the plate and dissolved in 50 μl of solvent.

F1:

PM-IRRAS (Al$_2$O$_3$ plate): $\tilde{\nu}_{max}$ [cm^{-1}] = 1495 (m) CH$_{aliph.}$ bend./scis.$^+$, 1478 (m) HCC$_{arom.}$ ip-bend.*, 1434 (s) CC$_{arom}$ stretch.*, 1279 (w) CH$_{arom.}$ ip-bend./CC$_{arom.}$ stretch.*, 1180 (s, br) HCC$_{arom.}$ ip-bend.*, 1157 (m, br) HCC$_{arom.}$ ip-bend.*, 1095 (s) PC stretch.*, 1068 (s) CC$_{arom.}$ stretch./HCC$_{arom.}$ ip-bend.*, 1057 (s) n.a.$^+$, 1027 (m) CH$_{arom.}$ op-bend.*, 1006 (w) CC$_{arom.}$ stretch./HCC$_{arom}$ ip-bend.*, 986 (s) n.a., 912 (w) n.a., 851 (w) n.a., 840 (w) n.a.; bands marked with * can be assigned to the PPh$_3$ ligands, bands with $^+$ to 2-PET

MALDI-MS (matrix: THAP, solvent: MeOH): m/z = 3357 [Au$_{11}$P$_4$Cl$_2$·2Cl]$^+$, 3095 [Au$_{11}$P$_3$Cl$_2$·2Cl]$^+$, 2834 [Au$_{11}$P$_2$Cl$_2$]$^+$, 2818 [Au$_9$P$_4$]$^+$, 2557 [Au$_9$P$_3$]$^+$, 2424 [Au$_7$P$_4$]$^+$, 2295 [Au$_9$P$_2$]$^+$, 2163 [Au$_7$P$_3$]$^+$, 2043 [Au$_{10}$Cl$_2$]$^+$, 1901 [Au$_7$P$_2$]$^+$, 1847 [Au$_9$Cl$_2$]$^+$, 1782 [Au$_7$P$_3$S]$^+$, 1769 [Au$_5$P$_3$]$^+$, 1586 [Au$_9$P$_2$Br]$^+$, 1408 [Au$_5$PBr$_2$]$^+$, 1376 [Au$_3$P$_3$]$^+$, 1114 [Au$_3$P$_2$]$^+$; with P = PPh$_3$ and S = -SC$_2$H$_4$Ph

F2:

PM-IRRAS (Al$_2$O$_3$ plate): $\tilde{\nu}_{max}$ [cm^{-1}] = 1495 (m) CH$_{aliph.}$ bend./scis.$^+$, 1477 (m) HCC$_{arom.}$ ip-bend.*, 1453 (w) CH$_{aliph.}$ bend./scis.$^+$, 1434 (s) CC$_{arom}$ stretch.*, 1328 (w) CH$_{arom.}$ ip-bend./HCP ip-bend.*, 1307 (w) n.a.$^+$, 1278 (w) CH$_{arom.}$ ip-bend./CC$_{arom.}$ stretch.*, 1250 (w) n.a., 1179 (s, br) HCC$_{arom.}$ ip-bend.*, 1096 (s) PC stretch.*, 1078 (m) CC$_{arom.}$ stretch./HCC$_{arom.}$ ip-bend.*, 1056 (s) n.a.$^+$, 1027 (m) CH$_{arom.}$ op-bend*, 998 (w) CC$_{arom.}$

stretch./HCCH$_{\text{arom.}}$ tors.*, 983 (s, br) n.a., 840 (w) n.a.; bands marked with * can be assigned to the PPh$_3$ ligands, bands with $^+$ to 2-PET

MALDI-MS (matrix: THAP, solvent: MeOH): m/z = 3356 [Au$_{11}$P$_4$Cl$_2\cdot$2Cl]$^+$, 3094 [Au$_{11}$P$_3$Cl$_2\cdot$2Cl]$^+$, 2832 [Au$_{11}$P$_2$Cl$_2$]$^+$, 2555 [Au$_9$P$_3$]$^+$, 2424 [Au$_7$P$_4$]$^+$, 2303 [Au$_{10}$PCl$_2$]$^+$, 2162 [Au$_7$P$_3$]$^+$, 2041 [Au$_{10}$Cl$_2$]$^+$, 1901 [Au$_7$P$_2$]$^+$, 1846 [Au$_9$Cl$_2$]$^+$, 1782 [Au$_7$P$_3$S]$^+$, 1769 [Au$_5$P$_3$]$^+$, 1585 [Au$_9$P$_2$Br]$^+$, 1407 [Au$_5$PBr$_2$]$^+$, 1375 [Au$_3$P$_3$]$^+$, 1114 [Au$_3$P$_2$]$^+$, 1054 [Au$_5$Cl$_2$]$^+$; with P = PPh$_3$ and S = -SC$_2$H$_4$Ph

7.4.2. Ligand Exchange of a Dropcast Film of Au$_{11}$(PPh$_3$)$_7$Cl$_3$ on Al$_2$O$_3$ with GSH

The Al$_2$O$_3$ plate was polished and cleaned according to the procedure described in Chapter 7.1.3. 1 eq. of Au$_{11}$(PPh$_3$)$_7$Cl$_3$ (2.5 mg, 6.1 $\cdot$ 10^{-4} mmol) was dissolved in a small amount of DCM and dropcasted onto the plate. After the cluster had completely dried up, a PM-IRRAS spectrum was recorded.
Next, the plate was placed in a solution of 160 eq. of GSH (30 mg, 0.098 mmol) in 10 ml 8:2 H$_2$O/MeOH and left at RT. PM-IRRAS spectra were recorded after 18, 44 and 66 h. Therefore, the plates were taken out of the solution, rinsed with n-pentane and small amounts of MeOH and let dry. After the spectrum had been recorded, the plate was placed back into the same solution. The procedure is visualized in Figure 7.8.

The PM-IRRAS and MALDI-MS spectra of the product **F3** are shown in Chapter 4.2.2. For the MS measurements, a small amount of sample was scratched off the plate and dissolved in 50 µl of MeOH.

F3:
PM-IRRAS (Al$_2$O$_3$ plate): $\tilde{\nu}_{\text{max}}$ [cm^{-1}] = 1726 (m) CO stretch.$^{++}$, 1710 (m) CO stretch.$^+$, 1689 (w) n.a., 1659 (s) amide I$^+$/H$_2$O def., 1642 (s) amide I^{++}/H$_2$O def., 1631 (m) amide I$^+$/H$_2$O def., 1611 (s, br) NH$_3^+$ def.$^+$, 1549 (s) amide II^{++}, 1531 (s) amide II$^+$, 1517 (w) n.a., 1433 (m) CC$_{\text{arom}}$ stretch.*, 1408 (m) S(COO$^-$) stretch.$^+$, 1313 (m) n.a., 1268 (w) n.a., 1233 (w) amide III^{++}, 1154 (m, br) n.a., 1120 (w) n.a., 1101 (m) PC stretch.*, 976 (s, br) n.a., 846 (w) n.a.; bands marked with * can be assigned to the PPh$_3$ ligands, bands with $^+$ to GSH and with $^{++}$ to GSH in H$_2$O

MALDI-MS (matrix: DCBT, solvent: MeOH): m/z = 4160 [Au$_{11}$P$_5$S$_2$Cl$_2$]$^+$, 3901 [Au$_{11}$P$_4$S$_2$Cl$_2$]$^+$, 3883 [Au$_{10}$P$_6$SCl$_2$]$^+$, 3855 [Au$_{11}$P$_5$SCl$_2$]$^+$, 3620 [Au$_{10}$P$_5$SCl]$^+$, 3565 [Au$_{11}$P$_3$S$_2$]$^+$, 3359 [Au$_{10}$P$_4$SCl]$^+$, 2425 [Au$_7$P$_4$]$^+$, 2227 [Au$_6$P$_4$]$^+$, 2166 Au$_{11}^+$ or [Au$_7$P$_3$]$^+$, 2028 [Au$_7$S$_2$Cl]$^+$, 1968 Au$_{10}^+$ or [Au$_6$P$_3$]$^+$, 1770 Au$_9^+$ or [Au$_5$P$_3$]$^+$, 1707 [Au$_6$P$_2$]$^+$; with P = PPh$_3$ and S = -SG

7.4.3. Attempted Ligand Exchange of $Au_{11}(PPh_3)_7Cl_3$ in Solution with a GSH Film on Al_2O_3

The Al_2O_3 plate was polished and cleaned according to the procedure described in Chapter 7.1.3. 60 eq. of GSH (22.4 mg, 0.073 mmol) dissolved in H_2O were dropcasted onto the plate and let dry for a day. A PM-IRRAS of the crystalline looking glutathione film on the plate was recorded.

The sample was then placed in a solution of 1 eq. of $Au_{11}(PPh_3)_7Cl_3$ (5 mg, 0.0012 mmol) in 10 ml $CHCl_3$. For measuring PM-IRRAS, the plate was taken out, rinsed with n-pentane and small amounts of DCM to remove excess cluster and let dry. The procedure is visualized in Figure 7.9.
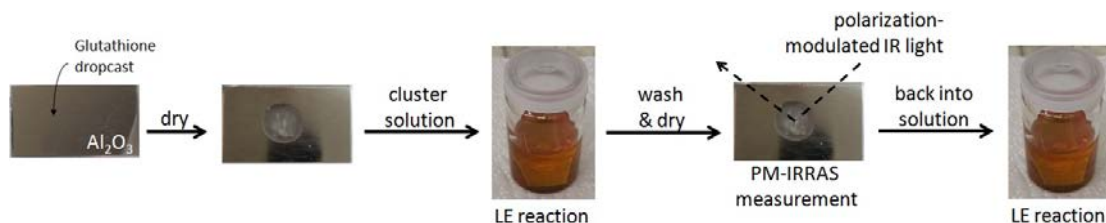
Figure 7.9.: Attempted ligand exchange reaction of $Au_{11}(PPh_3)_7Cl_3$ in solution with GSH immobilized on Al_2O_3, followed by PM-IRRAS

PM-IRRAS analysis showed that no exchange reaction had occurred. Instead, precipitation of $Au_{11}(PPh_3)_7Cl_3$ on the whole plate was noticed, resulting in a slightly reddish color of the surface.

7.4.4. Ligand Exchange of a Dropcast Film of $Au_{11}(PPh_3)_7Cl_3$ on ZnSe with GSH

The ZnSe crystal used was cleaned with EtOH and in an ultrasound bath. 1 eq. of $Au_{11}(PPh_3)_7Cl_3$ (5 mg, $1.2 \cdot 10^{-3}$ mmol) was dissolved in a small amount of EtOH and dropcasted onto the crystal with the help of a positioning device. After the solution had completely dried up, the crystal was placed into the flow cell, using a rubber sealing on the flow side and a teflon spacer on the other one (see Figure 7.10). The cell was then mounted into the optical path and positions optimized to reach high intensity on the detector.

A prepared 0.01 M solution of GSH in 8:2 H_2O/MeOH was pumped through the cell with a peristaltic pump at 0.05 ml/min over a period of 30 h, with the first 8 h monitored *in-situ*. Afterwards, the solution was removed and the crystal rinsed with 8:2 H_2O/MeOH to remove excess ligands. After the film was again completely dry, a final spectrum was recorded. The most intense bands of the end product **F4** are listed below, the spectra are displayed in Chapter 4.2.4.

F4:

ATR-IR (ZnSe crystal): $\tilde{\nu}_{max}$ [cm^{-1}] = 3300 (s, br) OH and NH stretch., 3144 (w) CH$_{arom}$ stretch., 3070 (m) CH$_{arom}$ stretch.*[++], 3054 (m) CH$_{arom}$ stretch.*[++], 3027 (w) CH$_{arom}$ stretch.[++], 3004 (w) CH$_{arom}$ stretch.[++], 2972 (m) CH$_{arom}$ stretch., 2926 (w, br) CH$_{arom}$ stretch.*[++], 2875 (w, br) CH$_{arom}$ stretch.[++], 1725 (w, br) CO stretch.[+], 1642 (m, br) amide I[++]/H$_2$O def.[+], 1572 (w) n.a.[++], 1548 (w, br) amide II[+], 1530 (w, br) amide II[+], 1479 (s) CC$_{arom}$*[++], 1435 (s) CC$_{arom}$ stretch.*[++], 1392 (w, br) n.a.[++], 1331 (w) CH$_{arom.}$ ip-bend./HCP ip-bend.*[++], 1311 (w) n.a.[++], 1223 (w, br) amide III[+], 1183 (w) HCC$_{arom.}$ ip-bend.*[++], 1161 (w) HCC$_{arom.}$ ip-bend.*[++], 1097 (m) PC stretch.*[++], 1049 (m) n.a., 1028 (m) CH$_{arom.}$ op-bend*[++], 997 (m) CC$_{arom.}$ stretch./HCCH$_{arom.}$ tors.*[++]; bands marked with * can be assigned to the PPh$_3$ ligands, bands with [+] to GSH and bands with [++] had already been present in the starting material Au$_{11}$(PPh$_3$)$_7$Cl$_3$

(a) cell parts   (b) closed cell   (c) ATR-IR set-up
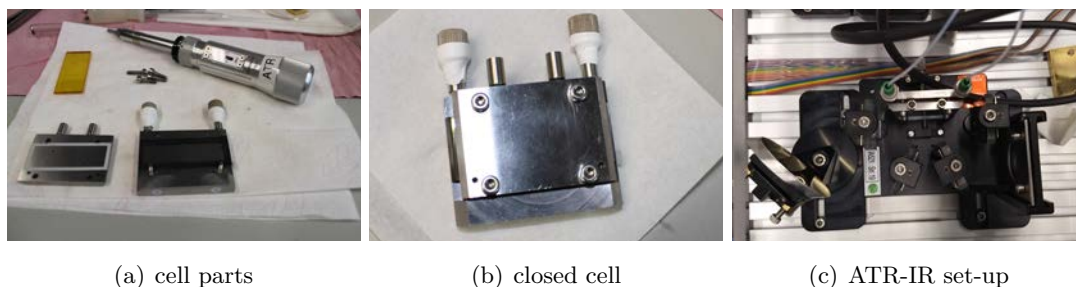
Figure 7.10.: ATR-IR flow cell used for the *in-situ* monitored ligand exchange between of Au$_{11}$(PPh$_3$)$_7$Cl$_3$ immobilized on ZnSe and GSH in solution. (a) Cell parts: backside with solution in- and outlet and rubber sealing, ZnSe crystal and frontside with teflon spacer (b) Closed cell (c) Top view on the measurement set-up

7.5. First Approach of Ligand Exchange Reactions of Au$_{11}$(PPh$_3$)$_7$Cl$_3$ Supported on Metal Oxide Materials

The reactions were conducted in two steps: First, Au$_{11}$(PPh$_3$)$_7$Cl$_3$ was immobilized on the chosen support material (SiO$_2$ or Al$_2$O$_3$). Next, the support-cluster mixture was suspended in a solution of the exchange ligand (2-PET or GSH) and stirred for 20 h at RT. The exact procedures are described in the following.

7.5.1. Supporting of Au$_{11}$(PPh$_3$)$_7$Cl$_3$ on SiO$_2$

For wet impregnation [102], 34 mg of Au$_{11}$(PPh$_3$)$_7$Cl$_3$ were dissolved in 30 ml of MeOH and added to 900 mg of SiO$_2$ (specific area 85-115 m^2/g, particle diameter $\approx$ 44 μm). The reddish suspension was stirred under N$_2$ atmosphere for 24 h, until the cluster had been completely

immobilized on the powder material. This was indicated by the color of the solution phase being clear.

The solvent was then removed by filtration and the red slurry washed with small portions of MeOH. Afterwards, it was dried in the oven at 65 °C for 2 h and then in an evacuated desiccator over silica gel for additional 24 h. The step in the oven can be left out, but results in 48 h of drying time under reduced pressure. The beige powder containing approximately 2 wt% Au was then ground and stored under inert atmosphere to prevent possible oxidation.

The samples were analyzed with UV-Vis and STEM. Spectra can be found in Chapter 4.3, a reference UV-Vis spectra of the support material SiO_2 can be found in Chapter A.3.

UV-Vis (solid, d = 0.5 cm): λ_{max} [nm] = 282, 300 (shoulder), 358 (shoulder), 400, 431, 467, 510 (shoulder), $\approx$ 650 (broad)

(a) MeOH suspension   (b) dry powder
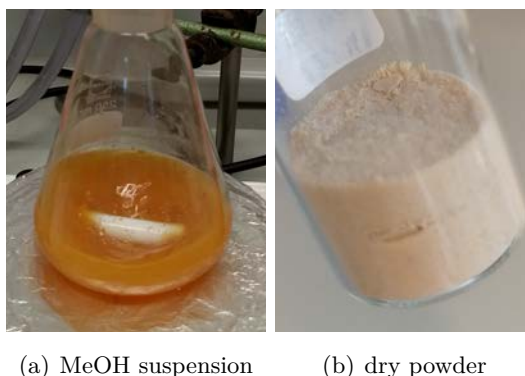
Figure 7.11.: Colors of $Au_{11}(PPh_3)_7Cl_3$ supported on SiO_2

7.5.2. Supporting of $Au_{11}(PPh_3)_7Cl_3$ on Al_2O_3

For wet impregnation [102], 61 mg of $Au_{11}(PPh_3)_7Cl_3$ were dissolved in 30 ml of MeOH and added to 1600 mg of Al_2O_3 (specific area 90-210 m^2/g, particle diameter $\approx$ 45 μm). The red suspension was stirred under N_2 atmosphere for 24 h, until the cluster had been completely immobilized on the powder material. This was indicated by the color of the solution phase being almost clear.

The solvent was then removed by filtration and the dark red slurry washed with small portions of MeOH. Afterwards, it was dried in the oven at 65 °C for 2 h and then in an evacuated desiccator over silica gel for additional 24 h. The step in the oven can be left out, but results in 48 h of drying time under reduced pressure. The reddish-brown powder containing approximately 2 wt% Au was then ground and stored under inert atmosphere to prevent possible oxidation.

The sample was analyzed with UV-Vis. The spectrum can be found in Chapter 4.3, a

reference UV-Vis spectra of the support material Al_2O_3 can be found in Chapter A.3.

UV-Vis (solid, d = 0.5 cm): λ_{max} [nm] = 282 (weak shoulder), 300, 330 (shoulder), 404, 431, 467, 510 (weak shoulder)

(a) MeOH suspension   (b) dry powder

Figure 7.12.: Colors of $Au_{11}(PPh_3)_7Cl_3$ supported on Al_2O_3

7.5.3. Reaction of SiO$_2$ Supported Au$_{11}$(PPh$_3$)$_7$Cl$_3$ with Thiol Ligands

Reaction with 2-PET

1 eq. of $Au_{11}(PPh_3)_7Cl_3$ (16 mg pure cluster, 422 mg with support, 3.9 mmol) were suspended in 25 ml of toluene and 50 eq. of 2-PET (26 µl, 195 mmol) were added. The reaction was stirred under air for 20 h. A color change of the suspension from red to brown was visible. The solvent was removed by filtration and the sample washed with toluene. Afterwards, the slurry was dried at 65 °C for 2 h and then in an evacuated desiccator over silica gel for another day. The step in the oven can be left out if the drying under reduced pressure is pursued for 3 d instead. The greyish powder **P1** was then ground and kept under N$_2$ atmosphere to avoid possible oxidation during storage.

UV-Vis (solid, d = 0.5 cm): λ_{max} [nm] = 282, 304 (shoulder), 430, 481, $\approx$ 630 (broad)

(a) 0 h   (b) 20 h
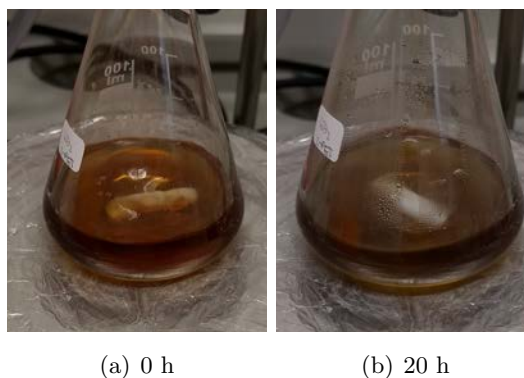
Figure 7.13.: Colors of the reaction mixture of SiO_2 supported $Au_{11}(PPh_3)_7Cl_3$ with 2-PET

Reaction with GSH

1 eq. of $Au_{11}(PPh_3)_7Cl_3$ (16 mg pure cluster, 422 mg with support, 3.9 mmol) were suspended in 25 ml of 8:2 H_2O/MeOH and 50 eq. of GSH (60 mg, 195 mmol) were added. The reaction was stirred under air for 20 h. A distinct color change of the suspension from beige to violet was visible.

The solvent was removed by filtration and the sample washed with water and MeOH. Afterwards, the slurry was dried at 65 °C for 2 h and then in an evacuated desiccator over silica gel for another day. The step in the oven can be left out if the drying under reduced pressure is pursued for 3 d instead. The light violet powder **P2** was then ground and kept under N_2 atmosphere to avoid possible oxidation during storage.

UV-Vis (solid, d = 0.5 cm): λ_{max} [nm] = 284, 481, $\approx$ 630 (broad)

(a) 0 h   (b) 20 h
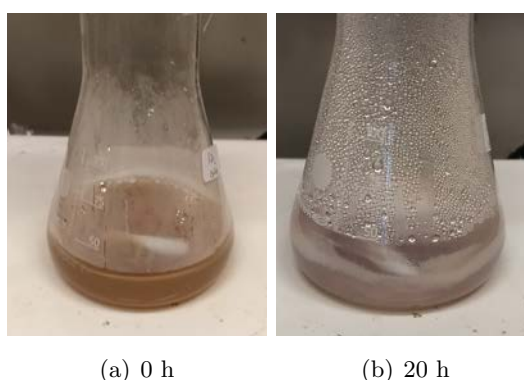
Figure 7.14.: Colors of the reaction mixture of SiO_2 supported $Au_{11}(PPh_3)_7Cl_3$ with GSH

Figure 7.15.: Colors of the dry powder samples on SiO_2: unreacted, after reaction with 2-PET (**P1**) and after reaction with GSH (**P2**); from left to right

The samples were analyzed with UV-Vis and STEM. The spectrum can be found in Chapter 4.3, a reference UV-Vis spectra of the support material SiO_2 can be found in Chapter A.3.

7.5.4. Reaction of Al$_2$O$_3$ Supported Au$_{11}$(PPh$_3$)$_7$Cl$_3$ with Thiol Ligands

Reaction with 2-PET

1 eq. of $Au_{11}(PPh_3)_7Cl_3$ (30 mg pure cluster, 791 mg with support, 7.3 mmol) were suspended in 25 ml of toluene and 50 eq. of 2-PET (49 µl, 365 mmol) were added. The reaction was stirred under air for 20 h. A distinct color change of the suspension from dark brown to dark violet was visible.

The solvent was removed by filtration and the sample washed with toluene. Afterwards, the slurry was dried at 65 °C for 2 h and then in an evacuated desiccator over silica gel for another day. The step in the oven can be left out if the drying under reduced pressure is pursued for 3 d instead. The light violet powder **P3** was then ground and kept under N_2 atmosphere to avoid possible oxidation during storage.

UV-Vis (solid, d = 0.5 cm): λ_{max} [nm] = 282, 300 (shoulder), 403, 485

(a) 0 h   (b) 20 h
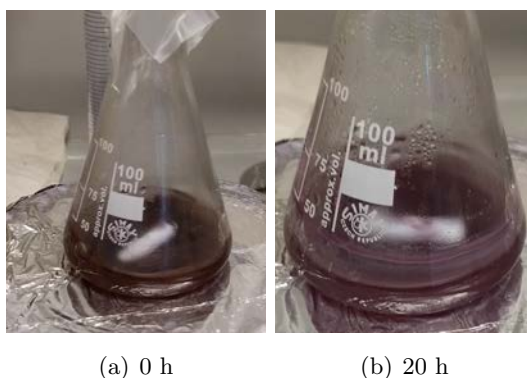
Figure 7.16.: Colors of the reaction mixture of Al$_2$O$_2$ supported Au$_{11}$(PPh$_3$)$_7$Cl$_3$ with 2-PET

Reaction with GSH

1 eq. of $Au_{11}(PPh_3)_7Cl_3$ (30 mg pure cluster, 791 mg with support, 7.3 mmol) were suspended in 25 ml of 8:2 H_2O/MeOH and 50 eq. of GSH (112 mg, 365 mmol) were added. The reaction was stirred under air for 20 h. Only a slight color change of the suspension from red-brown to lighter brown was visible.

The solvent was removed by filtration and the sample washed with water and MeOH. Afterwards, the slurry was dried at 65 °C for 2 h and then in an evacuated desiccator over silica gel for another day. The step in the oven can be left out if the drying under reduced pressure is pursued for 3 d instead. The brownish powder **P4** was then ground and kept under N_2 atmosphere to avoid possible oxidation during storage.

UV-Vis (solid, d = 0.5 cm): λ_{max} [nm] = 322, 485

(a) 0 h   (b) 20 h
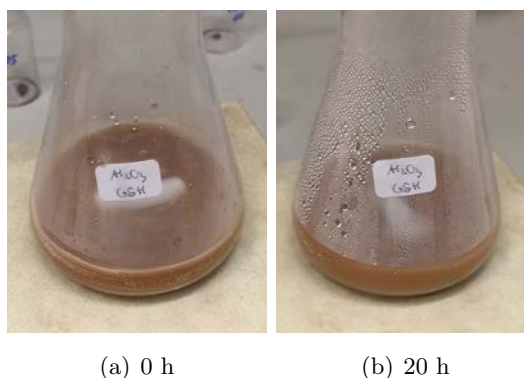
Figure 7.17.: Colors of the reaction mixture of Al_2O_2 supported $Au_{11}(PPh_3)_7Cl_3$ with GSH

Figure 7.18.: Colors of the dry powder samples on Al_2O_3: unreacted, after reaction with 2-PET (**P3**) and after reaction with GSH (**P4**); from left to right

The samples were analyzed with UV-Vis. The spectrum can be found in Chapter 4.3, a reference UV-Vis spectra of the support material Al_2O_3 can be found in Chapter A.3.

7.6. Ligand Exchange from Au$_{15}$(SG)$_{13}$ to Au$_{20}$(SC$_2$H$_4$Ph)$_{16}$

7.6.1. Synthesis of Au$_{15}$(GS)$_{13}$

$$\text{HAuCl}_4 \cdot 3\,\text{H}_2\text{O} + \text{exs. GSH} \xrightarrow[\text{2. TBAB}]{\text{1. 1M HNO}_3} \text{Au}_{15}(\text{SG})_{13}$$

393.83   6936.58
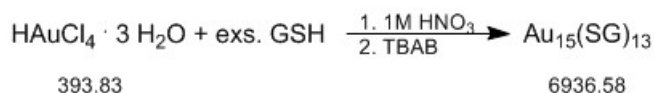
Figure 7.19.: Synthesis of Au$_{15}$(SG)$_{13}$

The synthesis of Au$_{15}$(SG)$_{13}$ was carried out as published in [58].

1 eq. of HAuCl$_4$ $\cdot$ 3 H$_2$O (50 mg, 0.13 mmol) and 3 eq. of L-glutathione (118 mg, 0.38 mmol) were dissolved in 94 ml of ultrapure H$_2$O, which resulted in an orange solution with the color slowly fading out until transparent. The pH of the solution was adjusted to 2.0 with 1 M HNO$_3$. Then, the mixture was left at RT for around 10 min until a murky white dispersion was observed. 10 eq. of borane *tert*-butylamine (TBAB) (100 mg, 1.26 mmol) dissolved in 125 ml of toluene were added and the reaction mixture stirred with 1000 rpm at RT for 4 h. Phases were separated and the slightly yellowish water phase washed with toluene three times. After evaporation of a majority of solvent, some white precipitate (residual TBAB or by-products) was formed and removed by centrifugation. The residual solution yielded Au$_{15}$(SG)$_{13}$ as a light yellow crude product.

Characterization was done by UV-Vis (spectrum in Chapter 5.1). As the sample could not be further purified as no separation method for H$_2$O soluble samples was available, the crude was used for the ligand exchange directly.

UV-Vis (MeOH): λ_{max} [nm] = 375, 410 (shoulder)

7.6.2. Ligand Exchange to Au$_{20}$(SC$_2$H$_4$Ph)$_{16}$
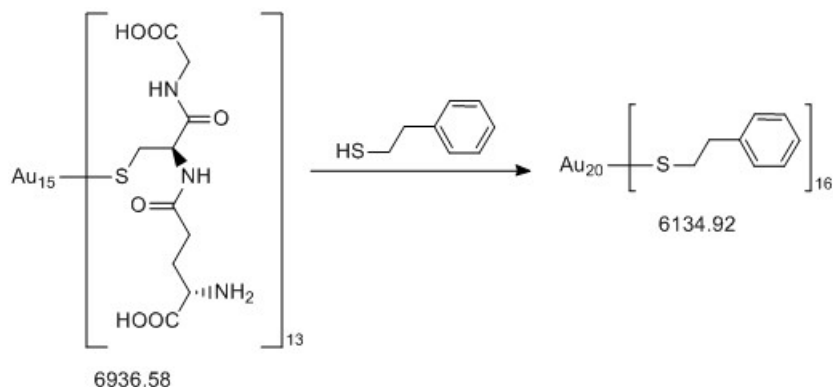
Figure 7.20.: Ligand Exchange of Au$_{15}$(SG)$_{13}$ with 2-PET

The ligand exchange procedure was based on previously reported ones [73, 104].

1 eq. of the crude Au$_{15}$(SG)$_{13}$ (29 mg, 0.004 mmol) was dissolved in 1 ml of MeOH. 150 eq. of 2-phenylethanethiol (84 µl, 0.63 mmol) in 1 ml of DCM were added and the mixture stirred moderately. The mixture started to get cloudy and yellow precipitate was formed even after 10 minutes.

After stirring at RT for 8 hours, the solution was clear and orange solid had been formed. The latter was collected by filtration and washed with MeOH. After extraction with DCM and size exclusion chromatography (SEC), Au$_{20}$(SC$_2$H$_4$Ph)$_{16}$ was obtained as an orange powder. The yield was about 65 %.

The product was analyzed with UV-Vis and MALDI-MS. For the EXAFS measurements at Au L3-edge at the SuperXAS beamline of SLS synchrotron, data analysis is still ongoing. Spectra can be found in Chapter 5.2.

UV-Vis (DCM): $\lambda_{\max}$ [nm] = 350 (shoulder), 420 (shoulder), 481

MALDI-MS (matrix: DCTB, solvent: toluene): m/z = 7162 [Au$_{28}$L$_{12}$]$^+$, 6628 [Au$_{27}$L$_{11}$]$^+$, 6525 [Au$_{22}$L$_{16}$]$^+$, 6433 [Au$_{25}$L$_{11}$]$^+$, 6190 [Au$_{21}$L$_{15}$]$^+$, 6099 [Au$_{24}$L$_{10}$]$^+$, 6007 [Au$_{27}$L$_5$]$^+$, 5855 [Au$_{20}$L$_{14}$]$^+$, 5763 [Au$_{23}$L$_9$]$^+$, 5671 [Au$_{26}$L$_4$]$^+$, 5428 [Au$_{22}$L$_8$]$^+$, 5336 [Au$_{25}$L$_3$]$^+$, 5265 [Au$_{17}$L$_{14}$]$^+$, 5126 [Au$_{17}$L$_{13}$]$^+$, 5034 [Au$_{20}$L$_8$]$^+$, 5001 [Au$_{24}$L$_2$]$^+$, 4930 [Au$_{16}$L$_{13}$]$^+$, 4791 [Au$_{16}$L$_{12}$]$^+$, 4700 [Au$_{19}$L$_7$]$^+$, 4667 [Au$_{23}$L]$^+$, 4596 [Au$_{15}$L$_{12}$]$^+$, 4365 [Au$_{18}$L$_6$]$^+$, 4030 [Au$_{17}$L$_5$]$^+$; with L = -SC$_2$H$_4$Ph

Appendix

A. Additional Spectra

A.1. Spectra of $Au_{11}(PPh_3)_7Cl_3$
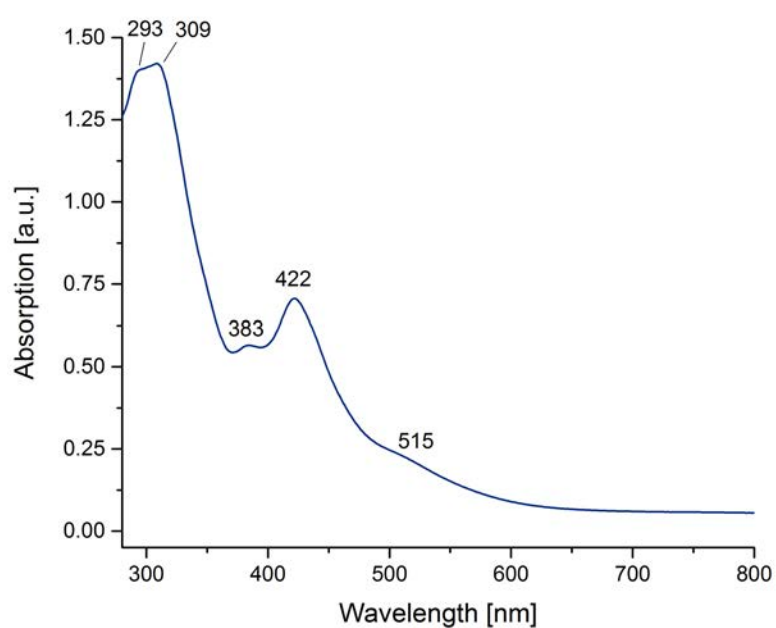
Figure A.1.: UV-Vis absorbance spectrum of $Au_{11}(PPh_3)_7Cl_3$ in DCM
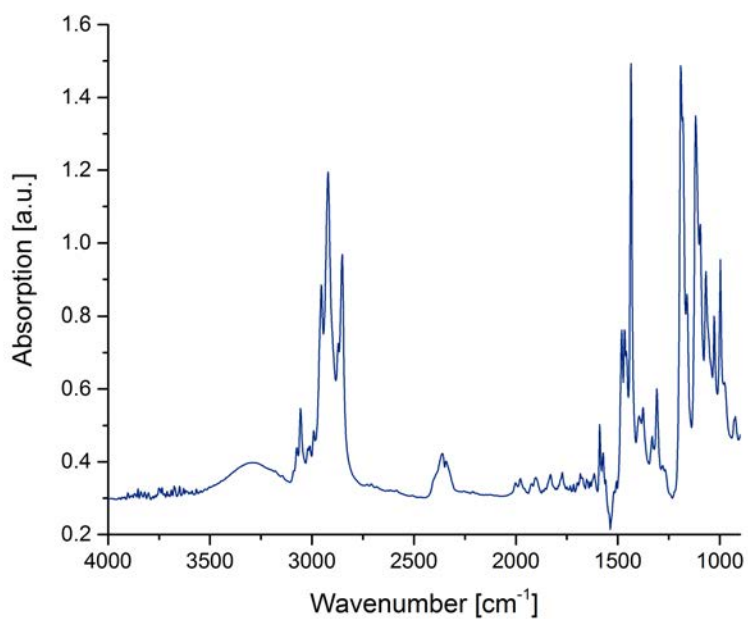
Figure A.2.: ATR-IR absorbance spectrum of $Au_{11}(PPh_3)_7Cl_3$ in solid phase (ZnSe crystal).

A.2. IR Reference Spectra of the Ligands

Phosphine, triphenyl-
INFRARED SPECTRUM

NIST Chemistry WebBook (http://webbook.nist.gov/chemistry)
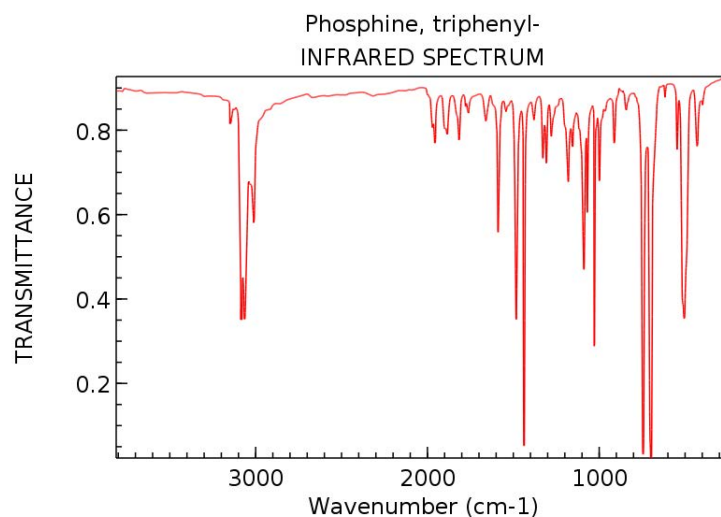
Figure A.3.: IR reference spectrum of PPh_3. Reproduced from NIST Chemistry WebBook [124].

PHENYLETHYLTHIOL
INFRARED SPECTRUM

NIST Chemistry WebBook (http://webbook.nist.gov/chemistry)
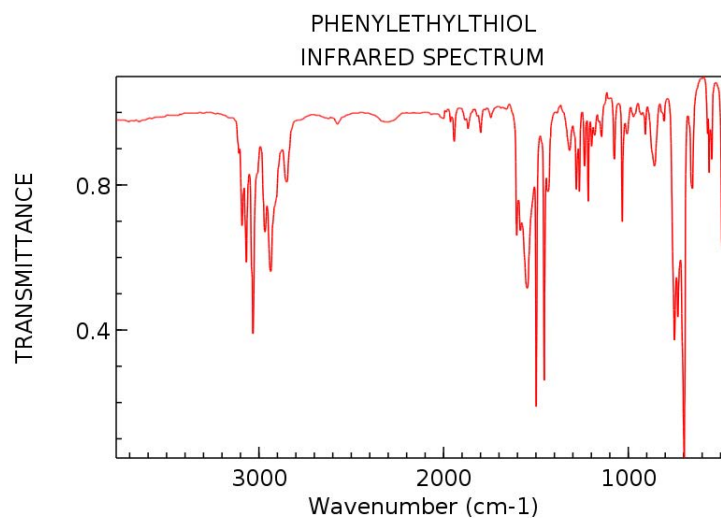
Figure A.4.: IR reference spectrum of 2-PET. Reproduced from NIST Chemistry WebBook [125].
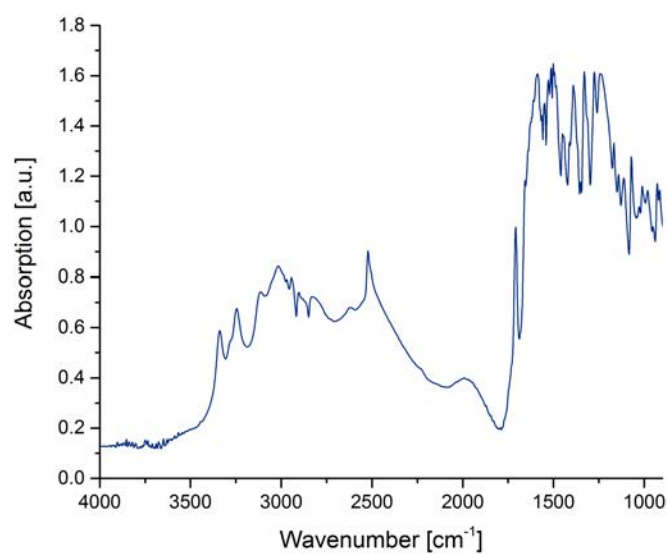
Figure A.5.: ATR-IR reference spectrum of GSH in solid phase (ZnSe crystal).
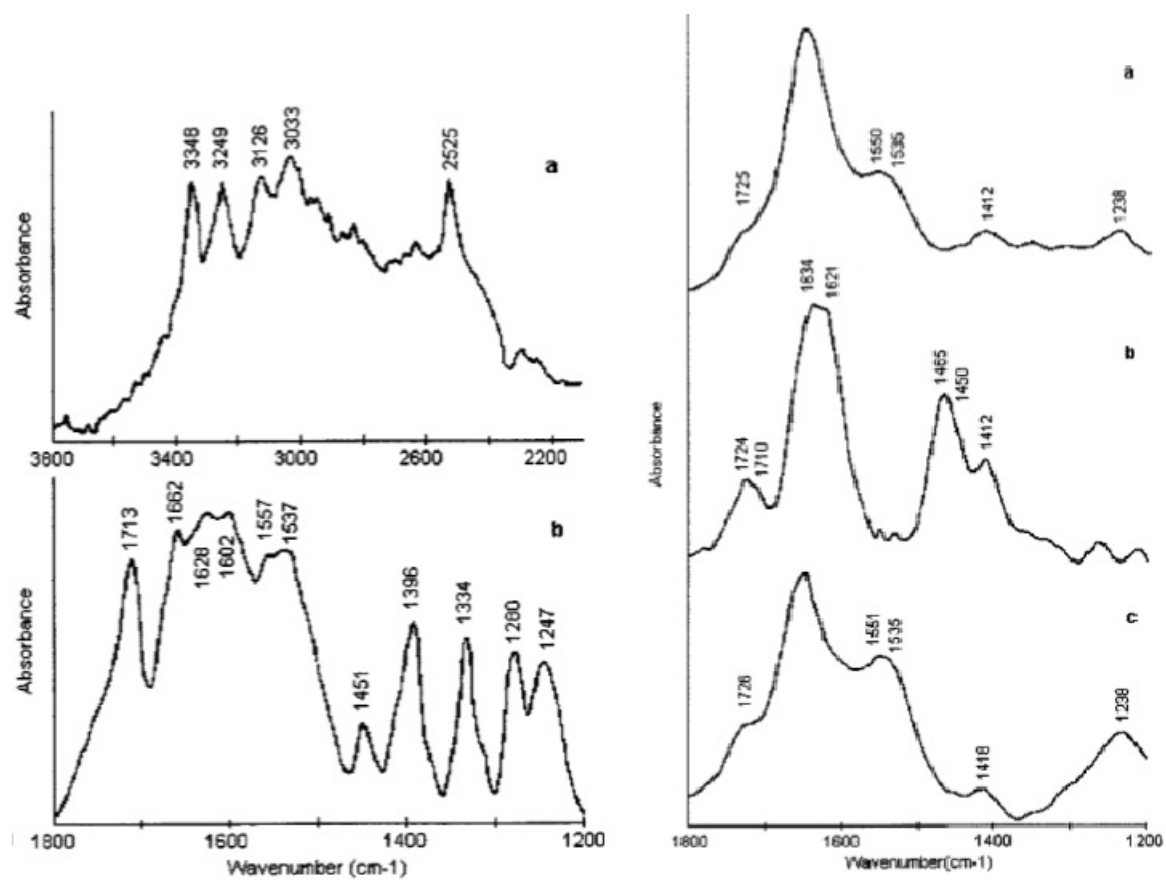
Figure A.6.: IR reference spectrum of GSH. Left side: GSH powder in KBr a pellet, right side: GSH in solution (a: H_2O, b: D_2O, c: H_2O with H_2O_2). Adapted from [101].

A.3. UV-Vis Spectra of the Support Materials
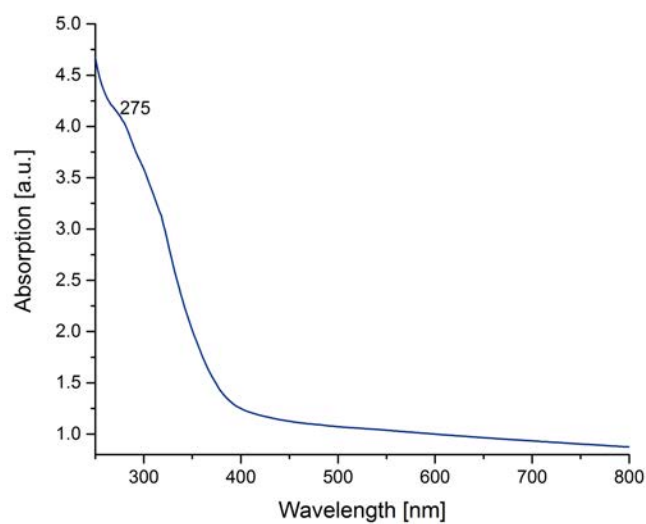
Figure A.7.: UV-Vis Absorbance spectrum of SiO_2. Measured in solid phase with d $= 0.5$ cm.
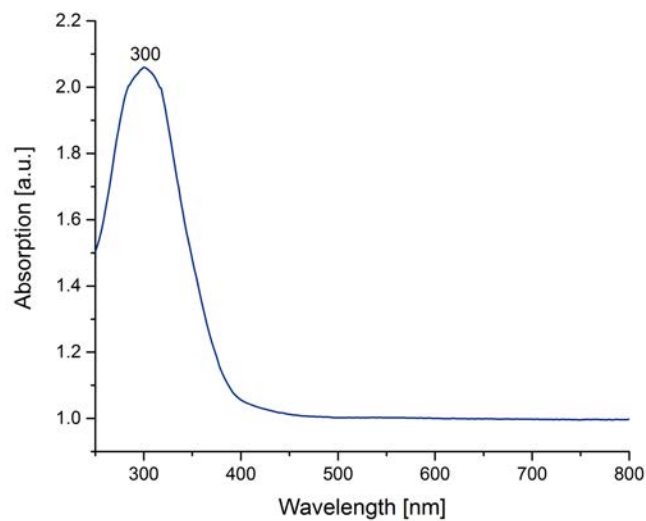
Figure A.8.: UV-Vis Absorbance spectrum of Al_2O_3. Measured in solid phase with d $= 0.5$ cm.

List of Figures

List of Tables

Bibliography

[1] S. Takano and T. Tsukuda. Controlled Synthesis: Size Control. In T. Tsukuda and H. Häkkinen, editors, *Protected Metal Clusters: From Fundamentals to Applications*, Frontiers of Nanoscience Vol. 9, pages 9–38. Elsevier, 2015.

[2] W. Kurashige, Y. Niihori, S. Sharma, and Y. Negishi. Recent Progress in the Functionalization Methods of Thiolate-Protected Gold Clusters. *J. Phys. Chem. Lett.*, 5(23):4134–4142, 2014.

[3] Y. Negishi, Y. Niihori, and W. Kurashige. Controlled Synthesis: Composition and Interface Control. In T. Tsukuda and H. Häkkinen, editors, *Protected Metal Clusters: From Fundamentals to Application*, Frontiers of Nanoscience, Vol. 9, pages 39–71. Elsevier, 2015.

[4] A. Corma and H. Garcia. Supported gold nanoparticles as catalysts for organic reactions. *Chem. Soc. Rev.*, 37(9):2096–2126, 2008.

[5] S. Yamazoe, K. Koyasu, and T. Tsukuda. Nonscalable Oxidation Catalysis of Gold Clusters. *Acc. Chem. Res.*, 47(3):816–824, 2014.

[6] M. Stratakis and H. Garcia. Catalysis by Supported Gold Nanoparticles: Beyond Aerobic Oxidative Processes. *Chem. Rev.*, 112(8):4469–4506, 2012.

[7] D. P. Anderson, J. F. Alvino, A. Gentleman, H. Al Qahtani, L. Thomsen, M. I. J. Polson, G. F. Metha, V. B. Golovko, and G. G. Andersson. Chemically-synthesised, atomically-precise gold clusters deposited and activated on titania. *Phys. Chem. Chem. Phys.*, 15(11):3917–3929, 2013.

[8] H. Häkkinen. Electronic Structure: Shell Structure and the Superatom Concept. In T. Tsukuda and H. Häkkinen, editors, *Protected Metal Clusters: From Fundamentals to Applications*, Frontiers of Nanoscience, Vol. 9, pages 189–222. Elsevier, 2015.

[9] Y.-K. Han, H. Kim, J. Jung, and Y. C. Choi. Understanding the Magic Nature of Ligand-Protected Gold Nanoparticle $Au_{102}(MBA)_{44}$. *J. Phys. Chem. C*, 114(17):7548–7552, 2010.

[10] J. Akola, M. Walter, R. L. Whetten, H. Häkkinen, and H. Grönbeck. On the Structure of Thiolate-Protected Au_{25}. *J. Am. Chem. Soc.*, 130(12):3756–3757, 2088.

[11] M. W. Heaven, A. Dass, P. S. White, K. M. Holt, and R. W. Murray. Crystal Structure of the Gold Nanoparticle $[N(C_8H_{17})_4][Au_{25}(SCH_2CH_2Ph)_{18}]$. *J. Am. Chem. Soc.*, 130(12):3754–3755, 2008.

[12] M. Walter, J. Akola, O. Lopez-Acevedo, P. D. Jadzinsky, G. Calero, C. J. Ackerson, R. L. Whetten, H. Grönbeck, and H. Häkkinen. A unified view of ligand-protected gold clusters as superatom complexes. *Proc. Natl. Acad. Sci.*, 105(27):9157–9162, 2008.

[13] B. Zhang, S. Kaziz, H. Li, M. G. Hevia, D. Wodka, C. Mazet, T. Bürgi, and N. Barrabés. Modulation of Active Sites in Supported $Au_{38}(SC_2H_4Ph)_{24}$ Cluster Catalysts: Effect of Atmosphere and Support Material. *J. Phys. Chem. C*, 119(20):11193–11199, 2015.

[14] B. Zhang. *Thiolate Protected Gold nanoclusters: Heteroatom Doping and Catalysis.* PhD thesis, Université de Genève, 2016.

[15] K. Konishi. Phosphine-Coordinated Pure-Gold Clusters: Diverse Geometrical Structures and Unique Optical Properties/Responses. In D. M. P. Mingos, editor, *Gold Clusters, Colloids and Nanoparticles I*, Struct. Bond. 161, chapter 49–86. Springer, 2014.

[16] P. Maity, H. Tsunoyama, M. Yamauchi, S. Xie, and T. Tsukuda. Organogold Clusters Protected by Phenylacetylene. *J. Am. Chem. Soc.*, 133(50):20123–20125, 2011.

[17] P. Maity, T. Wakabayashi, N. Ichikuni, H. Tsunoyama, S. Xie, M. Yamauchia, and T. Tsukuda. Selective synthesis of organogold magic clusters $Au_{54}(CCPh)_{26}$. *Chem. Commun.*, 48(49):6085–6087, 2012.

[18] P. Maity, S. Takano, S. Yamazoe, T. Wakabayashi, and T. Tsukuda. Binding Motif of Terminal Alkynes on Gold Clusters. *J. Am. Chem. Soc.*, 135(25):9450–9457, 2013.

[19] Y. Negishi, W. Kurashige, and U. Kamimura. Isolation and Structural Characterization of an Octaneselenolate-Protected Au_{25} Cluster. *Langmuir*, 27(20):12289–12292, 2011.

[20] X. Meng, Q. Xu, S. Wang, and M. Zhu. Ligand-exchange synthesis of selenophate-capped Au_{25} nanoclusters. *Nanoscale*, 4(14):4161–4165, 2012.

[21] W. Kurashige, M. Yamaguchi, K. Nobusada, and Y. Negishi. Ligand-Induced Stability of Gold Nanoclusters: Thiolate versus Selenolate. *J. Phys. Chem. Lett.*, 3(18):2649–2652, 2012.

[22] W. Kurashige, S. Yamazoe, M. Yamaguchi, K. Nishido, K. Nobusada, T. Tsukuda, and Y. Negishi. Au_{25} Clusters Containing Unoxidized Tellurolates in the Ligand Shell. *J. Phys. Chem. Lett.*, 5(12):2072–2076, 2014.

[23] Y. Wang, H. Yang, and N. Zheng. Structural Engineering of Heterometallic Nanoclusters. In T. Tsukuda and H. Häkkinen, editors, *Protected Metal Clusters: From*

Fundamentals to Applications, Frontiers of Nanoscience Vol. 9, pages 73–102. Elsevier, 2015.

[24] M. A. Boles, D. Ling, T. Hyeon, and D. V. Talapin. The surface science of nanocrystals. *Nature Materials*, 15:141–153, 2016.

[25] T. Bürgi. Properties of the gold–sulphur interface: from self-assembled monolayers to clusters. *Nanoscale*, 7(38):15553–15567, 2015.

[26] S. Knoppe and T. Bürgi. Chirality in Thiolate-Protected Gold Clusters. *Acc. Chem. Res.*, 47(4):1318–1326, 2014.

[27] G. H. Woehrle and J. E. Hutchison. Thiol-Functionalized Undecagold Clusters by Ligand Exchange: Synthesis, Mechanism, and Properties. *Inorg. Chem.*, 44(18):6149–6158, 2005.

[28] L. Malatesa, L. Naldini, G. Simonetta, and F. Cariati. Triphenylphosphine-gold(0)/gold(I) compounds. *Coord. Chem. Rev.*, 1(1–2):255–262, 1966.

[29] M. McPartlin, R. Mason, and L. Malatesa. Novel cluster complexes of gold(0)-gold(I). *J. Chem. Soc. D*, 0(7):334–334, 1969.

[30] S. Takano, S. Yamazoe, and T. Tsukuda. A gold superatom with 10 electrons in $Au_{13}(PPh_3)_8(p\text{-}SC_6H_4CO_2H)_3$. *APL Materials*, 5:053402, 2017.

[31] L. C. McKenzie, T. O. Zaikova, and J. E. Hutchison. Structurally Similar Triphenylphosphine-Stabilized Undecagolds, $Au_{11}(PPh_3)_7Cl_3$ and $[Au_{11}(PPh_3)_8Cl_2]Cl$, Exhibit Distinct Ligand Exchange Pathways with Glutathione. *J. Am. Chem. Soc.*, 136(38):13426–13435, 2014.

[32] R. K. Smith, S. U. Nanayakkara, G. H. Woehrle, T. P. Pearl, M. M. Blake, J. E. Hutchison, and P. S. Weiss. Spectral Diffusion in the Tunneling Spectra of Ligand-Stabilized Undecagold Clusters. *J. Am. Chem. Soc.*, 128(29):9266–9267, 2006.

[33] Z. Wu and R. Jin. Exclusive synthesis of $Au_{11}(PPh_3)_8Br_3$ against the Cl analogue and the electronic interaction between cluster metal core and surface ligands. *Chem. Eur. J.*, 19(37):12259–12263, 2013.

[34] V. G. Albano, P. L. Bellon, M. Manassero, and M. Sansoni. Intermetallic Pattern in Metal-Atom Clusters. Structural Studies on $Au_{11}X_3(PPh_3)_7$. *J. Chem. Soc. D*, 0(18):1210–1211, 1970.

[35] P. Bellon, M. Manassero, and M. Sansoni. Crystal and Molecular Structure of Triiodoheptakis(tri-p-fluorophenylphosphine)undecagold. *J. Chem. Soc. Dalton Trans.*, 0(14):1481–1487, 1972.

[36] X. Kang, Y. Song, H. Deng, J. Zhang, B. Liu, C. Panc, and M. Zhu. Ligand-induced change of the crystal structure and enhanced stability of the Au_{11} nanocluster. *RSC Adv.*, 5(82):66879–66885, 2015.

[37] K. Nunokawa, S. Onaka, M. Ito, M. Horibe, T. Yonezawa, H. Nishihara, T. Ozeki, H. Chiba, S. Watase, and M. Nakamoto. Synthesis, single crystal X-ray analysis, and TEM for a single-sized Au_{11} cluster stabilized by SR ligands: The interface between molecules and particles. *J. Organomet. Chem.*, 691(4):638–642, 2006.

[38] N. Zheng and G. D. Stucky. A General Synthetic Strategy for Oxide-Supported Metal Nanoparticle Catalysts. *J. Am. Chem. Soc.*, 128(44):14278–14280, 2006.

[39] Y. Liu, H. Tsunoyama, T. Akita, and T. Tsukuda. Preparation of $\approx$ 1 nm Gold Clusters Confined within Mesoporous Silica and Microwave-Assisted Catalytic Application for Alcohol Oxidation. *J. Phys. Chem. C*, 113(31):13457–13461, 2009.

[40] Y. Liu, H. Tsunoyama, T. Akita, and T. Tsukuda. Size Effect of Silica-supported Gold Clusters in the Microwave-assisted Oxidation of Benzyl Alcohol with H_2O_2. *Chem. Lett.*, 39(3):159–161, 2010.

[41] Y. Liu, H. Tsuyonama, T. Akita, S. Xie, and T. Tsukuda. Aerobic Oxidation of Cyclohexane Catalyzed by Size-Controlled Au Clusters on Hydroxyapatite: Size Effect in the Sub-2 nm Regime. *ACS Catal.*, 1(1):2–6, 2011.

[42] M. Turner, V. B. Golovko, O. P. H. Vaughan, P. Abdulkin, A. Berenguer-Murcia, M. S. Tikhov, B. F. G. Johnson, and R. M. Lambert. Selective oxidation with dioxygen by gold nanoparticle catalysts derived from 55-atom clusters. *Nature*, 454(7207):981–983, 2008.

[43] Y. Zhu, H. Qian, M. Zhu, and R. Jin. Thiolate-Protected Au_n Nanoclusters as Catalysts for Selective Oxidation and Hydrogenation Processes. *Adv. Mater.*, 22(17):1915–1920, 2010.

[44] Y. Zhu, H. Qian, and R. Jin. Catalysis opportunities of atomically precise gold nanoclusters. *J. Mater. Chem.*, 21(19):6793–6799, 2011.

[45] D.-C. Lim, R. Dietsche, G. Ganteför, and Y. D. Kim. Size-selected Au clusters deposited on SiO_2/Si: Stability of clusters under amibient pressure and elevated temperatures. *Applied Surface Science*, 256(4):1148–1151, 2009.

[46] D.-C. Lim, C.-C. Hwang, G. Ganteför, and K. Y. Kim. Model catalysts of supported Au nanoparticles and mass-selected clusters. *Phys. Chem. Chem. Phys.*, 12(46):15172–15180, 2010.

[47] D.-C. Lim, R. Dietsche, M. Bubeka, T. Ketterer, G. Ganteför, and Y. D. Kim. Chemistry of mass-selected Au clusters deposited on sputter-damaged HOPG surfaces: The unique properties of Au_8 clusters. *Chem. Phys. Lett.*, 439(4–6):364–368, 2007.

[48] M. Brust, M. Walker, D. Bethell, D. J. Schiffrin, and R. Whyman. Synthesis of Thiol-derivatised Gold Nanoparticles in a Two-phase Liquid-Liquid System. *J. Chem. Soc., Chem. Commun.*, 0(7):801–802, 1994.

[49] M. Zhu, E. Lanni, N. Garg, M. E. Bier, and R. Jin. Kinetically Controlled, High-Yield Synthesis of Au_{25} Clusters. *J. Am. Chem. Soc.*, 130(4):1138–1139, 2008.

[50] Z. Wu, J. Suhan, and R. Jin. One-pot synthesis of atomatically monodisperse, thiol-functionalized Au_{25}. *J. Mater. Chem.*, 19(5):622–626, 2009.

[51] X. Yuan, B. Zhang, Z. Luo, Q. Yao, D. T. Leong, N. Yan, and J. Xie. Balancing the Rate of Cluster Growth and Etching for Gram-Scale Synthesis of Thiolate-Protected Au_{25} Nanoclusters with Atomic Precision. *Angew. Chem. Int. Ed.*, 53(18):4623–4627, 2014.

[52] Y. Negishi, N. K. Chaki, Y. Shichibu, R. L. Whetten, and T. Tsukuda. Origin of Magic Stability of Thiolated Gold Clusters: A Case Study on $Au_{25}(SC_6H_{13})_{18}$. *J. Am. Chem. Soc.*, 129(37):11322–11323, 2007.

[53] A. Shivhare, S. J. Ambrose, H. Zhang, R. W. Purves, and R. W. J. Scott. Stable and recyclable Au_{25} clusters for the reduction of 4-nitrophenol. *Chem. Commun.*, 49(3):276–278, 2013.

[54] N. K. Chaki, Y. Negishi, H. Tsunoyama, Y. Shichibu, and T. Tsukuda. Ubiquitous 8 and 29 kDa Gold:Alkanethiolate Cluster Compounds: Mass-Spectrometric Determination of Molecular Formulas and Structural Implications. *J. Am. Chem. Soc.*, 130(27):8608–8610, 2008.

[55] H. Qian, Y. Zhu, and R. Jin. Size-Focusing Synthesis, Optical and Electrochemical Properties of Monodisperse $Au_{38}(SC_2H_4Ph)_{24}$ Nanoclusters. *ACS Nano*, 3(11):3795–3803, 2009.

[56] H. Qian and R. Jin. Ambient Synthesis of $Au_{144}(SR)_{60}$ Nanoclusters in Methanol. *Chem. Mater.*, 23(8):2209–2217, 2011.

[57] R. C. Price and R. L. Whetten. All-Aromatic, Nanometer-Scale, Gold-Cluster Thiolate Complexes. *J. Am. Chem. Soc.*, 127(40):13750–13751, 2005.

[58] Q. Yao, Y. Yu, X. Yuan, Y. Yu, J. Xie, and J. Y. Lee. Two-Phase Synthesis of Small Thiolate-Protected Au_{15} and Au_{18} Nanoclusters. *Small*, 9(16):2696–2701, 2013.

[59] Y. Yu, X. Chen, Q. Yao, Y. Yu, N. Yan, and J. Xie. Scalable and Precise Synthesis of Thiolated $Au_{10\text{-}12}$, Au_{15}, Au_{18}, and Au_{25} Nanoclusters via pH Controlled CO Reduction. *Chem. Mater.*, 25(6):946–952, 2013.

[60] S. Knoppe, N. Kothalawala, V. R. Jupally, A. Dass, and T. Bürgi. Ligand dependence of the synthetic approach and chiroptical properties of a magic cluster protected with a bicyclic chiral thiolate. *Chem. Commun.*, 48(38):4630–4632, 2012.

[61] M. Zhu, H. Qian, and R. Jin. Thiolate-Protected Au_{20} Clusters with a Large Energy Gap of 2.1 eV. *J. Am. Chem. Soc.*, 131(21):7220–7221, 2009.

[62] T. Tsukuda. Toward an Atomic-Level Understanding of Size-Specific Properties of Protected and Stabilized Gold Clusters. *Bull. Chem. Soc. Jpn.*, 85(2):151–168, 2012.

[63] X. Meng, Z. Liu, M. Zhu, and R. Jin. Controlled reduction for size selective synthesis of thiolate-protected gold nanoclusters Au_n (n = 20, 24, 39, 40). *Nanoscale Res. Lett.*, 7:277–283, 2012.

[64] A. C. Dharmaratne, T. Krick, and A. Dass. Nanocluster Size Evolution Studied by Mass Spectrometry in Room Temperature $Au_{25}(SR)_{18}$ Synthesis. *J. Am. Chem. Soc.*, 131(38):13604–13605, 2009.

[65] I. Odriozola, I. Loinaz, J. A. Pomposo, and H. J. Grande. Gold-glutathione supramolecular hydrogels. *J. Mater. Chem.*, 17(46):4843–4845, 2007.

[66] R. Jin. Quantum sized, thiolate-protected gold nanoclusters. *Nanoscale*, 2:343–362, 2010.

[67] A. Sels, G. Salassa, S. Pollitt, C. Guglieri, G. Rupprechter, and T. Barrabés, N. Bürgi. Structural Investigation of the Ligand Exchange Reaction with Rigid Dithiol on Doped (Pt, Pd) Au_{25} Clusters. *J. Phys. Chem. C*, 121(20):10919–10926, 2017.

[68] A. Sels. Ligand Exchange Reactions with Palladium, Platinum Doped $Au_{25}(SR)_{18}$. Master's thesis, Université de Genève, 2015.

[69] M. J. Hostetler, A. C. Templeton, and R. W. Murray. Dynamics of Place-Exchange Reactions on Monolayer-Protected Gold Cluster Molecules. *Langmuir*, 15(11):3782–3789, 1999.

[70] R. Guo, Y. Song, G. Wang, and R. W. Murray. Does Core Size Matter in the Kinetics of Ligand Exchanges of Monolayer-Protected Au Clusters? *J. Am. Chem. Soc.*, 127(8):2752–2757, 2005.

[71] C. L. Heinecke, T. W. Ni, S. Malola, V. Mäkinen, O. A. Wong, H. Häkkinen, and C. J. Ackerson. Structural and Theoretical Basis for Ligand Exchange on Thiolate Monolayer Protected Gold Nanoclusters. *J. Am. Chem. Soc.*, 134(32):13316–13322, 2010.

[72] V. R. Jupally, R. Kota, E. Van Dornshuld, D. L. Mattern, G. S. Tschumper, D. Jiang, and A. Dass. Interstaple Dithiol Cross-Linking in $Au_{25}(SR)_{18}$ Nanomolecules: A Combined Mass Spectrometric and Computational Study. *J. Am. Chem. Soc.*, 133(50):20258–20266, 2011.

[73] S. Knoppe and T. Bürgi. The fate of $Au_{25}(SR)_{18}$ clusters upon ligand exchange with binaphthyl-dithiol: interstaple binding vs. decomposition. *Phys. Chem. Chem. Phys.*, 15(38):15816–15820, 2013.

[74] S. Knoppe, S. Michalet, and T. Bürgi. Stabilization of Thiolate-Protected Gold Clusters Against Thermal Inversion: Diastereomeric $Au_{38}(SCH_2CH_2Ph)_{24-2x}(R\text{-}BINAS)_x$. *J. Phys. Chem. C*, 117(29):15354–15361, 2013.

[75] G. H. Woehrle, M. G. Warner, and J. E. Hutchison. Ligand Exchange Reactions Yield Subnanometer, Thiol-Stabilized Gold Particles with Defined Optical Transitions. *J. Phys. Chem. B*, 106(39):9979–9981, 2002.

[76] A. Das, T. Li, K. Nobusada, Q. Zeng, N. L. Rosi, and R. Jin. Total Structure and Optical Properties of a Phosphine/Thiolate Protected Au_{24} Nanocluster. *J. Am. Chem. Soc.*, 134(50):20286–20289, 2012.

[77] Y. Shichibu, Y. Negishi, T. Tsukuda, and T. Teranishi. Large-Scale Synthesis of Thiolated Au_{25} Clusters via Ligand Exchange Reactions of Phosphine-Stabilized Au_{11} Clusters. *J. Am. Chem Soc.*, 127(39):13464–13465, 2005.

[78] Y. Shichibu, Y. Negishi, T. Watanabe, N. K. Chaki, H. Kawaguchi, and T. Tsukuda. Biicosahedral Gold Clusters $[Au_{25}(PPh_3)_{10}(SC_nH_{2n+1})_5Cl_2]^{2+}$ (n = 2-18): A Stepping Stone to Cluster-Assembled Materials. *J. Phys. Chem. C*, 111(22):7845–7847, 2007.

[79] G. H. Woehrle, L. O. Brown, and J. E. Hutchison. Thiol-Functionalized, 1.5-nm Gold Nanoparticles through Ligand Exchange Reactions: Scope and Mechanism of Ligand Exchange. *J. Am. Chem. Soc.*, 127(7):2172–2183, 2005.

[80] H. Qian, M. Zhu, E. Lanni, Y. Zhu, M. E. Bier, and R. Jin. Conversion of Polydisperse Au Nanoparticles into Monodisperse Au_{25} Nanorods and Nanospheres. *J. Phys. Chem. C*, 113(41):17599–17603, 2009.

[81] H. Qian, W. T. Eckenhoff, M. E. Bier, T. Pintauer, and R. Jin. Crystal Structures of Au_2 Complex and Au_{25} Nanocluster and Mechanistic Insight into the Conversion of Polydisperse Nanoparticles into Monodisperse Au_{25} Nanoclusters. *Inorg. Chem.*, 50(21):10735–10739, 2011.

[82] M. I. Bruce, B. K. Nicholson, and O. Bin Shawkataly. Synthesis of Gold-Containing Mixed-Metal Cluster Complex. *Inorg. Synth.*, 26:324–328, 1989.

[83] P. Braunstein, H. Lehner, and D. Matt. A Platinum-Gold Cluster Chloro-1KCl-Bis(Triethylphosphine-1KP)-Bis(Triphenylphoshine)-2KP, 3KP-Triangulo-Digold-Platinum(1 +) Trifluoromethanesulfonate. *Inorg. Synth.*, 27:218–221, 1990.

[84] M. R. Richter. *Neue Goldcluster. Synthesen und Kristallstrukturen.* PhD thesis, Eberhard-Karls-Universität Tübingen, 2004.

[85] Y. Shichibu, K. Suzuki, and K. Konishi. Facile synthesis and optical properties of magic-number Au_{13} clusters. *Nanoscale*, 4(14):4125–4129, 2012.

[86] B. K. Teo, X. Shi, and H. Zhang. Pure gold cluster of 1:9:9:1:9:9:1 layered structure: a novel 39-metal-atom cluster $[(Ph_3P)_{14}Au_{39}Cl_6]Cl_2$ with an interstitial gold atom in a hexagonal antiprismatic cage. *J. Am. Chem. Soc.*, 114(7):2743–2745, 1992.

[87] F.-H. Hu, L.-S. Wang, and S.-F. Cai. Solubilities of Triphenylphosphine Oxide in Selected Solvents. *J. Chem. Eng. Data*, 54(4):1382–1384, 2009.

[88] K. Nobusada and T. Iwasa. Oligomeric Gold Clusters with Vertex-Sharing Bi- and Triicosahedral Structures. *J. Phys. Chem. C*, 111(39):14279–14282, 2007.

[89] B. K. Teo and K. Keating. Novel triicosahedral structure of the largest metal alloy cluster: hexachlorododecakis(triphenylphosphine)-gold-silver cluster $[(Ph_3P)_{12}Au_{13}Ag_{12}Cl_6]^{m+}$. *J. Am. Chem. Soc.*, 106(7):2224–2226, 1984.

[90] B. K. Teo, H. Zhang, and X. Shi. Cluster of Clusters: A Modular Approach to Large Metal Clusters. Structural Characterization of a 38-Atom Cluster $[p\text{-}Tol_3P)_{12}Au_{18}Ag_{20}Cl_{14}]$ Based on Vertex-Sharing Triicosahedra. *J. Am. Chem. Soc.*, 112(23):8552–8565, 1990.

[91] B. K. Teo and H. Zhang. Cluster of Clusters. Structure of a New 25-Metal-Atom Cluster $[(p\text{-}Tol_3P)_{10}Au_{13}Ag_{12}Cl_7](SbF_6)_2$ Containing a Nearly Staggered-Eclipsed-Staggered Metal Configuration and Five Doubly Bridging Ligands. *Inorg. Chem.*, 30(16):3115–3116, 1991.

[92] V. D. Thanthirige, E. Sinn, G. P. Wiederrecht, and G. Ramakrishna. Unusual Solvent Effects on Optical Properties of Bi-Icosahedral Au_{25} Clusters. *J. Phys. Chem. C*, 121(6):3530–3539, 2017.

[93] A. Dass, A. Stevenson, G. R. Dubay, J. B. Tracy, and R. W. Murray. Nanoparticle MALDI-TOF Mass Spectrometry without Fragmentation: $Au_{25}(SCH_2CH_2Ph)_{18}$ and Mixed Monolayer $Au_{25}(SCH_2CH_2Ph)_{18\text{-}x}(L)_x$. *J. Am. Chem. Soc.*, 130(18):5940–5946, 2008.

[94] S. Wang, H. Abroshan, C. Liu, T.-Y. Luo, M. Zhu, H. J. Kim, N. L. Rosi, and R. Jin. Shuttling single metal atom into and out of a metal nanoparticle. *Nature Communications*, 8(848):1–7, 2017.

[95] P. I. da S. Maia, A. Graminha, F. R. Pavan, C. Q. F. Leite, A. A. Batista, D. F. Back, E. S. Lang, J. Ellena, S. de S. Lemos, H. S. Salistre-de Araujo, and V. M. Deflon. Palladium(II) complexes with thiosemicarbazones. Syntheses, characterization and cytotoxicity against breast cancer cells and Anti-Mycobacterium tuberculosis activity. *J. Braz. Chem. Soc.*, 21(7):1177–1186, 2010.

[96] W. F. Edgell and M. P. Dunkle. The Infrared and Raman Spectra of a Triphenylphosphine Derivative of Ni(CO)$_4$. *Inorg. Chem.*, 4(11):1629–1636, 1965.

[97] E. Steger and K. Stopperka. Die Schwingungsspektren von Triphenylphosphin und Diphenylphosphin. *Eur. J. Org. Chem.*, 94(11):3023–3029, 1961.

[98] O. Dereli, Y. Erdogdu, and M. T. Gulluoglu. Study on molecular structure and vibrational spectra of (triphenylphosphoranylidene) acetaldehyde using DFT: A combined experimental and quantum chemical approach. *J. Mol. Struct.*, 1012:105–112, 2012.

[99] R. R. Shifrina, I. P. Romm, E. N. Gur'yanova, and Rozanel'skaya. IR spectra of methyl-substituted triphenylphosphine oxides. *J. Appl. Spectrosc.*, 34(1):84–88, 1981.

[100] B. Varnholt, P. Oulevey, S. Luber, C. Kumara, A. Dass, and T. Bürgi. Structural Information on the Au-S Interface of Thiolate-Protected Gold Clusters: A Raman Spectroscopy Study. *J. Phys. Chem. C*, 118(8):9604–9611, 2014.

[101] M. Picquart, L. Grajcar, M. H. Baron, and Z. Abedinzadeh. Vibrationional Spectroscopic Study of Glutathione Complexation in Aqueous Solutions. *Biospectroscopy*, 5(6):328–337, 1999.

[102] N. Nilius, T. Risse, S. Shaikhutdinov, M. Sterrer, and H.-J. Freund. Model Catalysts Based on Au Clusters and Nanoparticles. In D. M. P. Mingos, editor, *Gold Clusters, Colloids and Nanoparticles II*, Struct. Bond. 162, pages 91–138. Springer, 2014.

[103] Y. Negishi, K. Nobusada, and T. Tsukuda. Glutathione-Protected Gold Clusters Revisited: Bridging the Gap between Gold(I)-Thiolate Complexes and Thiolate-Protected Gold Nanocrystals. *J. Am. Chem. Soc.*, 127(14):5261–5270, 2005.

[104] A. Sels, N. Barrabés, S. Knoppe, and T. Bürgi. Isolation of atomically precise mixed ligand shell PdAu$_{24}$ clusters. *Nanoscale*, 8(21):11130–11135, 2016.

[105] Y. Shichibu, Y. Negishi, H. Tsunoyama, M. Kanehara, T. Teranishi, and T. Tsukuda. Extremely High Stability of Glutathionate Protected Au$_{25}$ Clusters Against Core Etching. *Small*, 3(5):835–839, 2007.

[106] R. Balasubramanian, R. Guo, A. J. Mills, and R. W. Murray. Reaction of Au$_{55}$(PPh$_3$)$_{12}$Cl$_6$ with Thiols Yields Thiolate Monolayer Protected Au$_{75}$ Clusters. *J. Am. Chem. Soc.*, 127(22):8126–8132, 2005.

[107] C. Gautier and T. Büergi. Chiral Inversion of Gold Nanoparticles. *J. Am. Chem. Soc.*, 130(22):7077–7084, 2009.

[108] Y. Song, T. Huang, and R. W. Murray. Heterophase Ligand Exchange and Metal Transfer between Monolayer Protected Clusters. *J. Am. Chem. Soc.*, 125(38):11694–11701, 2003.

[109] C. Zeng, C. Liu, Y. Pei, and R. Jin. Thiol Ligand-Induced Transformation of $Au_{38}(SC_2H_4Ph)_{24}$ to $Au_{36}(SPh\text{-}t\text{-}Bu)_{24}$. *ACS Nano*, 7(7):6138–6145, 2013.

[110] C. Zeng, C. Liu, Y. Chen, N. L. Rosi, and R. Jin. Gold-Thiolate Ring as a Protecting Motif in the $Au_{20}(SR)_{16}$ Nanocluster and Implications. *J. Am. Chem. Soc.*, 136(34):11922–11925, 2014.

[111] S. Kumar and A. K. Sood. *Reviews in Plasmonics 2015*, chapter Ultrafast Response of Plasmonic Nanostructures, pages 131–168. Springer, 2016.

[112] J. Mooney and P. Kambhampati. Get the Basics Right: Jacobian Conversion of Wavelength and Energy Scales for Quantitative Analysis of Emission Spectra. *J. Phys. Chem. Lett.*, 4(19):3316–3318, 2013.

[113] J. Mooney and P. Kambhampati. Correction to 'Get the Basics Right: Jacobian Conversion of Wavelength and Energy Scales for Quantitative Analysis of Emission Spectra'. *J. Phys. Chem. Lett.*, 5(20):3497, 2014.

[114] M. Zhu, C. M. Aikens, F. J. Hollander, G. C. Schatz, and R. Jin. Correlating the Crystal Structure of A Thiol-Protected Au_{25} Cluster and Optical Properties. *J. Am. Chem. Soc.*, 130(18):5883–5885, 2008.

[115] J. Li, X. Li, H.-J. Zhai, and L.-S. Wang. Au_{20}: A Tetrahedral Cluster. *Science*, 299(5608):864–867, 2003.

[116] Y. Pei, Y. Gao, N. Shao, and X. C. Zeng. Thiolate-Protected $Au_{20}(SR)_{16}$ Cluster: Prolate Au_8 Core with New $[Au_3(SR)_4]$ Staple Motif. *J. Am. Chem. Soc.*, 131(38):13619–13621, 2009.

[117] D. Jiang, W. Chen, R. L. Whetten, and Z. Chen. What Protects the Core When the Thiolated Au Cluster is Extremely Small? *J. Phys. Chem. C*, 113(39):16983–16987, 2009.

[118] K. L. Dimuthu, M. Weerawardene, and C. M. Aikens. Effect of Aliphatic versus Aromatic Ligands on the Structure and Optical Absorption of $Au_{20}(SR)_{16}$. *J. Phys. Chem. C*, 120(15):8354–8363, 2016.

[119] S. Calvin. *XAFS for Everyone*. CRC Press, 2013.

[120] M. A. MacDonald, D. M. Chevrier, P. Zhang, H. Qian, and R. Jin. The Structure and Bonding of $Au_{25}(SR)_{18}$ Nanoclusters from EXAFS: The Interplay of Metallic and Molecular Behavior. *J. Phys. Chem. C*, 115(31):15282–15287, 2011.

[121] D. M. Chevrier, M. A. MacDonald, A. Chatt, P. Zhang, Z. Wu, and R. Jin. Sensitivity of Structural and Electronic Properties of Gold-Thiolate Nanoclusters to the Atomic Composition: A Comparative X-ray Study of $Au_{19}(SR)_{13}$ and $Au_{25}(SR)_{18}$. *J. Phys. Chem. C*, 116(47):25137–25142, 2012.

[122] B. Ravel and M. Newville. ATHENA, ARTEMIS, HEPHAESTUS: Data Analysis for X-Ray Absorption Spectroscopy Using IFEFFIT. *J. Synchrotron Radiat.*, 12:537–541, 2005.

[123] W. W. Weare, S. M. Reed, M. G. Warner, and J. E. Hutchison. Improved Synthesis of Small ($d_{\text{CORE}} \approx 1.5$ nm) Phosphine-Stabilized Gold Nanoparticles. *J. Am. Chem. Soc.*, 122(51):12890–12891, 2000.

[124] NIST Chemistry WebBook. Phosphine, triphenyl-. http://webbook.nist.gov/chemistry, December 2017.

[125] NIST Chemistry WebBook. 2-Phenylethylthiol. http://webbook.nist.gov/chemistry, December 2017.